THESIS FOR THE DEGREE OF DOCTOR OF PHILOSOPHY

Chemical Modification of Cellulose Nanocrystals

Creating a Novel Toolbox Utilising the Overlooked Sulphate Surface Groups

KARIN SJÖVOLD

Department of Chemistry and Chemical Engineering

CHALMERS UNIVERSITY OF TECHNOLOGY

Gothenburg, Sweden 2021

Department of Chemistry and Chemical Engineering
Chalmers University of Technology
SE-412 96 Gothenburg
Sweden
Telephone + 46 (0)31-772 1000

Cover:
An illustration of a wooden toolbox containing various dialkylamine reagents, which have been used for functionalising the sulphate half-ester groups on a cellulose nanocrystal.

Chemical Modification of Cellulose Nanocrystals:
Creating a Novel Toolbox Utilising the Overlooked Sulphate Surface Groups

KARIN SJÖVOLD

Department of Chemistry and Chemical Engineering
Chalmers University of Technology

ABSTRACT

The move towards a bio-based economy has created an increasing demand for renewable, sustainably produced materials. For future generations, it is crucial to develop economically, socially and environmentally sustainable materials and processes. Cellulose, as the main component in plant biomass, has been an integral part of society since the dawn of age and still continues to provide new possibilities. The complex hierarchical structure of lignocellulosic materials makes it possible to liberate nano-sized cellulose particles with extraordinary and versatile properties, such as large surface area, transparency and excellent mechanical properties. However, the hydrophilic nature of nanocellulose can cause issues in certain applications, and in other instances it may be desirable to introduce additional properties to the CNCs. This can be achieved by functionalising the nanocellulose surface through chemical modification.

This thesis presents a novel approach to chemical modification of cellulose nanocrystals, by utilising the sulphate half-ester groups that decorate their surface. Cellulose nanocrystals produced by sulphuric acid hydrolysis were functionalised with dialkylamines through a ring-opening reaction with azetidinium salts, as well as through conjugation with dialkyl alkylchloride and dialkyl cyclocarbonate. The impact on thermal and rheological properties of the functionalised CNCs was evaluated and they were also incorporated as reinforcing elements in bio-based composites.

The functionalisation had a significant impact on the thermal stability, improving it by around $100\,°C$. The functionalised CNCs also exhibited a significantly higher viscosity compared to unmodified CNCs and were prone to network formation at considerably lower solid contents. The conjugation protocol was improved by a more robust synthesis path for the dialkylamine reagents and by shifting from using organic solvents to water, to facilitate scale-up. Incorporation of CNCs into a polymeric matrix resulted in a near three-fold increase in stiffness, depending on matrix, modification and processing techniques used. The modifications also created a stronger interphase between the CNCs and the matrix.

Keywords: Cellulose nanocrystals, Chemical modification, Dialkylamines, Azetidinium salts, Thermal stability, Composites, Scale-up

CONTRIBUTION REPORT

The author has made the following contribution to the papers:

I   Co-author. Involved in planning the study and designing the dialkylamine groups and experiments. Produced and desulphated the cellulose nanocrystals, produced the composites and performed initial surface characterisation. Contributed to writing the manuscript. The functionalisation of the CNCs was done together with Mikaela Börjesson, who also synthesised and characterised the reagents. Solid state NMR measurements were performed by Diana Bernin, AFM was performed by Anders Mårtensson.

II Shared main author. Involved in planning the study and designing the dialkylamine groups and chemical modification experiments. Produced, functionalised and characterised the cellulose nanocrystals, except for the rheological characterisation which was performed by Lilian Forsgren and the solid state NMR measurements performed by Diana Bernin. Synthesised and characterised the reagents and model reaction. The first draft of the manuscript was written together with Lilian Forsgren and the finalising was a joint effort by all co-authors.

III Co-author. Planned the study together with Lilian Forsgren and designed the dialkylamine groups and chemical modification experiments. Produced, functionalised and characterised the cellulose nanocrystals as well as the small-scale, neutralised composite. The mechanical testing was performed by Lilian Forsgren and Abhijit Venkatesh. The results were analysed and discussed together with all co-authors. The first draft of the manuscript was written together with Lilian Forsgren and Abhijit Venkatesh and the finalising was a joint effort by all co-authors.

IV Main author. Planned the study and designed the dialkylamine groups and experiments. Produced, desulphated, functionalised and characterised the cellulose nanocrystals. Synthesised and characterised the reagents. Wrote the manuscript with input from co-authors.

V   Co-author. Planned the study together with Lilian Forsgren and Abhijit Venkatesh and was involved in designing the dialkylamine groups and chemical modification experiments. Made initial synthesis of reagents and functionalisation of CNC, the large-scale modification was performed by internship student Florian Rigolet with assistance from Lilian Forsgren and characterised by the author. The composites were produced and characterised by Lilian Forsgren and Abhijit Venkatesh. Contributed to writing the manuscript.

ADDITIONAL PUBLICATIONS NOT INCLUDED IN THE THESIS

Rheological properties of nanocellulose suspensions: effects of fibril/particle dimensions and surface characteristics

Tobias Moberg, Karin Sahlin, Kun Yao, Shiyu Geng, Gunnar Westman, Qi Zhou, Kristiina Oksman, Mikael Rigdahl

Cellulose 24 (6), 2499–2510 (2017)

Electroosmotic dewatering of cellulose nanocrystals

Jonas Wetterling, Karin Sahlin, Tuve Mattsson, Gunnar Westman, Hans Theliander

Cellulose 25 (4), 2321–2329 (2018)

A revised solid-state NMR method to assess the crystallinity of cellulose

Tobias Sparrman, Leo Svenningsson, Karin Sahlin-Sjövold, Lars Nordstierna, Gunnar Westman, Diana Bernin

Cellulose 26, 8993–9003 (2019)

Melt Processing of Ethylene-Acrylic Acid Copolymer Composites Reinforced with Nanocellulose

Abhijit Venkatesh, Johannes Thunberg, Karin Sahlin-Sjövold, Mikael Rigdahl, Antal Boldizar

Polymer Engineering and Science 60 (5), 956-967 (2020)

Composition and structure of cell wall ulvans recovered from Ulva spp. along the Swedish west coast

Niklas Wahlström, Filip Nylander, Eric Malmhäll-Bah, Karin Sjövold, Ulrika Edlund, Gunnar Westman, Eva Albers

Carbohydrate Polymers 233, 115852 (2020)

SAMPLE NAME ABBREVIATIONS

CNC-OSO₃H	Sulphated CNCs produced by sulphuric acid hydrolysis
CNC-OSO₃Na	Commercial CNCs produced by CelluForce, Canada. Produced by sulphuric acid hydrolysis and neutralised
CNC-OSO₃H-part	Sulphated CNCs that are partially desulphated by an HCl-catalysed desulphation reaction
CNC-OSO₃H-self	Sulphated CNCs that are partially desulphated by a self-catalysed desulphation reaction
CNC-OH	Solvolytically desulphated CNCs
CNC-DEA-AzOH	Sulphated CNCs functionalized with 3-hydroxy azetidinium salts prepared from diethylamine
CNC-DEA-AzOMe	Sulphated CNCs functionalized with 3-methoxy azetidinium salts prepared from diethylamine
CNC-DHA-AzOH	Sulphated CNCs functionalized with 3-hydroxy azetidinium salts prepared from dihexylamine
CNC-DHA-AzOMe	Sulphated CNCs functionalized with 3-methoxy azetidinium salts prepared from dihexylamine
CNC-M-AzOH	Sulphated CNCs functionalized with 3-hydroxy azetidinium salts prepared from morpholine
CNC-M-AzOMe	Sulphated CNCs functionalized with 3-methoxy azetidinium salts prepared from morpholine
CNC-DAA-AzOH	Sulphated CNCs functionalized with 3-hydroxy azetidinium salts prepared from diallylamine
CNC-DAA-AzOMe	Sulphated CNCs functionalized with 3-methoxy azetidinium salts prepared from diallylamine
CNC-DAA-CC	Sulphated CNCs functionalized with diallyl cyclocarbonate
CNC-DAA-AC	Sulphated CNCs functionalized with diallyl alkylchloride
CNC-DAA-AC-alk	Sulphated CNCs functionalized with diallyl alkylchloride in alkali
CelluForce-DAA-CC	CelluForce CNCs functionalized with diallyl cyclocarbonate
CelluForce-DAA-AzOH	CelluForce CNCs functionalized with 3-hydroxy azetidinium salts prepared from diallylamine

TABLE OF CONTENT

1

INTRODUCTION

Wood has throughout history and across the world been an essential part of society. Not only is it a beautiful material, it is also strong, durable, renewable and biodegradable. It can be utilised unrefined, e.g.as firewood or for carpentry and building materials, or after various degrees of processing into e.g. paper, plastic and textiles. Sadly, the versatility and potential of wood as a raw material was to some extent forgotten after the discovery of fossil oil with the new, easily produced materials it brought with it. But climate change and the strives towards a bio-based society has reignited the interest in cellulose.

1.1 Background

The immense economic progress and the advances in science and technology over the past centuries has, for better or worse, been greatly facilitated by the discovery and refining of fossil resources, as it enabled a rapid expansion of power and material consumption. As time has passed, it has become increasingly clear that a lot of these advances have been made at the expense of our climate. Carbon dioxide emissions have led to global warming with rising sea-levels, more extreme weather and disturbances to the natural habitats of various animals. The urgent need for environment, social and economic sustainability has focused efforts on shifting to a bio-based, circular economy. Wood, with its vast potential, is therefore making a comeback as a material for the future.

Since wood is a complex, hierarchical material that can be utilised at different structural levels; from the raw wood logs down to the fibres and further to the polymeric and monomeric units. Cellulose fibres have historically been the main product when refining wood, primarily in the form of paper, but with the emergence of the digital era, the demand for printing paper has decreased substantially. It has therefore become critical for the pulp and paper industry to branch out and expand and diversify their product

1

portfolio and to better utilise the remaining wood components in order to maintain profitability. Utilising as much of the wood raw material as possible is the cornerstone in the biorefinery concept. For future generations, it is essential to develop economically, socially and environmentally sustainable processing of biomass with maximised conversion into materials, value-added chemicals, fuels, power and heat. It is about upgrading biomass by taking a more holistic approach, using as much as possible of the raw material and to do so by sustainable processes. Minimizing waste by more efficient and selective reactions is key, as is utilizing waste streams to produce chemicals, fuel and heat. More flexible processes and products could help to better meet market demands and prices and ensure competitiveness with fossil-based products.

To reach a bio-based economy, resting on the biorefinery concept more research is needed. Interdisciplinary collaborations are crucial for success, e.g. between chemistry, chemical engineering and biology. It is not only about creating new, functional materials, because if the materials cannot be produced by a sustainable, large scale process they are not likely to be commercially successful. Processes have to be sustainable, scalable and robust, and it is the responsibility of academia, research institutes and companies to together address these challenges.

1.1.1 Wallenberg Wood Science Center

The Wallenberg Wood Science Center (WWSC) is a research initiative that originated between The Royal Institute of Technology and Chalmers University of Technology in 2009, but has since grown to also include Linköping University as well as research groups from Stockholm University and Luleå University. The focus of the research centre is on creating new materials from wood, with the mission "*to create knowledge and build competence that can form the basis for an innovative future value creation from forest raw material*". It does so by educating PhD students in subjects ranging from process technology and biotechnology to molecular dynamics, polymer science and nanotechnology. The centre is based on funding from the Knut and Alice Wallenberg Foundation.

1.1.2 Nanocellulose

Nanocellulose is a nanomaterial produced by liberating the nanoscale structural element of wood. It has several interesting and versatile properties such as large surface area, transparency, excellent mechanical properties, lightweight, low density and has many suggested applications in very diverse areas. It was discovered already during the 1950s

that cellulose can form colloidal particles (Rånby 1949), but it wasn't until the 1980s with the rise of nanotechnology, encouraged by the discovery of fullerenes and AFM microscopy (U. S. National Nanotechnology Initiative) along with the Nobel prize in chemistry in 1987 on "supramolecular chemistry" (Nobel Media AB, 1987), that this discovery would gain the attention of the research community. There are applications where some of the inherent properties of the nanocellulose could pose an issue, such as high moisture uptake and compatibility with non-polar media, such as when incorporated as reinforcing elements in bio-based composites. The insufficient compatibility between the hydrophobic matrix and the hydrophilic nanocellulose can result in poor stress transfer and dispersion in the matrix, which could deteriorate the mechanical properties rather than enhance them. This could be addressed by e.g. adding compatibilizers or by chemically modifying the particle surfaces, where the latter is the approach taken in this thesis. Chemical modification of cellulose is typically done on the plentiful hydroxyls, but this thesis presents a method that instead utilises the characteristic sulphate half-ester groups of cellulose nanocrystals to achieve new properties and better interactions with the matrix.

1.2 Aim and Outline of Thesis

The overall aim of the project has been to contribute to the WWSC mission of generating knowledge and creating new materials from wood. The more specific aims for this project have been to find an industrially plausible method to functionalise cellulose nanocrystals as well as to improve the mechanical properties of thermoplastic bio-composites by incorporation of chemically modified cellulose nanocrystals. A new chemical modification method was developed, based on utilising the sulphate half-ester groups decorating the surface of cellulose nanocrystals. The latter aim was achieved in collaboration with Lilian Forsgren and Abhijit Venkatesh at the Department of Industrial and Materials Science at Chalmers University of Technology.

To provide an introduction to the field, Chapter 2 describes the history, structure and properties of cellulose and cellulose nanocrystals. The experimental work and characterisation techniques are presented in Chapter 3 and the outcome of the synthesis work and chemical modification is presented and discussed in Chapter 4. In Chapter 5 is a shorter summery given, describing the results from the composite collaboration with Lilian Forsgren and Abhijit Venkatesh at the Department of Industrial and Materials Science at Chalmers University of Technology. Lastly, some concluding remarks and future outlook are presented in Chapter 6.

2

CELLULOSE

Cellulose is considered to be the most abundant polymer on earth (Pérez and Mazeau, 2004, Klemm et al., 2005) as it is the main constituent in plant biomass. It was discovered by Anselme Payen in 1838 after he extracted a seemingly insoluble material from plant tissue (Payen, 1838). He found that the main hydrolytic product was glucose, but the properties of the extracted material differed from those of starch. The substance was given the name cellulose, derived from French and Latin, meaning plentiful in small cells.

Cellulose is not only found as the structural, load-bearing polymer in plant biomass, it is also found in some species of bacteria, algae, fungi and animals. The mechanical strength, low density and its recalcitrance are important properties of this ubiquitous polymer. It is an integral part of various complex biological systems and even small structural changes can have a huge impact on its mechanical and biological properties.

2.1 The Structure of Cellulose

Cellulose is a carbohydrate, i.e. empirically, it consists of hydrated carbons; $C_x(H_2O)_y$. A seemingly simple molecule, yet the complex and anisotropic hierarchical structure provide challenges at every structural level during processing and characterisation. It would take nearly 100 years from when Anselme Payen first discovered cellulose, until its molecular structure was determined. Attempts at understanding the nature of the linkages between the sugar residues in cellulose was done by hydrolysis of methylated cellulose and analysing the residual sugars (Denham and Woodhouse, 1917, Irvine and Hirst, 1922). Hydrolysis of a near completely methylated cellulose yielded only one hydrolysis product, namely 2,3,6-trimetylglucose (Irvine and Hirst, 1923), thus confirming that the linkage between the glucose units could only include the two non-methylated hydroxyl groups. Irvine & Hirst firmly believed that cellulose was comprised of furanoses, rather than pyranoses, as was the generally accepted view at the time (Haworth, 1925), and thus suggested that the linkages would be at the C1 and C5 positions. Haworth, Charlton, Peat

later established that this was not the case as glucose in fact had a pyranose structure (Charlton et al., 1926). During this period, the concept of macromolecules, i.e. small, organic molecules connected through covalent bonds rather than colloidal association, started to win acceptance and Staudinger proposed that cellulose was such a macromolecule (Staudinger et al., 1927). Haworth and Machemer were able to present a final piece of evidence, supporting the claim that cellulose was a linear polysaccharide, by isolating small amounts of tetramethyl glucose units from hydrolysed trimethyl cellulose, and could thus demonstrate that cellulose does indeed have end groups and therefore has to be a large, linear molecule (Haworth and Machemer, 1932). The model they suggested is the molecular structure of cellulose as we know it today.

While the molecular structure of cellulose has been established, there is still controversy regarding the more complex supramolecular structure. An early model was the fringed micellar model, where cellulose chains would pass in and out of ordered regions, micelles, without any distinct boundaries (Herrmann et al., 1930). Hearle (1958) proposed a modification of this model, suggesting that the ordered regions should have a fibrillar structure, rather than micellar. Both models accounted for the observed lack of crystallinity in cellulose samples observed in X-ray diffraction experiments, but the model put forward by Rowland and Roberts (1972) is considered to best describe the current understanding of the supramolecular structure of cellulose. They described a model with highly crystalline fibrils with distorted surface chains as well as distorted regions along the fibril axis caused by stresses or twists, which would result in less frequent hydrogen bonds, making these regions more accessible to chemical reactions.

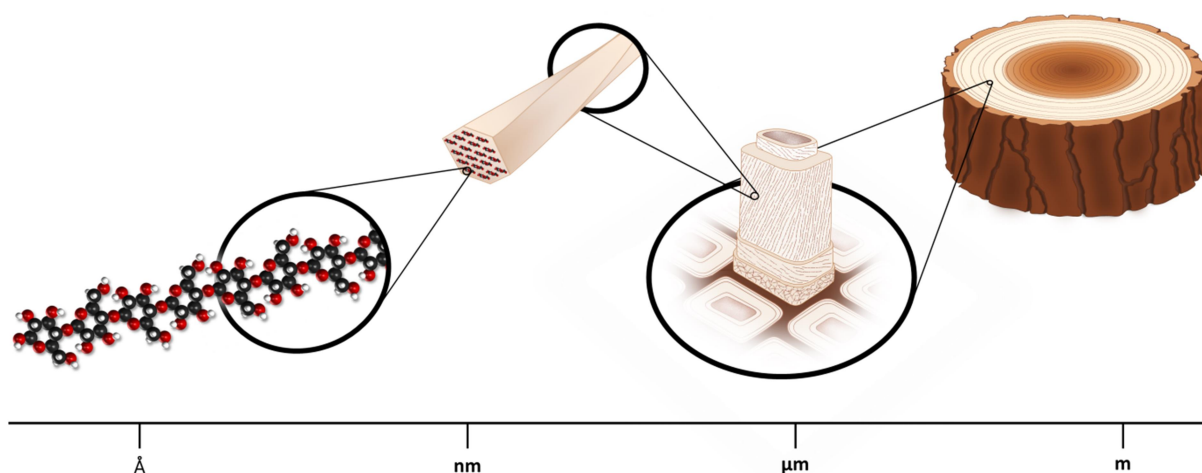| Å | nm | μm | m |

Figure 2.1. Wood is a hierarchical structure with distinctive structural elements at the different length scales.

2.1.1 Molecular Structure

Cellulose is an unbranched, linear homopolysaccharide comprised of anhydrous β-D-glucopyranoses (commonly referred to as an anhydrous glucose unit, abbreviated to AGU), linked by β-1,4-glycosidic bonds, see Figure 2.2. The AGUs are assembled in a

6

syndiotactic manner, where every other AGU is rotated 180° around the glycosidic bond. This gives rise to a structural disaccharide unit referred to as cellobiose, which is commonly, although incorrectly, claimed to be the repeating unit of cellulose (French, 2017). Due to the inherent directionality of the cellulose chain, it has two chemically different end groups; a non-reducing end group, and a reducing end group, containing a cyclic hemiacetal which is in equilibrium with its open aldehyde isomer, see Figure 2.2. The $^4C_1$ chair conformation of the AGUs arranges the hydroxyl groups in equatorial positions, i.e. they will be in the same plane as the ring, while the hydrogens will be axial. This enables intramolecular hydrogen bonding and restricts the AGUs from rotating freely around the glycosidic bond, thus creating a stiff polymer chain with a more hydrophilic nature on the sides and a more hydrophobic nature above and below the flat chain, as seen in Figure 2.3.
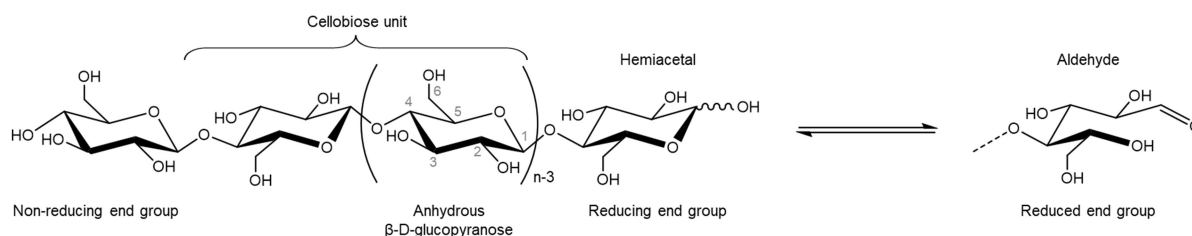

Figure 2.2. The molecular structure of cellulose, illustrating the repeating anhydrous glucose unit, the cellobiose unit and the non-reducing and reducing end groups as well as the equilibrium for reducing end group between the aldehyde and hemiacetal.

The molecular weight of cellulose varies greatly with its origin and method of isolation as well as with any other treatments the material may have been subjected to. It is often referred to in terms of degree of polymerisation (DP) which gives an average distribution of the number of repeating units per polymer chain. As the molecular weight is affected by the isolation method, isolated native celluloses has a high polydispersity (D. Klemm, 2004), with the DP estimated to be around 10 000 for wood cellulose (Sjöström, 1993), but may reach as high as 18 500 when isolated from the algae Valonia (Marx-Figini, 1969).

2.1.2 Supramolecular Structure

The supramolecular structure has its origin in the conformation of the AGUs and the stiffness of the cellulose chain. The conformation not only enables intramolecular hydrogen bonding, but also intermolecular bonding, making it energetically favourable for cellulose to form sheets. Due to attractive van der Waals forces and hydrophobic interactions between the sheets, they stack into highly ordered, three-dimensional crystal structures, often referred to as elementary fibrils which are then organised into fibril aggregates. The size and shape of the fibrils depend on the source, species, growth conditions and isolation method. Typical reported widths for wood derived fibrils are usually around 1.5-3.5 nm (Klemm et al., 2005, Jakob et al., 1994, Guerriero et al., 2010).

There are still ambiguities about the size and shape of a typical wood cellulose elementary fibril, and while it is commonly said to consist of 36 chains, recent research suggests models with 18-24 chains with cross-sections varying from square or hexagonal to rhombus or rectangular (Cosgrove, 2014, Haigler and Roberts, 2019). The terminology in literature when it comes to the fibrils is not completely consistent; elementary fibrils and the term microfibrils are sometimes used synonymously, while some considered microfibrils as bundles of elementary fibrils, although of varying sizes. This confusion may be due to the measuring techniques used having insufficient resolution or due to artefacts from the sample preparations, causing difficulties in distinguishing between elementary fibrils and fibril aggregates. Additionally, the distinction between fibril and aggregate is not necessarily a representative model for all cellulose sources, adding to the confusion.
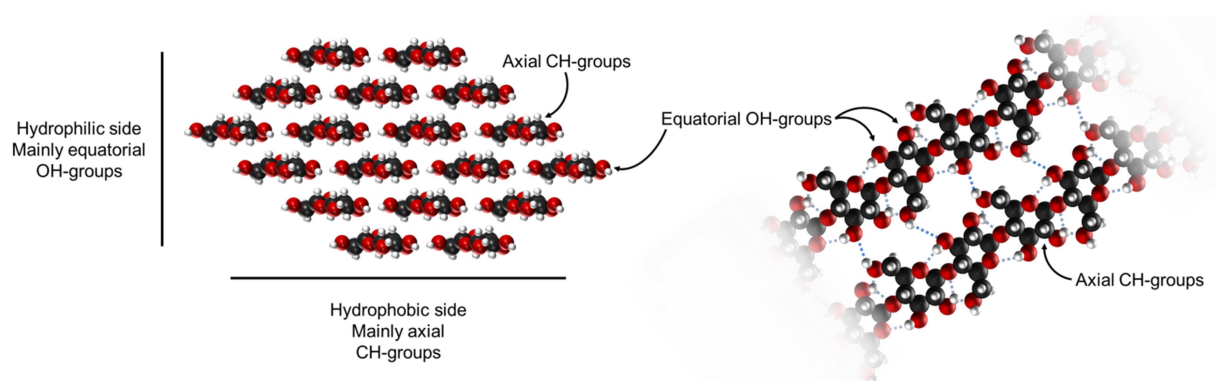

Figure 2.3. To the right; a cross section of an 18-chain cellulose fibril displaying the more hydrophilic and hydrophobic sides of the fibril caused by the dominant bond types in the axial and equatorial positions. To the left; the hydrogen bonding pattern in I$_\beta$ cellulose with the equatorial C2 and C3 OH-groups and the axial C-H bonds indicated.

Current discussions about the structure of cellulose fibrils are often concerning the shape and size, as well as how the non-ordered domains are distributed in the fibrils. The prevailing idea has for a long time been a straight, untwisted fibril. However, new evidence suggests a right-handed twist of the fibril core, a model which is gaining popularity in the research community (Haigler and Roberts, 2019, Conley et al., 2016, Revol and Marchessault, 1993, Revol et al., 1992).

Cellulose has several different crystal structures (O'Sullivan, 1997), where cellulose I and II are the most common polymorphs. Cellulose I, native cellulose, was found to be comprised of two different polymorphs; I$_\alpha$ and I$_\beta$, where I$_\beta$ is the dominant in wood and plant cellulose and I$_\alpha$ is the dominant in bacterial cellulose (O'Sullivan, 1997). Cellulose II is the thermodynamically most favoured structure, while the native cellulose I is a metastable structure occurring at a local energy minimum. Subjecting cellulose to various chemical and thermal treatments results in the formation of different polymorphs, where cellulose II is produced by precipitation of dissolved cellulose or by mercerisation of cellulose I. The surface of the fibril is often considered to be paracrystalline, as the surface

chains will be slightly askew compared to the bulk lattice, due to the desire to reduce surface energy, as well as having to twist more compared to the core chains.

A molecule such as cellulose with a high capacity for hydrogen bonding would at first glance be expected to be soluble in water. That is however not the case, nor is cellulose soluble in typical organic solvents. There are in fact very few solvents capable of dissolving cellulose. This recalcitrance is attributed to the strong intermolecular bonding, mainly the van der Waals forces and hydrophobic interactions between the C-H groups in the skeleton rings, together with entropic and enthalpy effects linked to the conformational rigidity and the molecular weight of the polymer (Medronho et al., 2012, Glasser et al., 2012). As cellulose has both strong hydrogen bonding and hydrophobic interactions, solvent systems that can break both types of interactions are required. Amphiphilic solvents, such as some ionic liquids as well as ionising solvents such as cold alkali have been found to dissolve cellulose, although complete molecular dissolution is rarely obtained (Glasser et al., 2012). The NMMO process is a commercial ionic liquid-based process used for the production of Lyocell fibres (Reddy and Yang, 2015) as is the newly invented Ioncell process (Sixta et al., 2015).

2.1.3 Morphological structure

Both the supramolecular, and even more so, the morphological structure, varies greatly with origin, e.g. bacterial cellulose is nearly pure while cellulose found in wood and plants is part of a complex, three-dimensional matrix mainly composed of lignin and other polysaccharides such as hemicelluloses and pectins as well as proteins. The cellulose structure is determined in the biosynthesis, a complex multistep process that controls the shape, size, crystallinity and morphology of the cellulose (Moon et al., 2011). Wood mainly consists of matured, dead cells, usually referred to as fibres. The wood cell is comprised of several layers (Sjöström, 1993), with the primary cell wall being the outermost layer, where the cellulose fibril aggregates are more or less randomly ordered. The secondary cell wall contains three sub-layers; S1, S2 and S3, and constitutes the bulk of the cell wall with highly aligned fibril aggregates. The fibres are held together by the pectin and lignin rich middle lamella. Exactly how the different cell wall constituents are organised with in the cell wall, and the nature of their interactions is still researched to this day.

2.2 Nanocellulose

Materials with one or more dimension in the nanometer range can exhibit new, unexpected properties compared to their associated bulk material. As the dimensions get smaller, the surface to volume ratio becomes larger and chemical and physical surface effects, such as interactions with the surface, becomes more pronounced. Maybe more

importantly, subtle features that affect self-assembly and organization becomes important (Kumar and Kumbhat, 2016). Cellulosic nanomaterials can be obtained by a top-down approach by utilising the hierarchical structure of cellulose. There are several different types of nanocelluloses with different morphological, chemical and biological properties, depending on both source and isolation method (Moon et al., 2011). In this thesis only cellulose nanocrystals (CNCs) will be discussed further in depth.

2.2.1 Cellulose Nanocrystals

CNCs[1] are highly crystalline cellulose nanoparticles with a high aspect ratio, typically 100-200 nm in length and 3-5 nm in width when produced from wood (Habibi et al., 2010, Beck-Candanedo et al., 2005). The nanocrystals are isolated by liberating crystalline domains by acid-catalysed hydrolysis, utilising the difference in reactivity between the ordered and non-ordered domains, causing the more accessible non-ordered domains to be hydrolysed at a faster rate than the denser, ordered domains. This difference in reactivity was reported by Nickerson and Habrle (1947) who observed a rapid initial drop of the DP, followed by a slower degradation where the DP almost ceased to decrease, an effect called the levelling off degree of polymerisation (LODP). A few years later, Bengt Rånby (1949) described how he obtained colloidal cellulose suspensions, what we today would call CNCs, after subjecting cellulose fibres to concentrated sulphuric acid. Sulphuric acid is still the most commonly used acid for producing CNCs, although several acids have been investigated, such as other mineral acids like hydrochloric acid (Araki et al., 1999, Yu et al., 2013), hydrobromic acid (Sadeghifar et al., 2011) and phosphoric acid (Camarero Espinosa et al., 2013) and organic acids like acetic acid (Braun and Dorgan, 2009), butyric acid (Braun and Dorgan, 2009), maleic acid (Filson and Dawson-Andoh, 2009) and oxalic acid (Li et al., 2017). The detailed mechanism for the heterogeneous acid-catalysed hydrolysis of cellulose is still not fully comprehended, but in general it transpires through cleavage of the glycosidic bond by addition of a water molecule, involving a hydrolytic attack catalysed by acidic protons (Fan et al., 1987), as shown in the schematic in Figure 2.4. Although the acidic hydrogen is the active species in the chain scissioning of the glycosidic bond, the counter ion has a significant impact on the reaction conditions, due to swelling (Fan et al., 1987).

A consequence of the sulphuric acid hydrolysis is that a small amount of the hydroxyl groups on the surface will undergo an esterification to form sulphate half esters, illustrated in Figure 2.4, which provides colloidal stability to the particles above their pKa (approx. 2.5) (ISO 21400:2018). Other acids can also impart a characteristic surface charge, although hydrochloric acid and hydrobromic acid does not, or to a very low degree,

---

[1] Sometimes referred to as nanocrystalline cellulose, cellulose whiskers, cellulose nanowhiskers or colloidal cellulose in literature. Cellulose nanocrystal is the agreed upon terminology according to ISO/TS 20477:2017
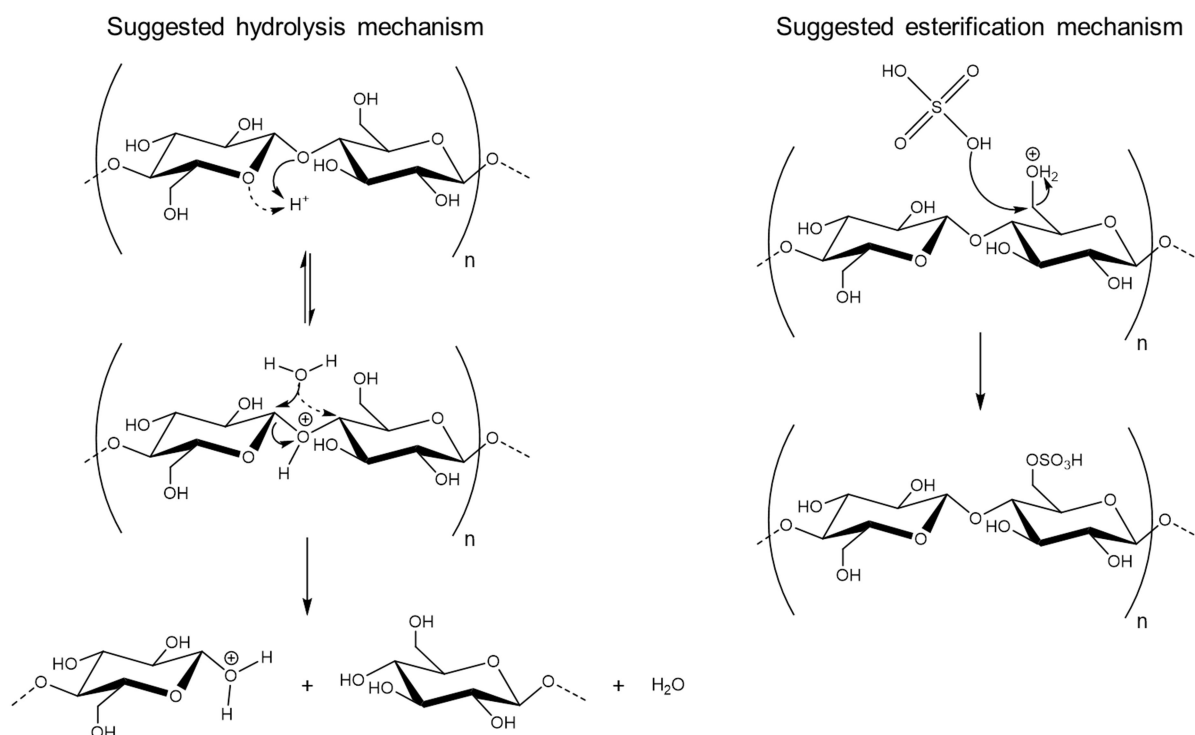
Figure 2.4. Suggested mechanism of acid hydrolysis of cellulose and the simultaneous sulphate surface esterification. Protonation of the bridging oxygen is the more probable path due to the strong hydrogen bond between OH at the C3 position and the ring oxygen. The degradation reaction proceeds through cleavage of the formed hemiacetal, presumable on the anomeric carbon as it has two electron withdrawing oxygens. The esterification is likely a nucleophilic acyl substitution reaction at the more easily accessed primary alcohol at C6.

introduce any charges, resulting in lower colloidal stability (Sadeghifar et al., 2011, Habibi, 2014). The surface charge in conjunction with the twisted core of the fibrils is believed to be responsible for the chiral nematic liquid crystalline phase exhibited by CNCs at higher concentrations (Araki and Kuga, 2001). A disadvantage with the sulphate half-esters is that they induce an acid-catalysed dehydration reaction that decreases the thermal stability of the CNCs significantly (Roman and Winter, 2004, Wang et al., 2007). It is, however, possible to inhibit the reaction by ion exchange to the neutral sodium form (Wang et al., 2007). Sulphated CNCs can also undergo a self-catalysed desulphation, both in aqueous solution and when dried (Beck and Bouchard, 2014). This process is accelerated by elevated temperatures, although still occurs at room temperature, however at a slower rate. The desulphation can be substantially slowed down or inhibited by cool storage or neutralisation (Beck and Bouchard, 2014).

The size and cross sections as well as polydispersity of CNCs will vary due to the intrinsic differences in morphology of samples, owing to origin and isolation method. CNCs produced from wood are generally produced from high purity cellulose grades, produced by Kraft or sulphite pulping of hardwoods or softwoods (Beck-Candanedo et al., 2005, Revol et al., 1992, Orts et al., 2005), but have for research purposes also been isolated from

a great variety of sources, including microcrystalline cellulose (MCC) (Strømme et al., 2002, Bondeson et al., 2006, Elazzouzi-Hafraoui et al., 2008), cotton (Dong et al., 1996, Heux et al., 2000, Orts et al., 2005, Revol et al., 1994, Elazzouzi-Hafraoui et al., 2008), bast fibres (Garcia de Rodriguez et al., 2006, Siqueira et al., 2009, Habibi and Dufresne, 2008, Luzi et al., 2014, Cao et al., 2007, Csiszár and Nagy, 2017), and assorted agricultural residues (El-Sakhawy and Hassan, 2007, Lu and Hsieh, 2012, Zhang et al., 2020, Börjesson, 2018, Smyth et al., 2017, Melikoğlu et al., 2019, Jiang and Hsieh, 2015, Coelho et al., 2018, Dai et al., 2018), as well as from algae (Strømme et al., 2002, Revol, 1982), bacteria (Orts et al., 2005, Grunert and Winter, 2002, Roman and Winter, 2004) and animals (tunicate) (Elazzouzi-Hafraoui et al., 2008, Chazeau et al., 1999, Azizi Samir et al., 2004, Sugiyama et al., 1992, Heux et al., 2000). During the pulping process, cellulose will undergo degradation reactions which will decrease the DP. In addition to chemical reactions that occur during the cooking, physical changes of the material can also take place, both during the cooking, but also during the subsequent drying, which will impact the properties and reactivity of the isolated cellulose. Hornification is a term used to describe the phenomena where the cellulose structure partially collapses, resulting in stiffer fibres (Hubbe et al., 2007). Studies have showed that both during the cooking as well as drying stages of the pulping process, there is an increase in the lateral fibril aggregation dimension, suggesting the occurrence of co-crystallisation between fibril aggregates (Hult et al., 2001, Idström et al., 2013, Newman, 2004). The irreversible aggregation of fibrils appears to introduce tension within the fibrils resulting in an increase in the susceptibility to acid hydrolysis in the non-ordered regions (Kontturi and Vuorinen, 2009). Additionally, Atalla et al. (2017) argues that native celluloses are highly hydrated with an even twist along the fibril, that upon subjection to elevated temperatures change the distribution of the twist from an even distribution to instead occur within a shorter distance while maintaining the overall periodicity, thus generating regions with higher stress which are more susceptible to acid attacks. Accordingly, in addition to key parameters such as temperature, agitation, hydrolysis time and acid-to-cellulose ratio, the isolation method and additional treatments the material may have been subjected to also affects the processing parameters. It should be noted that the more treatments the material has been subjected to and the smaller the isolated structure is, the less significant the origin of the material becomes.

The size and shape of CNCs have a significant impact on their rheological behaviour, especially the percolation threshold, i.e. the point where the particles are concentrated enough to form a continuous network, and the gelation point (Salas et al., 2014). CNCs display a shear thinning behaviour and both viscosity and moduli increase rapidly with concentration, until the percolation threshold is reached, followed by a less pronounced

concentration dependence at high concentrations. The shear thinning is attributed to flow-induced alignment of the CNCs (Moon et al., 2011).

The excellent mechanical properties of CNCs along with their high aspect ratio and large surface area have generated a lot of interest in composite applications. Although the current knowledge of the intrinsic mechanical properties of CNCs is insufficient due to limitations of the current characterisation techniques, indirect measurements suggests the tensile strength to be in the range of 0.3-22 GPa and the axial modulus between 58 and 180 GPa (Lee et al., 2014). In order to achieve good reinforcing ability, the particle concentration should be above the percolation, in order to have continuous contact between the CNCs (Dufresne, 2017). Consequently, the anisotropy and distribution of the CNCs in the matrix are of great importance. The crystallites can also act as nucleation points, thus increasing the matrix crystallinity and thereby affecting the mechanical properties of the composite. Another crucial part of the reinforcing ability is to transfer the stress from the matrix to the stiff CNC which requires a good interphase.

The mechanical, rheological and optical properties as well as the renewable origin and abundant raw material of CNCs has generated a lot of research interest and led to a wide variety of suggested applications including both high-end niche products and high-volume bulk products, mainly within materials science and life science, such as composite materials, paperboard and packaging, food additive, biomedical and medical products, hygiene products, barrier applications, antimicrobial films, and electronics. There are a few commercial pilot plants producing CNCs, most located in North America, such as CelluForce, USDA Forest Products Laboratory and Alberta Innovates Technology Futures, producing up to 1 tonne CNCs per day (CelluForce, 2016). Production is also starting up in Europe with Melodea that opened up a pilot plant in Sweden in 2016 (Processum, 2015).

Current research indicates that CNCs exhibit no oral or dermal toxicity, although there are indications of pulmonary toxicity as well as somewhat conflicting results regarding the cytotoxicity (Roman, 2015). The results are based on just a few studies, which use different cell lines as well as CNCs from different sources and processes, hence the influence of surface chemistry and morphology as well as impurities from the processing may have had an influence on the interpretation of the results. Harper et. al. (Harper et al., 2016) found no significant changes in toxicity when CNCs with anionic, cationic and neutral surface characteristics where evaluated.

2.3 Chemical Modification of Cellulose Nanocrystals

The list of potential applications for CNCs is long, and for certain applications some of the intrinsic properties of nanocellulose can pose a challenge, such as high moisture uptake

and poor dispersibility in non-polar solvents or polymer matrices. Changing the surface chemistry can address this while still maintaining the desired properties of the CNCs. Both covalent and non-covalent surface modifications techniques can be applied, with different advantages and drawbacks depending on the specific application. The typical chemical approach usually involves derivatisation of the surface hydroxyl groups or grafting. The two techniques are often combined as it can be necessary to derivatise in order to create a handle for further reactions. This can be done either by a grafting onto approach, i.e. attaching a large molecule to the handle, or by a grafting from approach, i.e. the handle is used as an initiator for polymerisation. Modifications are generally performed after isolation, although as discussed in the previous section, the hydrolysis itself generally induces some surface groups. The obtained properties of the CNCs will be governed by the nature of the substituents, the quantity and their distribution on the crystallites.

Many of the chemical modification routes originate in classical cellulose chemistry, and rely on the free hydroxyl groups, such as esterification, etherification, oxidation and silylation, using reagents prone to react with alcohols such as isocyanates, epoxides, acid halides, acid anhydrides (Eyley and Thielemans, 2014, Moon et al., 2011, Klemm et al., 2011). The reaction conditions often require adjusting, as the reactions have historically been applied either to merely functionalise the fibre surface or, on the contrary, to produce cellulose derivatives, i.e. derivatising to the point of solubilising the cellulose chains and further. Too harsh conditions can cause swelling, which alters the particles core structure and can cause the surface chains to solubilise, essentially peeling the crystals layer by layer.

The AGUs constituting the cellulose backbone each have three free hydroxyl groups with somewhat different reactivity. The two secondary alcohols at the C2 and C3 positions, should according to fundamental organic chemistry be more reactive than the primary alcohol at the C6 position, see Figure 2.2. However, it is not just the nature of the covalent bonds that determines the reactivity, the hydrogen bonding patterns, and the supramolecular structure also play a very important role. The accessibility for the reagent is affected by both the inter- and intramolecular hydrogen bonding as well as by steric hindrance caused by the dense packing in the crystal structure. As a result, the C6 hydroxyl group is generally the most reactive and the hydroxyl at the C3 position has the lowest reactivity (Eyley and Thielemans, 2014). Common description of organic chemical reactions usually neglects solvent interactions and supramolecular aggregation of the molecules involved in the reaction, effects that are highly relevant in chemical modification of cellulose in water.

Sulphate half-esters, introduced during heterogeneous reactions with cellulose, have been shown to react mainly at the C6 position (Chen et al., 2013). Although the sulphate groups are important for the colloidal and thermal stability, they are rarely considered during surface modification of CNCs. Within organic chemistry, they are generally seen as good leaving groups, and are considered a soft nucleophile, and are thus expected to react with soft electrophiles.

Granted both amount and distribution of substituents play important parts in the properties of the CNCs, it can be very difficult to determine these, especially when the DS is low as is generally the case with surface modifications. The most common techniques for direct, non-derivatising, measurements are solid state techniques such as Fourier transfer infrared spectroscopy, elemental analysis, solid state magic angle spinning NMR techniques and X-ray photoelectron spectroscopy (King et al., 2018). The main challenges with the current techniques are that they are generally semi quantitative, have insufficient resolution and do not differentiate between bulk and surface, nor between covalent bonds and adsorbed moieties. Because of this, a combination of characterisation techniques is usually required to convincingly show that a reaction has occurred. Recently, King et al. (2018) developed a promising solution state NMR technique which allow for qualitative and quantitative characterisation of grafted CNCs with low DS, by dissolution in a combination of ionic liquids and NMR solvents.

For chemical modifications of CNCs intended for use in high-volume applications, such as composites, the scalability of the reaction is crucial. Nanocelluloses are usually produced as water suspensions, while many functionalisation reactions are carried out in various organic solvent systems. This can be problematic as solvent exchanges are time-consuming and the use of organic solvents should be avoided (Anastas and Eghbali, 2010). Thus, performing the modification reactions in water has huge advantages for the scalability. Chemical reactions in water have gained a lot of attention during the last 10 to 20 years and may become the preferred reaction solvent in the future (Li and Chen, 2006, Lindström, 2008).

3

MATERIALS AND METHODS

This chapter provides a brief description of the materials and methods used in this thesis. For detailed descriptions of the experimental procedures, please see the appended papers.

3.1 Materials

Microcrystalline cellulose (MCC) PH-101 (Fluka, Morris Plains, NJ) with an average particle size of 50 μm, was used as the starting material for the sulphuric acid hydrolysis of the CNCs used in Papers I-IV.

Commercial grade sulphuric acid hydrolysed CNCs (CelluForce, Canada), was used for the large-scale composites produced in Paper V. The CNC was obtained as a powder and was dispersed in deionized water to a 6-7 % dry content, using an IKA T25 digital Ultra Turrax at a rotational speed of 7400 rpm for 10 min.

In Paper I a linear low-density polyethylene (LLDPE), purchased from Sigma-Aldrich, was used a matrix. According to the supplier, the melting point was 100-125 °C, the density 0.918 g/cm³ and a melt flow rate of 1.0 g/10 min (ISO 1133).

In Paper III a poly(ethylene-acrylic acid) copolymer (EAA) provided by BIM Kemi AB, Sweden was used as the composite matrix. It was obtained as a 20 wt.-% dispersion at pH 9.7. According to the supplier, the acrylic acid content of the polymer was 15% (denoted EAA15), its melting point and density were 88 °C and 0.994 g/cm³, respectively, and the melt flow rate was 36 g/10 min (ISO 1133-1:2011).

In Paper V, two polymers matrices were used; a poly(ethylene-acrylic acid) copolymer containing 7 % acrylic acid (denoted EAA7) obtained from Dow Chemical Company, Sweden, and a low-density polyethylene (LDPE), obtained from Olefins and Polymers, Sweden. According to the supplier the EAA7 had a melting point of 88 °C, a density of

0.932 g/cm³ and a melt flow rate of 8 g/10 min (ISO 1133-1:2011) and the LDPE a melting point of 108 °C, a density of 0.92 g/cm³ and a melt flow rate of 8 g/10 min (ISO 1133-1:2011).

Chemicals were used as purchased from Sigma-Aldrich, Fluka or Alfa Aesar without further purification. NMR solvents were purchased from Teknolab sorbent or Sigma-Aldrich. Spectra/Por 2 Dialysis Membrane (MWCO 12–14 kDa) tubing was purchased from Spectrum Labs (Los Angeles, CA). The mixed bed ion exchange resin Dowex® Marathon™ MR-3 hydrogen and hydroxide form (20-50 mesh particle size) was purchased from Sigma-Aldrich. The strong acid cation exchange resin Dowex® Marathon™ C hydrogen form (23-27 mesh particle size) was purchased from Sigma-Aldrich and rinsed with ethanol until the filtrate was clear and then air-dried prior to use.

3.2 Experimental

3.2.1 Preparation of Cellulose Nanocrystals
Cellulose Nanocrystals
CNCs were prepared according to the procedure described by Hasani et al. (2008), with adjustments based on the raw material. Aqueous CNC suspensions were prepared from MCC by a sulphuric acid hydrolysis using 64 w.-% sulphuric acid and continuously stirred at 45 °C for 2 h. The reaction was quenched by dilution in deionized water, followed by centrifugation and subsequent dialysis against deionized water for batches on an 80 g scale, whereas batches on a half kilogram scale where immediately dialysed against deionized water. The CNC particles were dispersed by sonication until a colloidal dispersion was achieved.

Uncharged Cellulose Nanocrystals
For Paper I and IV, uncharged CNCs were prepared through solvolytic desulphation. An aqueous CNC suspension was neutralized with pyridine and subsequently lyophilized. The freeze-dried CNCs were dispersed in DMSO by sonication. Methanol was then added, and the mixture was heated at 80 °C for 2 h with constant stirring in a heating bath. The reaction was stopped by cooling in an ice bath. The mixture was centrifuged, the supernatant was removed, and the precipitate was re-dispersed in deionized water and re-centrifuged several times and finally put on dialysis against deionized water.

Low Charge Cellulose Nanocrystals
For Paper I and IV, CNCs with a low amount of sulphate half esters were prepared by either hydrochloric acid-catalysed desulphation (Paper I and IV) or self-catalysed desulphation (Paper IV) of CNCs. For the hydrochloric acid-catalysed desulphation an aqueous CNC suspension was heated to 80 °C followed by an addition of hydrochloric acid

and was kept at 80 °C with constant stirring for 2.5 h. The reaction was stopped by cooling in an ice bath, followed by centrifugation. The supernatant was removed, and the precipitate was dialysed against deionized water. For the self-catalysed desulphation, an aqueous CNC suspension was heated to 90 °C for 24 h and was then dialysed against deionized water.

High Charge Cellulose Nanocrystals

For Paper I CNCs with a higher amount of sulphate half esters as compared to the unmodified CNCs were prepared according to the procedure described by Araki et al. (1999), with minor modifications. Sulphuric acid was added to an aqueous CNC suspension and heated for 2 h at 40 °C. The reaction was quenched by dilution in deionized water, immediately followed by centrifugation. The supernatant was removed, and the precipitate was re-dispersed in deionized water and re-centrifuged. The precipitate was then dialysed against deionized water.

3.2.2 Synthesis of Reagents

Three different types of reagents have been used for the dialkylamine functionalisation of CNCs; *N,N*-dialkyl-3-hydroxy-azetidinium and *N,N*-dialkyl-3-methoxy-azetidinium chlorides, 1-chloro-3-dialkylaminopropan-2-ol and 4-((dialkylamino)methyl)-1,3-dioxolan-2-one, referred to in this thesis as azetidinium salts, dialkyl alkylchloride and dialkyl cyclocarbonate, respectively.

Synthesis of Azetidinium Salts

We were unable to find any general reaction conditions that yielded azetidinium salts regardless of amine, instead suitable solvents and temperatures had to be evaluated for each dialkylamine. Additionally, the azetidinium salt synthesis proved to have low reproducibility. For Paper I-III the synthesis of the azetidinium salts was based on procedures described by Chattopadhyay et al. (2012) where equimolar amounts of epichlorohydrin was added to a secondary amine dissolved in a solvent and placed in an ice bath, solvent varying depending on which secondary amine was used. The reaction was stirred at room temperature for 2-4 days and then purified by washing with diethyl ether and removal of the solvent by evaporation under reduced pressure. This procedure showed to give complex mixture of products for some dialkylamines and for Paper IV the azetidinium salt synthesis was changed into a two-step process, inspired by Krishna Reddy et al. (2011) and Parzuchowski et al. (2018), using water as the solvent. In the first step equimolar amounts of epichlorohydrin was added to a secondary amine in deionised water and the two-phase mixture was stirred vigorously at room temperature for approx. 24 h. The mixture was then heated at 90 °C for 10 h in the sub-sequent step. The final product was water soluble.

Methylation of Azetidinium salts

In Paper I and II methylation of the azetidinium salts was done in order to increase the hydrophobicity. The *N,N*-dialkyl-3-methoxyazetidinium salts were prepared by adding potassium-*tert*-butoxide (1.1 mol equiv.) to the *N,N*-disubstituted azetidinium salt dissolved in dichloromethane. After 2 min, methyl-*p*-toluenesulphonic acid (1.2 mol equiv.) was added and the reaction was stirred for 1 h at room temperature. A small amount of water was added to quench the reaction. The mixture was concentrated under reduced pressure to yield the crude product. The product was triturated with acetonitrile, filtered, and then concentrated once again under reduced pressure.

Synthesis of Dialkyl Cyclocarbonate

The synthesis of the dialkyl cyclocarbonate 4-((diallylamino)methyl)-1,3-dioxolan-2-one outlined in Paper II was based on a two-step procedure by Krishna Reddy et al. (2011) and Parzuchowski et al. (2018). In the first step equimolar amounts of epichlorohydrin was added to a secondary amine in isopropanol and was stirred at room temperature for 24 h to form dialkyl alkylchloride. For the second step the solvent was removed by evaporation under reduced pressure, unless acetonitrile was used as solvent in step 2 in which case it was not removed. Acetonitrile was added to the crude product, along with an excess of sodium bicarbonate (1.5-3.5 mol equiv.) and the mixture was then heated at 80 °C and continuously stirred for an additional 10 h. The inorganic salts were removed by filtration and the solvent was removed by evaporation under reduced pressure.

Synthesis of Dialkyl Alkylchloride

1-chloro-3-dialkylaminopropan-2-ol was obtained from adding epichlorohydrin to a dialkylamine in isopropanol (other solvent including water, methanol, ethanol, isopropanol, acetonitrile, ethyl acetate, tetrahydrofuran, triethylamine, toluene, n-heptane, hexane and cyclohexane also yielded the dialkyl alkylchloride depending on amine) for 24 h. The 1-chloro-3-dialkylaminopropan-2-ol was used for synthesis of azetidinium salts and dialkyl cyclocarbonate as well as for conjugation with CNCs.

Synthesis of Secondary Amines

Asymmetrical secondary amines that were not commercially available were synthesised by reductive amination. An aldehyde (nonanal or undecanal) was added to an amine (propylamine, methylamine or benzylamine) dissolved in THF and stirred for 3 h under N_2-flow. $NaBH_4$ was added along with additional THF. After 24 h aqueous sodium bicarbonate (1 M) was added to stop the reaction. The product was extracted with DCM and the solvent was removed by evaporation under reduced pressure.

3.2.3 Conjugation Reactions

The dialkylamine functionalisation of CNCs through grafting onto the surface sulphate half-ester groups has been evolved and improved as part of the work in this thesis.

Initially, the conjugation was performed in a DMSO-toluene system (Paper I and II) based on procedure outlined by Chattopadhyay et al. (2012), where the CNCs were solvent exchanged from an aqueous suspension to DMSO through an azeotrope with toluene. An excess of *N,N*-dialkylazetidinium salts (3 mol equiv. per AGU) was added to the CNCs and then reacted for 22 h at 90 °C. The reaction mixture subsequently washed with acetonitrile, ethanol and deionised water through repeated centrifugation steps.

In the work leading up to Paper III it was found that the conjugation worked well in water, so for the conjugations performed in Paper III, the solvent exchange step was omitted. The excess of azetidinium salt was reduced to 0.1 mol equiv. per AGU.

As the azetidinium salt synthesis proved to have issues with reproducibility, as well as the salts being difficult to handle due to their highly hygroscopic and viscous nature, an alternative reagent was sought after. The dialkyl cyclocarbonate was found to react under the same conditions as had been used for the azetidinium salts; in aqueous CNC suspensions heated to 90 °C for 24 h. For Paper IV, the conjugation with the dialkyl cyclocarbonate was also done at 90 °C, but was found to have finished prior to 2 h. The conjugation was also performed with the dialkyl alkylchloride at 90 °C for 2 h, as well as in alkaline conditions at 50 °C for 6 hours. The conjugation reactions in Paper IV were subjected to either dialysis, ion exchanged with Dowex® Marathon™ C strong acid cation exchange resin or both.

Control reactions as reference, with only aqueous CNC suspensions and without any reagent, were prepared by heating at 30, 50 and 70 °C and taking out small aliquots at 5, 15, 30, 120 min, 4 h and 24 h, to study the impact of the water on the sulphate content.

3.2.4 Model Reactions

As the amount of available surface sulphate half-ester groups per CNC is very low, it is very difficult to directly characterise the link between the reagent and the CNCs. Therefore, model reactions were performed in Paper I and II. The reaction conditions were the same as for the initial conjugation; *p*-toluenesulphonic acid or 2-methyl-2-propene-1-sulphonic acid were mixed with equimolar amounts of *N,N*-dialkylazetidinium salt in a DMSO-toluene mixture (90:10 ratio). The reaction was heated at 90 °C for 22-24 h with constant stirring. For the reaction with *p*-toluenesulphonic acid, the product was obtained by removing the solvent via bulb-to-bulb distillation, while for the reaction with 2-methyl-2-propene-1-sulphonic acid the product precipitated once the reaction mixture cooled to room temperature and was subsequently washed with diethyl ether and dried at room temperature.

3.3 Manufacturing of Composites

CNC composites were produced for Papers I, III and V by different methods. In Paper I, composites were prepared on a small scale by hot-melt extrusion of a wet-mixed CNC coated LLDPE powder using a mini twin extruder. In Paper III, CNCs were incorporated into the polymer matrix by mixing aqueous dispersions of CNC with an EAA15 dispersion which was then air dried and compression-moulded. Reference samples to enable comparisons between Paper III and V were prepared with the same technique as the composites in Paper III but with the materials from Paper V. The large-scale composites prepared for Paper V were produced by water-assisted melt processing on a 3 kg scale, using a twin-screw extruder, followed by injection moulding.

3.4 Characterisation

3.4.1 Molecular characterisation

Molecular characterisation provides information about the chemical or molecular nature of a sample, such as the chemical structures, the composition or the surface charge.

Fourier Transform Infrared Spectroscopy

Fourier Transform Infrared Spectroscopy (FTIR) provides information about functional groups in a sample. It utilises the differences in vibrational energy of different bonds, which can be measured by the transmission of infrared light through a sample. Both solid and liquid samples can be analysed. The potassium bromide (KBr) pellet technique and the attenuated total reflectance (ATR) technique are commonly used. The ATR method is a surface technique and while the KBr pellet method provides information about the bulk of the sample.

KBr-FTIR was recorded on a Perkin Elmer Spectrum One spectrometer. Approximately 3 mg of freeze-dried sample was mixed with 300 mg potassium bromide and pressed into a pellet. The spectra were recorded between 4000 and 400 cm^{-1} and 32 scans were collected. The resolution was 4 cm^{-1} and the interval scanning 1 cm^{-1}.

ATR-FTIR was recorded on a Perkin Elmer Frontier FT-IR Spectrometer (Waltham, MA, USA) equipped with a diamond GladiATR attenuated total reflectance (ATR) attachment from Pike Technologies. The samples were placed directly on the ATR-crystal without further preparation. The spectra were recorded between 4000 and 400 cm^{-1} and 32 were scans collected. The resolution was 2 cm^{-1} and the interval scanning 0.5 cm^{-1}.

In-situ ATR-FTIR was recorded on the dialkylamine reagents and used for monitoring reactions, with a ReactIR 700 with a gold sealed diamond (DiComp) probe (Mettler-

Toledo). The spectra were recorded between 3000 and 650 cm^{-1} with 8 cm^{-1} resolution. For the *in-situ* measurements of the syntheses 159 scans were collected with 1-minute intervals, for the dissolution measurements 256 scans were collected with 1-hour intervals, and for the reference spectra of the reagents 128 were scans collected.

Nuclear Magnetic Resonance Spectroscopy

Nuclear magnetic resonance (NMR) spectroscopy provides information about the chemical environment of atoms, and thereby the structure of a compound. It utilises the fact that certain nuclei have a magnetic moment and can be excited by radiofrequency electromagnetic radiation at specific wavelengths, determined by the local electronic environment, while placed in a magnetic field. NMR can be performed either in solution state or in solid state.

Solution NMR was used to verify product outcome. Spectra were recorded at room temperature on a Varian MR-400 (Varian, Palo Alto, CA, USA) operating at 399.95 MHz for proton detection and 100.58 MHz for carbon detection.

Solid state magic angle spinning (MAS) NMR analyses were done on CNC samples in Paper I and II, and were performed on a 14.1 T Agilent Inova (Agilent, Palo Alto, CA) with a ^{13}C and ^{1}H Larmor frequency of 150.9 and 600.1 MHz, equipped with a 3.2 mm double-resonance MAS probe. ^{13}C cross polarization (CP) and ^{13}C insensitive nuclei enhanced polarization transfer (INEPT) were recorded at a MAS rate of 9 kHz using a ^{13}C spectral width of 30.48 kHz, a repetition delay of 3.3 s, 8192 signal accumulations, and the decoupling scheme proton small-phase incremental alternation. The CP time was set to 1 ms, and the delays for INEPT were set to 3.6 and 2.2 ms. The chemical shift was referenced to adamantine.

Raman Spectroscopy

Raman Spectroscopy provides information about functional groups in a sample, similar to FTIR. It measures the low-probability, inelastic scattering of photons, utilising differences in vibrational and rotational energy of the bonds.

Raman measurements were performed using a Bruker MultiRAM Fourier-Transform Raman spectrometer (Bruker, Billerica, MA) equipped with a Nd:YAG laser (1064 nm) and a liquid nitrogen-cooled Ge-diode detector. The resolution was 2 cm^{-1} (full width at half maximum), and the Blackman–Harris three-term window function was used for apodization. Experiments were performed at room temperature with an exposure time of 2 h (1000 scans) and a laser power of 400 mW.

ζ-potential

ζ-potential is a measure of the electric potential of the double layer of colloidal particles and is a useful tool to predict colloidal stability of a suspension as well as an indicator of the surface charge. The technique uses electrophoresis to cause the particles to migrate, while measuring the particle velocity by a laser Doppler anemometer.

ζ-potential was measured on a Zetasizer Nano ZS (Malvern Instruments, UK). The Smoluchowski approximation was used for converting the electrophoretic mobility to ζ-potential. The light source was a 50 mW diode-pumped solid-state laser emitting light at 532 nm. All measurements were carried out at 25 °C using DTS1070 disposable folded capillary cells. The samples were stabilized for 120 s inside the device and five measurements per sample were recorded with a minimum of 10 runs per measurement and three replicates. Samples were prepared by dilution to 0.05 wt.-% dry content, adjusting of the pH to 3.5 followed by ion exchange (Dowex® Marathon™ MR-3 hydrogen and hydroxide form) overnight and subsequent removal of resin beads by filtration.

Conductometric titration

Conductometric titration can be used to determine the total surface charge content of particles. Measuring the change in conductivity as a function of the added volume of a strong base provides information about the amount of strong and weak acidic groups as well as weak basic groups on the nanoparticle surface.

Typically, a sample volume of 75-100 ml was prepared, containing around 0.1 g CNCs (dry weight). The samples were subjected to different pre-treatments to converted any charged species into hydrogen form; The suspension was either put on extensive dialysis until the conductivity of the effluent remained below 5 μS prior to titration or ion exchanged by either strong acid cationic ion exchange resin (Dowex® Marathon™ C hydrogen form) or pH-adjusting the suspension to below 3.5 with 0.01 M HCl. The titrations were either done manually by adding 0.1-1 mL aliquots 10 mM NaOH in 30-60 s intervals and logging the conductivity (Eutech Instruments) until sufficiently many data points were collected after the equivalence point, or by using an automated titrator (Mettler-Toledo) were 0.1 mL aliquots 10 mM standardised[2] NaOH was added in 50-70 steps with 30-60 s intervals.

The surface charge was calculated graphically from the intersect points determined by plotting the conductivity against the volume of added NaOH solution, as shown in Figure 3.1. A more detailed description is provided in Appendix A1.

---

[2] Standardised using potassium hydrogen phthalate (KHP)
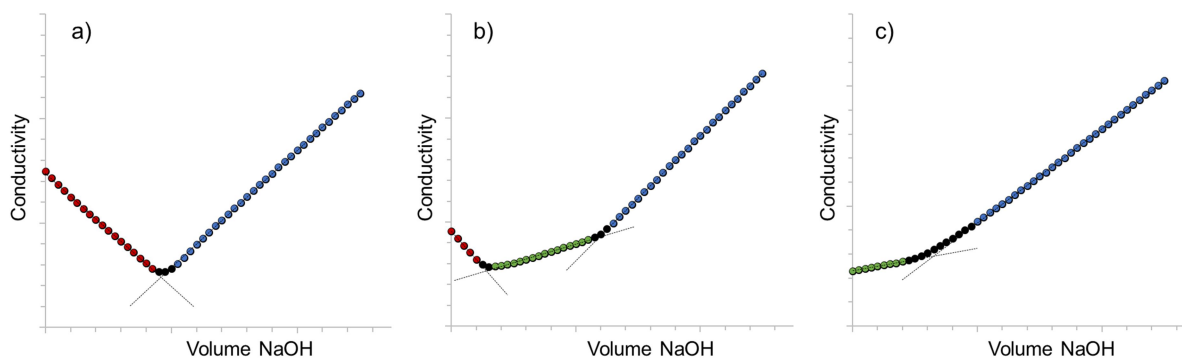
Figure 3.1. Typical titration curves for samples containing a) strong acid surface groups, b) strong and weak acid or base surface groups and c) only weak acid or base groups.

Elemental analysis

Sulphur (%S) and nitrogen (%N) content was measured on CNC samples in Paper I with elemental analysis provided by the Mikroanalytisches Laboratorium, Kolbe, Germany.

3.4.2 Material characterisation

Material characterisation provides information about e.g. the thermal properties, physical appearance, flow properties and mechanical behaviour.

Thermal Properties

Thermal degradation processes and the thermal stability of a sample can be assessed by thermogravimetric analysis (TGA), which monitors the changes in the mass of a sample as a function of temperature. TGA was measured on CNC and composite samples in Paper I-V using a TGA/DSC 3+Star system (Mettler Toledo, Columbus, OH, USA). A 5 °C/min heating rate was used to heat approximately 10 mg sample from 25 °C to 350-550 °C under nitrogen atmosphere at a flow rate of 50 mL min^{-1}.

Another experiment was conducted to visually assess the thermal stability of the CNC composites in Paper III by observing colour changes with increasing temperature. Small pieces of CNC composite and pure matrix were placed at five different positions along a heat gradient on a Kopfler Bench (Wagner & Munz, Germany). Samples were positioned at 120, 130, 140, 150 and 160 °C for 8 minutes to determine at which temperature discoloration occurred and thus provide an indication for when the onset of thermal degradation.

Information about thermal transitions and crystallinity can be determined by differential Scanning Calorimetry (DSC), which measures the differences in energy required to heat a sample in comparison to a reference as a function of temperature. For Papers III and V, DSC was performed on a Perkin-Elmer DSC7. The endotherms were recorded in a nitrogen atmosphere, while the temperature was increased from either 25 or -20 to 150 °C at a scan rate of 10 °C/min. No second temperature scan was used.

The crystallinity (X_c) can be calculated according to:

$$X_c = \frac{\Delta H_c}{w_{matrix} \Delta H_o}$$

Where ΔH_c is the specific heat of fusion of the composite, w_{matrix} the weight fraction of matrix and ΔH_o the specific heat of fusion for 100% crystalline polyethylene, 277.1 J/g (Brandrup et al., 1999). The melting point (T_m) of the polymer matrix was taken as the peak value of the DSC endotherm.

Appearance

To attempt to quantify the perceived differences in appearance of the composites in Papers I and V, the colour was assessed using a Datacolor 600 spectrophotometer with a d/8° spherical measurement device and 9 mm diameter opening, and expressed in the 1976 CIELAB system (ISO/CIE 11664-4:2019) with coordinates L* (lightness), a* (red-green) and b* (yellow-blue). The lightness L* ranges from 0 (black) to 100 (white), -a* is green, +a* red, -b* is blue and +b* yellow. The gloss was measured with a Konica Minolta Uni Gloss 60Plus having an incidence angle of 60 ° at room temperature. A white printer paper was used as background and reference. The reported values were the average of three measurements at different positions on the sample.

Atomic Force Microscopy

Atomic force microscopy (AFM) is a microscopic technique that provides information about the surface topology on an Å scale as well as phase information. A cantilever scans across the surface, either in an oscillating movement above the sample surface (tapping mode), sensing the forces the sample imposes on it, or in constant contact with the sample (contact mode).

AFM measurements were conducted using a Digital Instruments Nanoscope IIIa equipped with a type G scanner (Digital Instruments Inc., Santa Barbara, CA). The measurements were done in tapping mode and in air using a Micro Masch silicon cantilever NSC 15. Samples for analysis were casted on mica plates from 9 ppm (wt/wt) solutions.

AFM measurements were also conducted using a Veeco Multimode Scanning Probe (Santa Barbara, USA) in tapping mode with the Nanoscope V software to obtain height and amplitude information of individual cellulosic elements. The measurements were performed on dilute suspensions (10^{-4} wt.-%) that were placed on a mica surface and allowed to dry at room temperature prior to analysis. The average values of the dimensions of the elements and their standard deviations were based on measurements of about 200 fibrils/particles.

Rheological Properties

Rheological measurements describe flow characteristics of fluids and solids and provide indications on e.g. processability and mechanical properties.

Rheological measurements on the aqueous CNC suspensions in Paper II were carries out on an Anton Paar MCR 702 rheometer (Graz, Austria) with a cone-plate configuration (cone diameter 50 mm and cone-plate angle 1.991°) at 25 °C and two different CNC concentrations. The steady-state shear viscosity was determined as a function of the applied shear rates, which were varied between 1 and 1000 s^{-1}, and the dynamic-mechanical shear properties, given by the storage modulus G' and the loss modulus G", were determined by a strain sweep at 1 Hz in which the G' and G" were measured as functions of the applied shear strain amplitude.

The same equipment was used for small-amplitude oscillatory shear tests (SAOS) on the extruded composites in Paper V, but using a parallel plate geometry (15 mm plate diameter) set-up. The measurements were performed at 170 °C as the thermal degradation of composites could be considered negligible at this temperature for the duration of the measurement. The disk-shaped samples, with a thickness of 1.5 mm, were gradually squeezed to a plate gap of 1 mm. The linear viscoelastic region was first assessed using a strain sweep from 1 to 100 % at a constant angular frequency of 1 s^{-1}. In addition, angular frequency sweeps were made in the range of 0.08 – 200 s^{-1} at strain amplitudes of 0.04 - 0.7 %.

The shear viscosity of the composite melts in Paper V was determined as a function of the shear rate using a capillary viscometer (Göttfert Rheograph 2002, Germany) at a melt temperature of 170 °C. Two cylindrical capillaries of different lengths (10 and 20 mm) but with the same diameter (1 mm) were used in order to make it possible to estimate the pressure entrance losses (Bagley correction of the applied pressure). A 500 bar (50 MPa) pressure transducer (Dynisco, USA) was used to record the pressure applied when the melt was pushed through the capillary at different speeds. The piston speed was varied between 0.05 and 2 mm/s, corresponding to shear rates of 58 - 2300 s^{-1}. The measured shear rates were subjected to a Rabinowitch-correction.

Mechanical properties

Mechanical properties of polymeric materials can be obtained by e.g. tensile testing and dynamic mechanical thermal analysis (DMTA), the former providing information about e.g. strength, stiffness, elasticity and stress at break and the latter on transitions, such as glass transition and crystalline transitions.

The tensile properties of the small-scale composites produced in Paper I were measured with an Instron 5565A (Instron, Norwood, MA) equipped with 5 kN load cell. The dog-

bone shapes were punched from hot-pressed nanocomposite films and were conditioned at 23 °C and 50% relative humidity prior to measurement. The measurements were done in atmosphere pressure and at ambient temperature. The gauge dimension was ~30 mm × 4.1 mm × 0.4 mm, the cross-head speed was 6 mm min⁻¹.

The tensile properties of the composites in Papers III and V were measured with a Zwick/Z2.5 tensile tester equipped with a 500 N (Paper III) or 2 kN (Paper V) load cell. The test bars had a gauge length of 40 mm, cut from compression-moulded (Paper III) or injection-moulded (Paper V) plaques, with the length oriented in the injection direction for the latter. The samples were conditioned at 25 °C and 55 % relative humidity prior to measurement. The measurements were done in atmosphere pressure at 25 ℃ with a strain rate of 6 mm min⁻¹.

The dynamic-mechanical properties of the composites in Papers III and V were measured using a Rheometrics RSA II. A pre-strain of 0.13-0.15% tensional strain was applied to the specimens and maintained during the measurement, while a sinusoidal deformation was superimposed at a temperature of 23 ℃. The measured loss and storage moduli of the materials were recorded.

4

DIALKYLAMINE FUNCTIONALISATION OF CNCS

Chemical modification of CNCs can be a useful tool to obtain new and unique properties. Typically, functionalisation is carried out on the abundant surface hydroxyl groups, but in this chapter a method that utilises the sulphate half-ester groups that decorate the CNC surface is presented and discussed.

4.1 Background

For various reasons chemical modification of CNCs is needed, e.g. to overcome compatibility issues in order to better utilise the excellent mechanical properties of CNCs, or to introduce active functional groups for tuning the properties and function of the CNC's, making them useful in a plethora of applications. Chemical modification of CNCs originates in the classical cellulose chemistry where the hydroxyl groups are the focus, such as esterification and etherification reactions (Eyley and Thielemans, 2014). However, already during the hydrolysis new functionalities are introduced which can influence the properties and reactivity of the CNCs. A small amount of sulphate half-esters forms on the surface of the crystals during the sulphuric acid hydrolysis, in the range of 80-400 µmol/g (Hamad and Hu, 2010). Although the sulphate half-esters are often taken into account with regards to the colloidal and thermal stability, they are rarely considered when further reacting CNCs. Sulphates are regarded as a good leaving group, and consequently overlooked as a functional group useful as a handle for chemical functionalization. However, alkylsulphates can be considered as weak nucleophiles and are known to react with alcohols under basic conditions forming dialkylsulphates, and it has been shown for biopolymer such as carrageenan that some of their sulphates react with hydroxyl groups under basic conditions.

4.1.1 Azetidinium salt

Chemical modification of the sulphate groups on CNCs is not a very explored area, but inspiration can be found by looking at reagents that work well with other functional groups with a reactivity similar to the sulphate group such as carboxylates, phosphates and phenols. A compound found to react with these types of soft nucleophiles is azetidinium salts (Börjesson and Westman, 2016, Higgins et al., 1994, Bakalarz-Jeziorna et al., 2001), which is also a component in the traditional pulp and paper wet strength agent PAE (Obokata and Isogai, 2007, Siqueira et al., 2015). Azetidinium salts are organic compounds containing a saturated heterocyclic four-membered ring where one of the ring atoms is a quaternized nitrogen. Due to the inherent four-atom ring strain they react readily even at mild conditions through a ring-opening reaction at the α-carbon to form a Y-shaped grafting, demonstrated in Figure 4.1. Azetidinium salts can be synthesised by reacting epichlorohydrin with equimolar amounts of a secondary amine or by reacting epichlorohydrin with a primary amine to form an azetidine which can then be alkylated to give a quaternized nitrogen center (Chattopadhyay et al., 2012, Ross et al., 1964). The use of various amines, with symmetrical and asymmetrical substituents, opens up possibilities to a plethora of functionalities, facilitating straightforward tailoring of the functionalities of the finished materials. The reaction pathway also has the potential to be scaled-up since epichlorohydrin is a commodity chemical and many dialkylamines are produced on tonne scale. When reacting epichlorohydrin with a secondary amine, two possible products may form, which apart from forming azetidinium salts, may also form additional, in this case, undesired products, such as diamines and quaternary ammonium salts, shown in Figure 4.2.
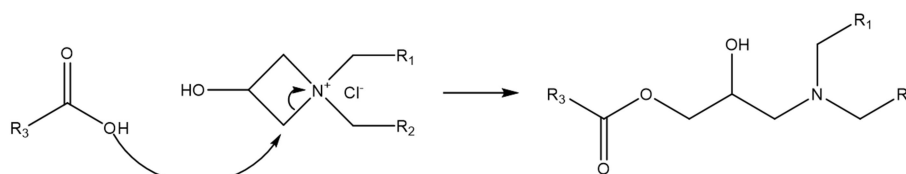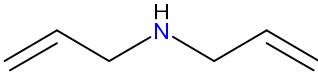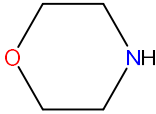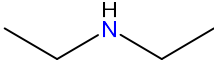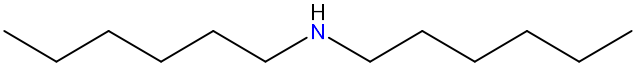
Figure 4.1. Reaction scheme of the formation of azetidinium from a secondary amine and epichlorohydrin (to the left) as well as the ring-opening when reacted with a carboxylic acid (to the right).

4.2 Dialkylamine Reagent Synthesis
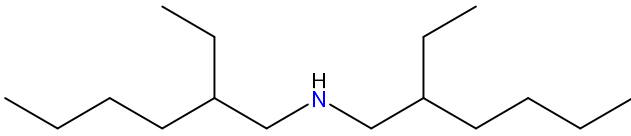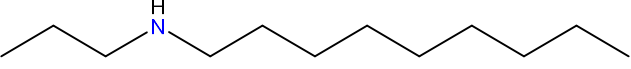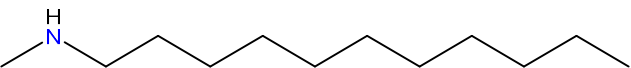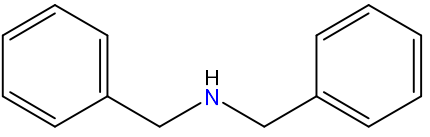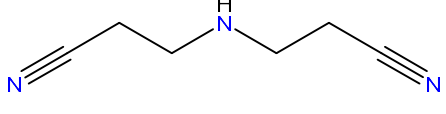
The syntheses of the dialkylamine reagents were not optimised, the intention was simply to develop a convenient way to make them, with good enough parameters. Following protocols from Chattopadhyay et al. (2012), azetidinium salts were synthesised from secondary amines and epichlorohydrin, simply by mixing the reactants while cooling and then letting the reaction mixture stir for a few days at room temperature. During the work with synthesising azetidinium salts, it was noted that the chemical structure of the dialkylamines had a strong effect on the reaction outcome. Some of the dialkylamines gave azetidinium salts in high yields whereas other dialkylamines seemed to only give the

chloro-2-hydroxy-propyldialkylamine. We were unable to find any general reaction conditions that yielded azetidinium salts regardless of amine, so different solvent and amine combinations were tried and tested to find suitable combinations, as can be seen in Table 4.1. Despite the seemingly simple reaction protocol, when reactions where repeated they would sometimes give the azetidinium salt as the major product and sometimes gave the dialkyl alkylchloride as the major product. Both symmetrical and asymmetrical amines were investigated, where the dialkylamines that where not commercially available were prepared by reductive amination, starting from appropriate aldehyde and amine via reduction of the formed imine by $NaBH_4$. Furthermore, the synthesis seemed to give variation in the product outcome.

Table 4.1. Screening of solvents for reactions between epichlorohydrin and various secondary amines when mixed at room temperature.

Substituent/Secondary amine	Solvent	Type
Diallylamine – DAA	Acetonitrile	Mixed[3]
	Water	Dialkyl alkylchloride
	Methanol	Dialkyl alkylchloride
	Ethanol	Dialkyl alkylchloride
	Isopropanol	Dialkyl alkylchloride
	n-Heptane	Dialkyl alkylchloride
	Ethyl acetate	Dialkyl alkylchloride
	THF	Dialkyl alkylchloride
	Triethylamine	Dialkyl alkylchloride
Morpholine – M	Water	Azetidinium salt
Diethylamine – DEA	Water	Azetidinium salt
Dihexylamine – DHA	Isopropanol	Azetidinium salt
	Hexane	Mixed
	THF	Mixed
	-	Azetidinium salt

---

[3] Sometimes only formation of azetidinium salt, sometimes mixed product formation and sometimes only diallyl alkylchloride when repeated.

Di(ethylhexyl)amine – DEHA	Isopropanol	Dialkyl alkylchloride	
	Hexane	Dialkyl alkylchloride	
	THF	Dialkyl alkylchloride	
	-	Dialkyl alkylchloride	
Propylnonylamine – PNA	Isopropanol	Mixed	
	Hexane	Mixed	
	THF	Mixed	
	-	Mixed	
Methylundecylamine – MUA	Isopropanol	Mixed	
	Hexane	Mixed	
	THF	Mixed	
	-	Mixed	
Dibenzylamine – DBA	Isopropanol	Dialkyl alkylchloride	
	Hexane	Dialkyl alkylchloride	
	Cyclohexane	Dialkyl alkylchloride	
	Toluene	Dialkyl alkylchloride	
Iminodipropionitrile – IDPN	Water	Dialkyl alkylchloride	
	Ethanol	Dialkyl alkylchloride	
	Acetonitrile	Dialkyl alkylchloride	
	Ethyl acetate	Dialkyl alkylchloride	
	Isopropanol	Dialkyl alkylchloride	
	Hexane	Dialkyl alkylchloride	
	THF	Dialkyl alkylchloride	
	-	Dialkyl alkylchloride	

As a consequence, a better, more robust and reliable synthesis protocol was needed. A two-step reaction inspired by Krishna Reddy et al. (2011) and Parzuchowski et al. (2018) was investigated, where the dialkyl alkylchloride was first formed and then further reacted with sodium bicarbonate in a second step to form the azetidinium salt. With primary amines this protocol yielded an azetidine that could be alkylated by an alkyl halide in the second, ring-closing, step, but with the secondary amines investigated, another product was formed. At first glance it appeared to be the desired azetidinium salt since the NMR peak pattern was very similar. However, after further analysis we realised that a cyclic carbonate is formed, shown in Figure 4.2. The first step, forming the dialkyl

alkylchloride, is fairly straight-forward, equimolar amounts of epichlorohydrin and (di)alkylamine reacted in isopropanol, and usually does not require any purification before moving on to the second step. For the second step, an excess of sodium carbonate or sodium bicarbonate was used to form the cyclic carbonate, which was easily removed by filtration when the reaction was done. This procedure worked well for all the amines used in these studies. So far, the dialkyl cyclocarbonate synthesis seems robust and gives rather pure product, but the scope needs to be investigated further and the reaction parameters optimised.
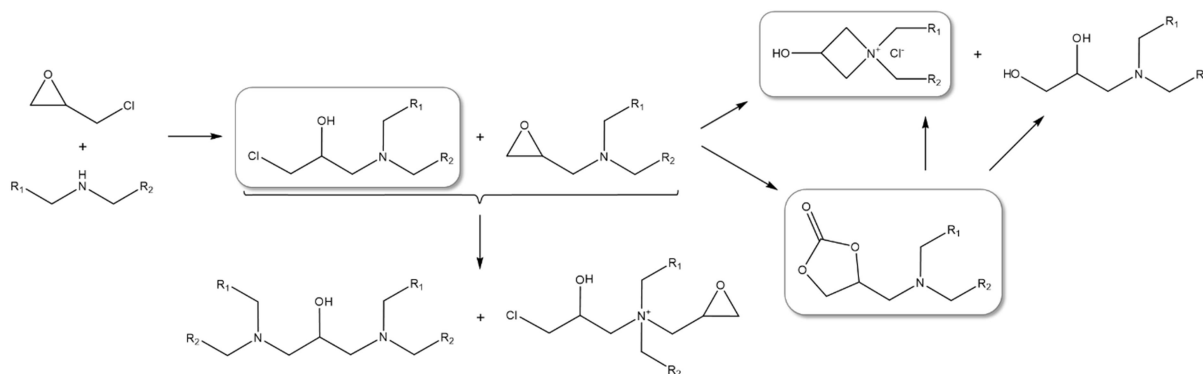
Figure 4.2. Possible products and side reactions when reacting epichlorohydrin and secondary amines.

An alternative two-step route for azetidinium was also found (Cunkle, 2001). The first step is the same as for the dialkyl cyclocarbonate synthesis, but for the second step the dialkyl alkylchloride is heated at 100 °C in water, which causes the dialkyl alkylchloride to cyclise into azetidinium salts with high purity. We also noted that in an aqueous solution of dialkyl cyclocarbonate, upon standing for a long time, the dialkyl cyclocarbonate hydrolyses into dialkyl diol and azetidinium salt, as illustrated in Figure 4.2.

4.3 Cellulose Nanocrystal Properties

CNCs were produced through sulphuric acid hydrolysis, which results in a small amount of sulphate half-esters decorating the surface. An in-house protocol on a half-kilo scale was used for producing the CNCs. The width was determined to be 6.0 ± 1.5 nm and the length 211 ± 114 nm by AFM.

CNCs with different sulphate contents were prepared through oversulphation and desulphation reactions. Similar to previous reports, acid-catalysed desulphation results in a partial desulphation and in order to reach full desulphation a solvolytical methodology has to be employed (Jiang et al., 2010). The characteristic sulphate peak in both FTIR and Raman disappears after solvolytic desulphation, as shown in Figure 4.4, indicating complete removal of the sulphate groups, which was also supported by the elemental
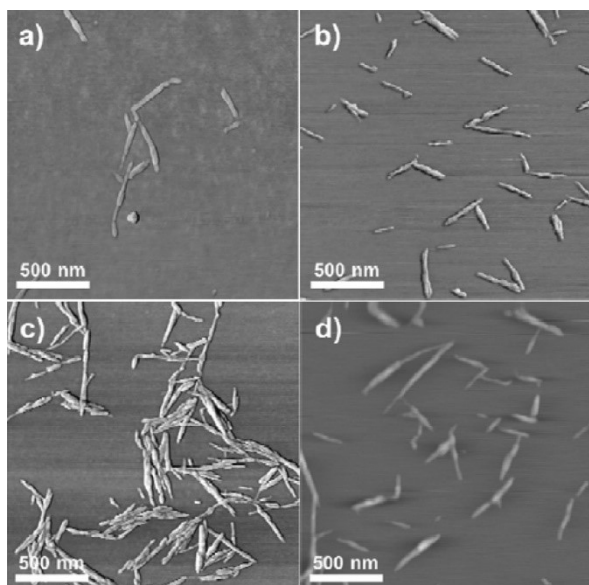
Figure 4.3. AFM images of a) solvolytically desulphated CNCs, b) HCl-catalysed partially desulphated CNCs, c) unmodified CNCs and d) oversulphated CNCs
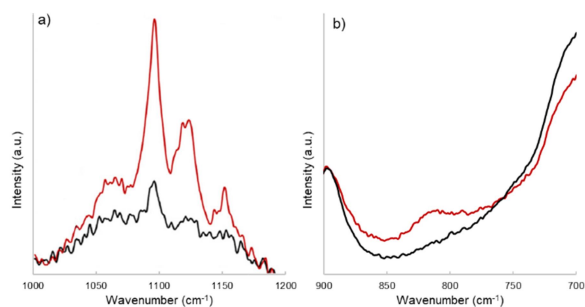
Figure 4.4. a) Raman and b) FTIR spectra zoomed in on the characteristic sulphate peak, shown for sulphated (red) and solvolytically desulphated CNCs.

Table 4.2. Sulphate half-ester content and onset of thermal degradation of the non-functionalised CNCs from the different batches used.

Sample	Sulphate half-ester content		Onset of thermal degradation (°C)
	(S-%)	(µmol/g)	
CNC-OH	0.00[a]	0[a]	277
CNC-OSO$_3$H-part	0.47[a]	146[a]	158
CNC-OSO$_3$H	0.55[a]	171[a]	156
CNC-OSO$_3$H-over	0.85[a]	265[a]	155
CNC-OSO$_3$H	1.12[b]	350[b]	157
CNC-OH	0.08[b]	20[b]	201
CNC-OSO$_3$H-self	0.38[b]	129[b]	156
CNC-OSO$_3$H-part	0.44[b]	136[b]	152
CNC-OSO$_3$H	0.59[b]	187[b]	152
CNC CelluForce	1.05[b]	293[b]	236

[a] determined by elemental analysis

[b] determined by conductometric titration

analysis, see Table 4.2. The TGA results support the complete removal of sulphate groups when using solvolytic desulphation as the thermal stability is increased to over 270 °C, compared to 150 °C for the unmodified. Near complete desulphation results in a smaller increase of the thermal stability, due to the few residual sulphate groups. The increased thermal stability is attributed to the removal of the acidic hydrogen associated to the sulphate groups, which catalyses a dehydration of the cellulose. The CNCs can also be stabilised by replacing the associated hydrogen to a sodium ion, thus inhibiting the dehydration reaction (Wang et al., 2007). AFM confirmed that the treatments had no impact on the dimensions of the CNCs, see Figure 4.3.

4.4 The Dialkylamine Functionalisation

The Westman research group have previously demonstrated that azetidinium salts react with carboxylic acids on hemicellulose (Börjesson and Westman, 2016). A little simplified, sulphate half-esters and carboxylic acids may be considered as soft nucleophiles with similar orbital arrangement and thus, may have similar reactivity. It was therefore hypothesised that azetidinium salts could be used to introduce dialkylamine functionalities to nanocellulose. CNCs with different sulphate contents were reacted with a large excess of azetidinium salts. Elemental analysis results, shown in Figure 4.5, indicated a correlation between the nitrogen content after conjugation and the sulphur content prior to conjugation. Reacting the azetidinium salts with CNCs should equate to one reagent per sulphate group, as they are expected to react in equal molar ratio. Upon modification, the thermal stability was increased by around 100 °C, see Table A1 in Appendix A2, and the FTIR sulphate peak was slightly shifted from 814 to 796 cm^{-1}, see Figure 4.6, indicating that the sulphate half-esters have been stabilised by reacting to form
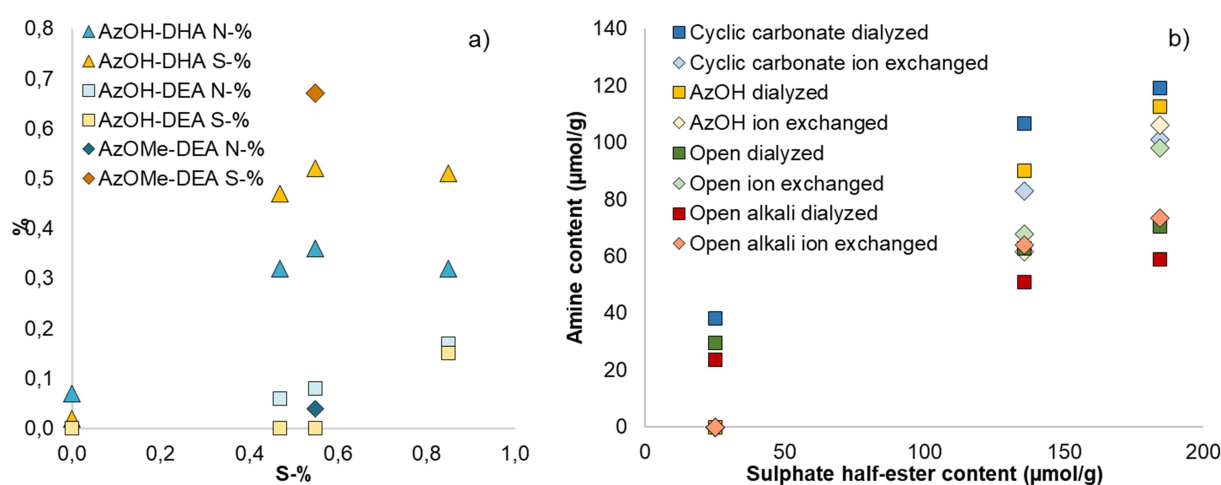
Figure 4.5. Elemental analysis results and conductimetric titration showing the correlation between amine content and sulphate half-ester groups for the dihexyl and diethyl functionalised samples in a) Paper I and b) the samples in Paper IV functionalised with the diallyl cyclocarbonate, the diallyl azetidinium salt and the dialkyl alkylchloride in both acidic and alkaline reaction conditions.
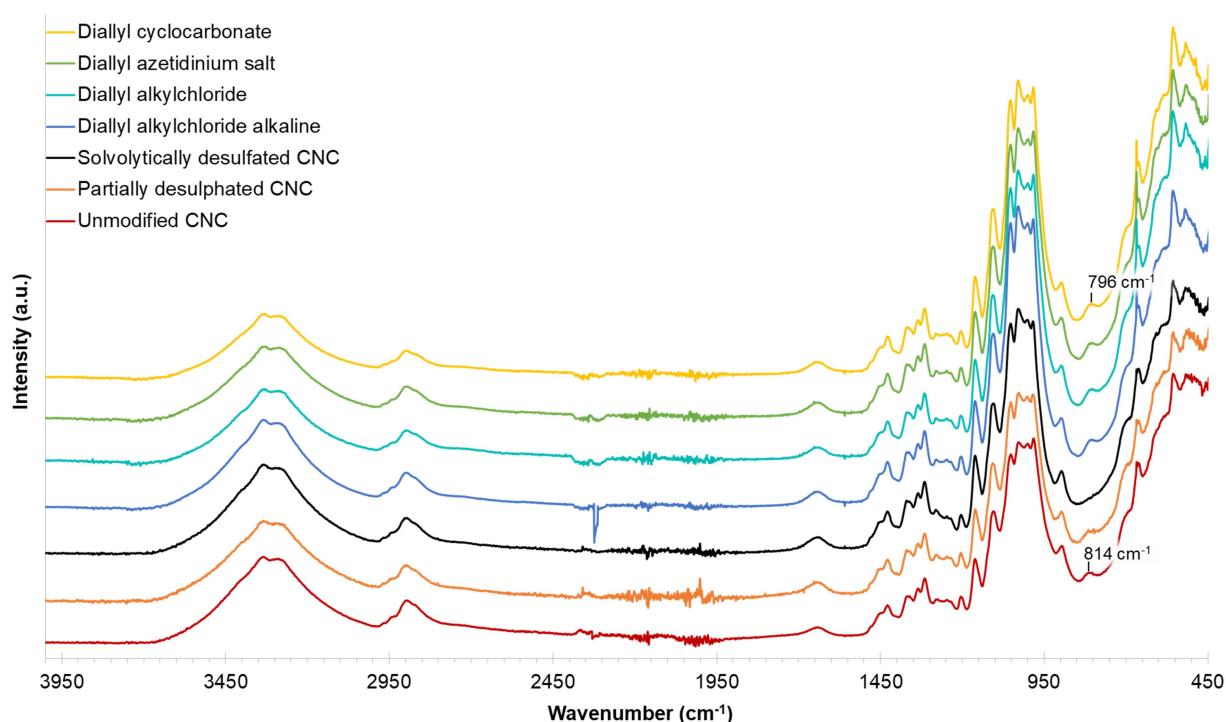
Figure 4.6. FTIR spectra of representative samples, with the characteristic sulphate peak marked on a sulphated CNC sample and on a dialkylamine functionalised CNC sample.

a di-ester, thus inhibiting the low temperature dehydration process. For the short-chained AzOH-DEA, a reduction in the sulphate content was observed after conjugation, which was not noticed for the longer chained AzOH-DHA. It was hypothesised that this was due to an intramolecular cyclization, similar to that of azetidinium-functionalized phosphorodithioates (Jeziorna et al., 2003), which caused the desulphation. Methylation of the azetidinium salt (AzOMe-DEA) prevented the desulphation, see Figure 4.5 a).

The low degree of substitution along with the recalcitrance of cellulose makes it very difficult to directly qualitatively characterise the actual linkage, thus model reactions using *p*-toluenesulphonic acid and 2-methyl-2-propene-1-sulphonic acid was done to verify that sulphonates can react with azetidinium salts, which was confirmed by NMR.

The conjugation was initially done in a DMSO-toluene system which required solvent exchange from water to DMSO-toluene, and then again back to water once the reaction was done. DMSO and toluene are hazardous solvents and the high boiling point of DMSO makes it difficult to remove. The protocol was consequently not scalable beyond the lab scale from an environmentally and economically sustainable perspective. Therefore, an alternative solvent system was sought after. After some investigation, it turned out that the conjugation worked in water. In addition to the improved solvent system, the molar ratio was decreased from 3 reagents per AGU to 0.1, corresponding to around 2 mol equiv., rather than over 50 mol equiv., per sulphate half-ester group. The methylation of the azetidinium salts was omitted for the CNCs prepared for Paper III, as the results in

Paper I indicated that larger substituents did not undergo an intramolecular cyclization. As the functionalisation of the CNC samples prepared in Paper III was successful, it was therefore concluded that the methylation step is, in most cases, redundant.

As discussed previously, issues with reproducibility had emerged with the azetidinium salt and alternative reagents were investigated. The new dialkylamine reagent that was used was the dialkyl cyclocarbonate, which was found to react with CNCs under the same conditions used for the azetidinium salts. Neither of the conjugation reactions had been optimised, although the azetidinium conjugation had been greatly improved. We attempted to optimise the dialkyl cyclocarbonate conjugation and preliminary results indicated a very quick reaction that worked at low temperatures. This seemed too good to be true, and after further investigation we realised that upon addition of the dialkylamine reagents to the acidic CNCs, the nitrogen is protonated and forms an ionic complex with the sulphate half-esters, which would be deprotonated during titration. In a titration curve, this would give the same appearance as if they had been covalently bound to the CNCs. These complexes are so strong so that they are not broken during dialysis, but required ion exchange with a strongly acidic cationic resin, as demonstrated in Figure 4.7. Based on this information it could be concluded that the fast reaction kinetics previously observed were not an exceptionally fast conjugation reaction, but simply ionic interactions. It turned out that the conjugation works already at room temperature, as seen from Figure 4.7 e).
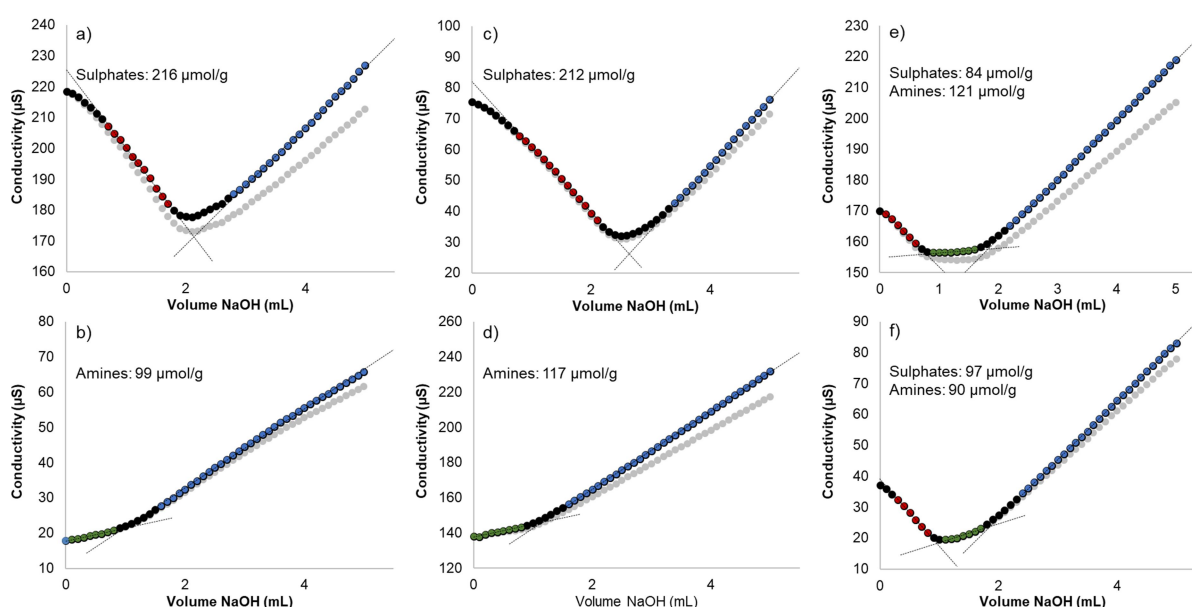
Figure 4.7. Titration curves of sulphated CNCs a) after dialysis and ion exchange with strong acid cationic exchange resin, b) after 5 minutes mixing with diallyl cyclocarbonate reagent before and c) after ion exchange with strong acid cationic exchange resin, as well as d) after dialysis (no ion exchange). Sulphated CNCs and after mixing with diallyl cyclocarbonate reagent e) for 24 hours at room temperature or f) after heating at 90 °C for 20 minutes, with subsequent ion exchange with strong acid cationic exchange resin.

We also explored if the dialkyl alkylchloride conjugates to the CNC surface, as this method is commonly used for traditional functionalisation of cellulose and alcohols. It was investigated both under acidic and alkaline conditions. Based on Merima Hasani's previous work (Hasani et al., 2008) as well as fundamental organic chemistry knowledge, alkylchlorides are expected to react with alcohols under alkaline conditions. The hypothesis was that the dialkyl alkylchloride should react with the hydroxyl groups, rather than the sulphate groups. Surprisingly, the reaction outcome showed a clear correlation with the amount of sulphate groups, see Figure 4.5. In fact, all investigated dialkylamine reagents showed a clear dependency between amine and sulphate content, see Figure 4.5 b). Whether the reaction occurs through conjugation with the sulphate half-ester, transforming it into a di-ester or a trialkyl sulphonamide, or if it is a substitution reaction, replacing the sulphate group to form a tetraalkyl ammonium group on the surface, is difficult to say and can based on current data only be speculated upon. The FTIR data suggests that the sulphate ester linkage is still present, but this may be from the residual sulphate groups uncovered by the ion exchange. What should be noted though is that the amines appear to have a protective effect on the sulphate groups, preserving them despite high temperatures which should make them prone to self-desulphation. The self-catalysed desulphation of CNCs in aqueous suspensions is observed already at room temperature (Beck and Bouchard, 2014), but increases with increasing temperature, as demonstrated in Figure 4.8.
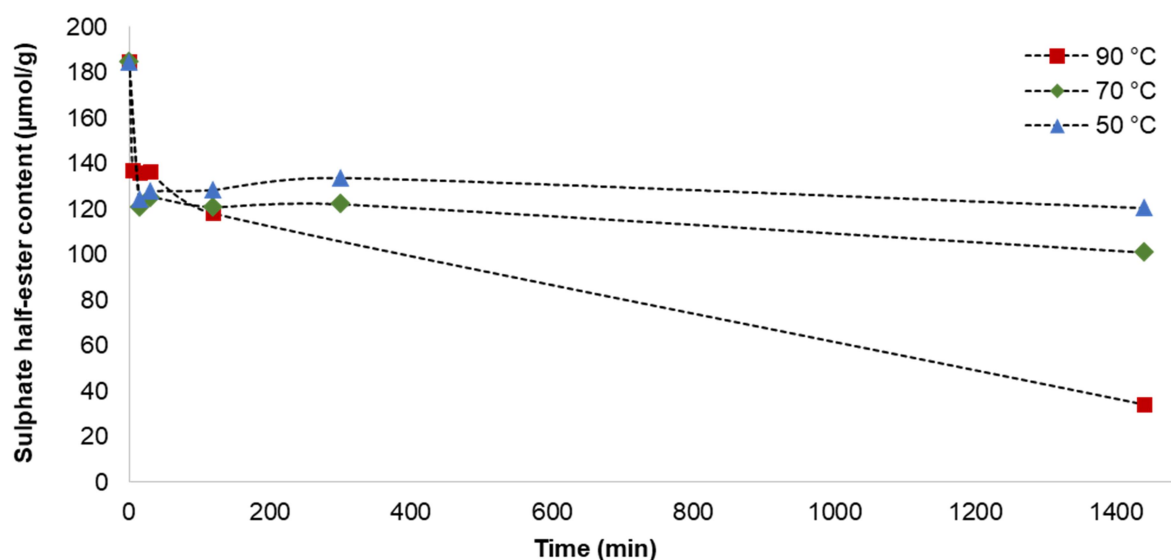
Figure 4.8. The surface sulphate content of CNCs in aqueous suspension over time when heated at 50, 70 and 90 °C.

Production of dialkylamine functionalised CNCs at a larger scale was attempted. We decided to use commercially available CNCs, CelluForce, to show the possibilities for large-scale production. The reaction appeared to have worked, as discussed previously, titration indicated only weak cationic surface charges (i.e. the dialkyl amines) and FTIR showed the characteristic sulphate peak and TGA a high thermal stability. When it was
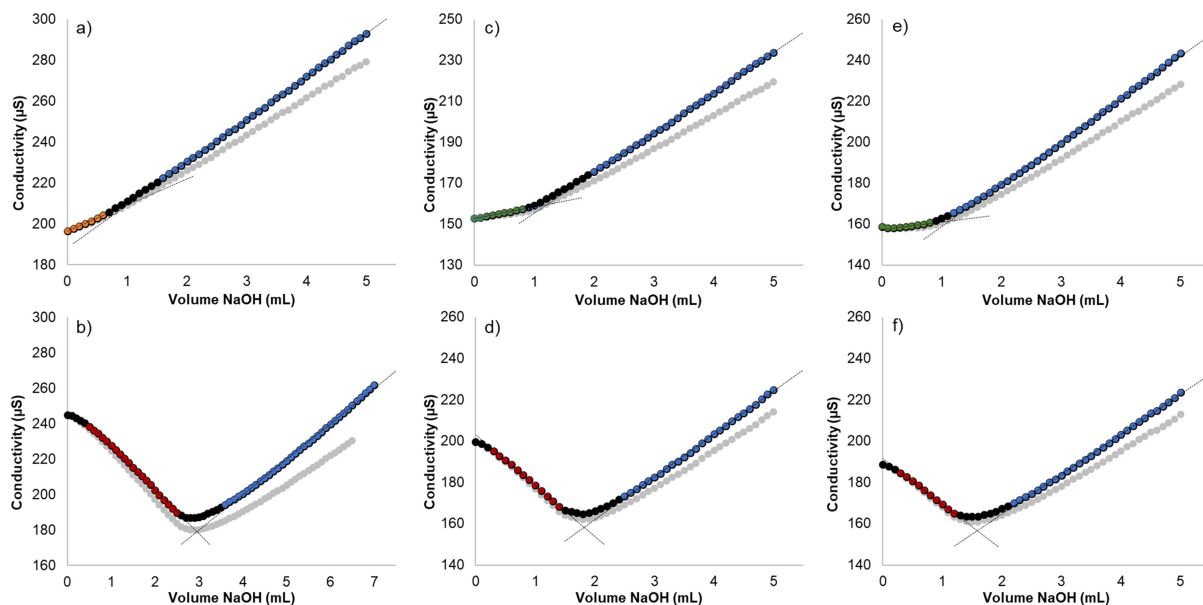
Figure 4.9. CelluForce CNC a) dispersed in deionised water without any pre-treatment, b) after ion exchange with a strong acid cationic resin, c) after reaction with DAA-cc before and d) after ion exchange with a strong acid cationic resin and e) after reaction with DAA-AzOH before and f) after ion exchange with a strong acid cationic resin.

realised that dialysis was not sufficient to remove unreacted dialkylamines, the functionalised CelluForce CNC samples were also subjected to ion exchange. The new titration results shown no, or very small amounts of amine, i.e. the conjugation did not work with the neutralised CNCs.

4.4.1 Rheological properties of the Functionalised CNCs

The methoxyazetidinium functionalised CNCs in Paper II were also characterised by measuring the shear viscosity and the percolation threshold was determined by Lilian Forsgren and Tobias Moberg at the Department of Industrial and Materials Science at Chalmers University of Technology. Below is a short summary of the rheological characterisation.

Both the dialkyl functionalised and the unmodified CNC samples exhibited clear shear thinning behaviour both at 1.3 wt.-% and 0.65 wt.-%. The shear thinning behaviour was even more pronounced for the functionalised samples, which at low shear rates (<50 s^{-1}) had around ten times higher shear viscosity as compared to the unmodified CNCs, while the curves started to converge at the higher shear rates. The increased viscosity indicates a change in the particle interactions upon modification, which may be interpreted as that the introduced dialkyl groups facilitated the formation of a network structure. The dialkyl groups are predominantly lipophilic compounds and thus are not prone to attractive interactions with water, nor with the hydroxyl groups on the CNC surface. The diallyl functionalisation resulted in the highest shear viscosity, suggesting that the allyl groups promote the formation of a comparably stronger network, possibly through interactions between their π-π bonds. These interactions would be expected to be stronger compared

than the van der Waals forces likely to be dominant for the dihexyl and morpholine modifications. The reach and flexibility of the substituents are also likely to affect the tendency to form networks and could help explain the observed differences in shear viscosity. The smaller and stiffer morpholine substituent would be less prone to form a strong network compared to the longer dihexyl, but as the dihexyl chains having a higher degree of conformational freedom would tend to form a more flexible network, reflected in the lower shear viscosity. The tendency for strong network formation for the dialkyl functionalised CNCs was further supported by the onset of percolation, which was determined to be 2 percentage points higher for the unmodified CNC, at around 2.5 wt.-%, than that of the functionalised CNCs, at around 0.2-0.4 wt.-%.
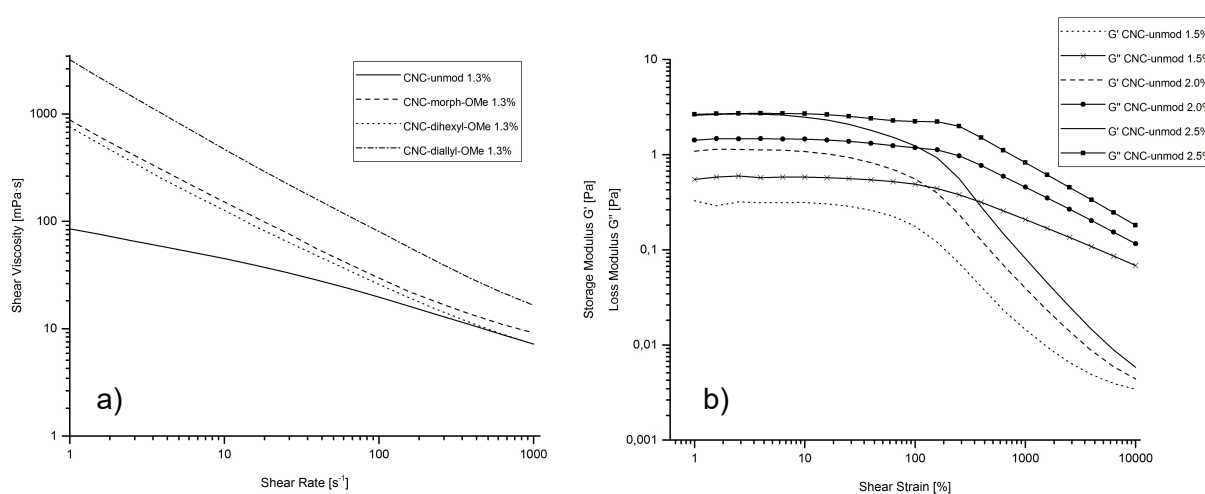
Figure 4.10. a) The shear viscosity and b) storage and loss moduli as a function of the shear rate in the region between 1 and 1000 s^{-1}.

<div align="right">

5

</div>

DIALKYLAMINE FUNCTIONALISED CNC COMPOSITES

Incorporating nano-sized fillers into a polymeric matrix can be an efficient way to improve the mechanical properties of a material. The excellent mechanical properties of cellulose nanocrystals make them suitable as reinforcing elements in bio-based nanocomposites. This chapter provides a brief background and summary of the results from the nanocomposites produced with dialkyl surface-functionalised as well as unmodified CNCs reported in Papers I, II and V.

5.1 Background

The strive towards a bio-based, circular economy has created a demand for strong, light-weight materials from renewable resources. CNCs' low density, excellent specific mechanical properties and low abrasion toward processing equipment, along with its biodegradability and renewable origins has made it popular as a reinforcing element in polymeric matrices (Gan et al., 2020). There are however some drawbacks to consider, such as the rather low thermal stability, with the onset of thermal decomposition being below the processing temperature of many engineering polymers, as well as the potentially poor compatibility between the matrix and CNCs. When mixing CNCs with common polymers, such as polyolefins, the differences of the respective material characteristics can result in poor adhesion and a weak interphase, which is likely to have a negative impact in the dispersibility of the CNC in the matrix. Chemical modification can be a way to address these issues as the surface of the CNCs can be adapted to suit the matrix, while still maintaining its desired mechanical properties of the CNCs. If the chemical modification is performed on the sulphate half-esters, like the dialkyl functionalisation discussed in the previous chapter, the thermal stability can also be increased above the processing temperature of some common engineering polymers.

The commercial availability of CNCs has made it possible to produce composites on a large scale, but most composites reported in literature are produced by solvent casting (Azizi Samir et al., 2004, Lee et al., 2014), a method that is not viable on an industrial scale. In Paper V, composites containing 10 wt.-% CNC are produced using conventional processing equipment, while Papers I and III uses different forms of solvent casting. A summary of the results for the composites in Papers I, III and V are presented and discussed in this chapter.

5.2 Summary of Results

With the exception of the composites in Paper I and the neutralised composite in Paper III, all other composites were produced and characterized by Lilian Forsgren and Abhijit Venkatesh at the Department of Industrial and Materials Science at Chalmers University of Technology. A compilation of the properties can be found in Appendix A3 and the detailed results can be found in the appended papers, only a brief background and summary is given below.

The composites in Papers I, III and V were produced with three different manufacturing techniques at three different scales with four different polymer matrices. Therefore, the results cannot be compared without taking these factors into consideration. Reference samples with CelluForce CNC, both unmodified and diallyl surface functionalised, and with EAA7 as well as EAA15 as matrix were produced by dispersion mixing and compression moulding in the same manner as Paper III to try to understand the effect of the change of CNC source, matrix and production method. Comparing the CNC sources, no significant differences in mechanical behaviour was observed when the same matrix and processing method was employed.

EAA is a rather ductile polymer and was chosen as matrix due its compatibility with cellulose (Ariño and Boldizar, 2012). LDPE and EAA are both made up of a polyethylene backbone, with EAA also containing a certain amount of carboxylates, derived from acrylic acid units, making it more hydrophilic. The functionalities of the dialkyl groups were also varied. The morpholine substituent was chosen based on its hydrogen bonding capabilities and NMMO-like structure, the diallyl functionality was chosen for the potential to form strong networks through π-π bond interactions as well as the possibility to do further chemical reactions or crosslinking with the double bond, and the dihexyl group was chosen as its fairly long aliphatic chains might be prone to interact with the lipophilic matrix. The diethyl group was chosen to compare the influence of short compared to long aliphatic chains on the CNC surface.

Incorporating CNCs into the various polymeric matrices had a significant impact on the mechanical properties, regardless of modification. The increased stiffness and decreased tensile strength and ductility seen are expected when incorporating a rigid reinforcing element such as CNCs into a polymeric matrix (Nielsen, 1974). No significant impact on matrix crystallinity was observed, suggesting that the impact stems from the CNC network itself and not matrix crystallinity changes. Although the actual values and magnitudes differ quite a bit between the different production methods, as can be seen in Figure 5.1, the general trends are in agreement. These discrepancies are, as discussed above, expected when comparing dispersion mixed, compression-moulded samples with extruded and injected moulded samples. The LLDPE composites from paper I produced using the mini-extruder showed a two-fold increase in Young's modulus when incorporating CNCs (at around 3 wt.-%) and a more than three-fold increase was seen for the EAA15 dispersion mixed composites in Paper III (with 10 wt.-% CNC) while a more modest increase of 40-80 % was noted for the large-scale twin-screw extruded composites in paper V (with 10 wt.-% CNC), as shown in Figure 5.1. The greatest improvement in stiffness for the composites in Paper III was seen for the 10 % unmodified CNC, closely followed by the 10 % CNC-AzOH-DAA. At low loadings (0.1 and 1 %) the CNC-AzOH-M exhibited the highest modulus, but showed the least improvement at the high loading, which may have been due to defects. The cause of the defects was not determined. In paper V there was no significant difference in the mechanical properties when comparing the dialkyl cyclocarbonate functionalised CNC and the unmodified CNC, similar to the finding in Paper I where no significant difference was noted between the unmodified and
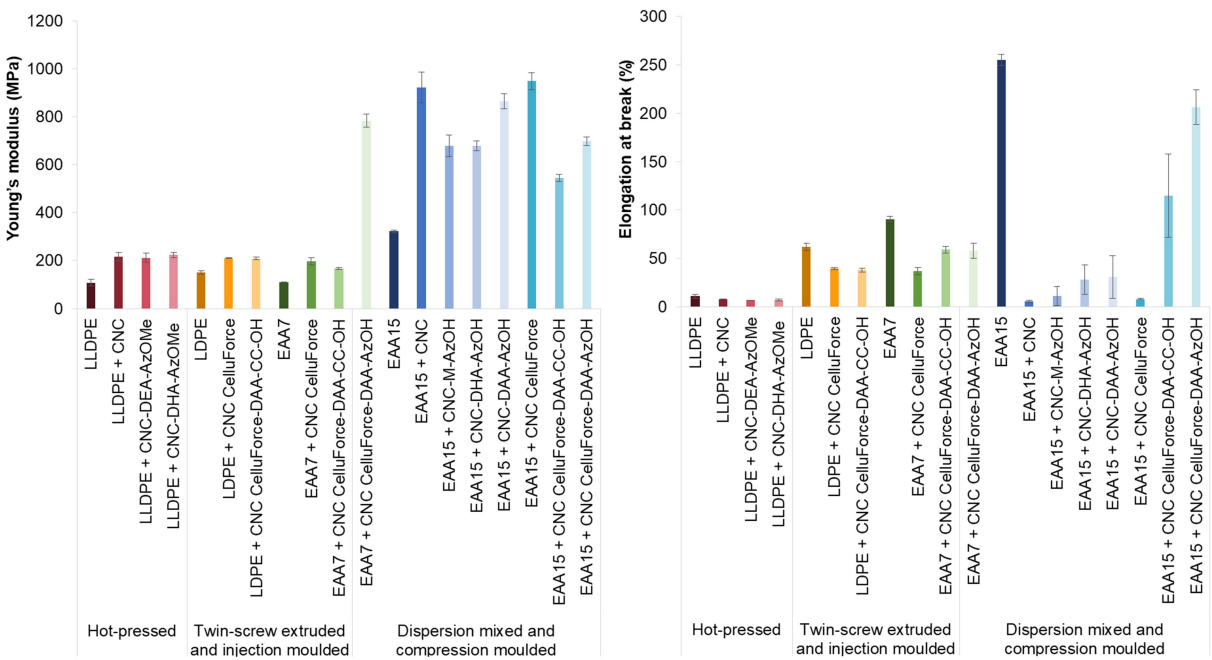
Figure 5.1. To the left; Young's modulus, indicating the stiffness of the composites, and to the right; the elongation at break, as a measure of the ductility of the composites.

43

the diethyl and dihexyl functionalised CNCs, despite that the composites were processed at the at the onset of thermal decomposition for the unmodified CNC. Surprisingly, the difference in mechanical properties comparing the unmodified CNC and diallyl functionalised CNC composites in Paper V was greater than what was reported in Paper III, with the unmodified showing a near doubling in stiffness, compared to a mere 50 % increase for the diallyl functionalised CNC composite. Dynamic mechanical analysis of the composites in Paper III and V showed that the diallyl modification appears to create a stronger, more stable interphase between the EAA matrix and the CNC, while the morpholine and dihexyl modifications creates a more flexible interphase. The same trend was not seen for the LDPE matrix, where no significant differences between the modified and unmodified CNC were seen. Melt rheology revealed a shear-thinning behaviour for all samples, but with little impact of the modification.

The composites in Paper III were produced with varying amounts of CNCs, where at low loadings (0.1 and 1 wt.-%) the composites displayed an increased ductility, suggesting that that the modification had a plasticizing effect, while a more typical reinforcing behaviour was observed at higher loading (10 wt.-%).
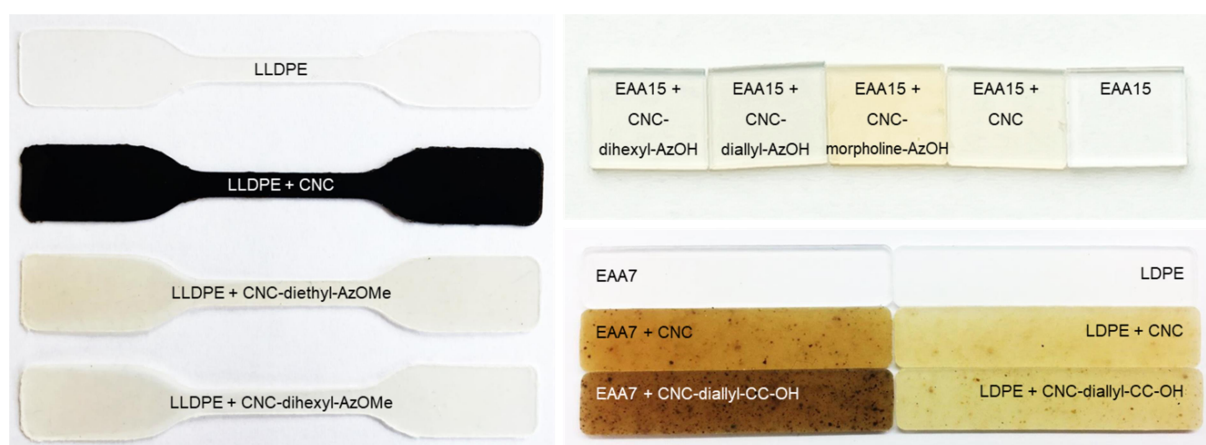
Figure 5.2. Appearance of the composites after processing.

The result of the improved thermal stability for the modified CNC was most prominent in the composites produced in Paper I, where the composites were processed at the onset of decomposition for the unmodified CNC. This caused the composite with unmodified CNC to char during the production, unlike the modified which were only slightly darker and more yellow, as shown with the colorimetric analysis. The EAA15 were processed well below the onset thermal degradation temperature and showed no visible signs of degradation, with the exception of the 10 wt.-% CNC-M-AzOH composite which showed some yellowing and defects, seen in Figure 5.2, which is most probably from N-oxide formation. Many amines show a yellowish colour due to impurities resulting from air-oxidation (Krauklis and Echtermeyer, 2018). For the large scale production the maximum

processing temperature was set to 200 °C in certain heating zones along the extruder barrel. In addition to the heat, the materials were also subjected to high shear forces during the mixing and compounding, so it is not unexpected that the composites were discoloured (Shafizadeh and Bradbury, 1979). That the EAA7 composites were darker compared to the LDPE composites, especially the composite with diallyl functionalised CNC, which may be due to the alkalinity of the EAA7 matrix.

In addition to the issue with discolouration of the large-scale composites, there is also a clear difference in how well dispersed the CNCs are. Just from visual inspection aggregates can be seen in the large-scale composites while the compression-moulded samples are transparent and without any visible aggregates, photos of the composites are shown in Figure 5.2. The compression-moulded samples were prepared by mixing an aqueous CNC suspension with a polymeric dispersion and are thus expected to have a better distribution as compared to twin-screw extruded, wet mixed composites, as the mixing is enabled at a much smaller length-scale. In a twin-screw extruder, the mixture is under a stronger, directed shear that may affect how the crystallites align. As a consequence of the aggregation in the large-scale composites, less than the added 10 % CNCs will act as the intended reinforcing element. The crystals may not be dispersed as single crystals but may also have formed aggregates of a few CNC crystallites up to the large agglomerates seen by eye. Thus, from a practical point of view the effective reinforcing elements could be considered to be less than the added 10 wt.-%.
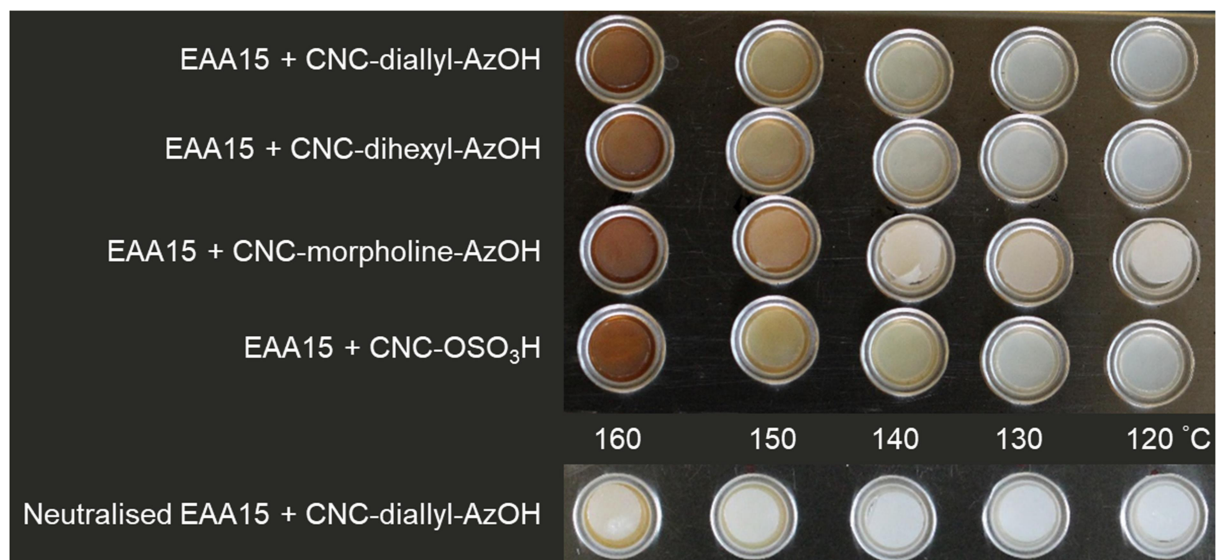
Figure 5.3. The composites in Paper III were placed on a Kopfler bench with a heat gradient to visualise the thermal degradation.

EAA was chosen as matrix as its carboxylate content was expected to have more favourable interactions with cellulose compared to more conventional polymers like LDPE, which could also be seen from the results in Paper V and consistent with previous

reports (Venkatesh et al., 2018). It was noted that the increased thermal stability of the surface modified CNCs was not maintained when they were incorporated into the EAA composites, regardless of production method. The cause of this may lay with the carboxylates and the high pH of the matrix. Sulphates are well-known within organic chemistry to act as good leaving groups under alkaline conditions in the presence of nucleophiles, such as carboxylates and hydroxide. At this high pH, combined with elevated temperatures, the functionalised sulphate di-esters are likely cleaved off by the carboxylates and/or hydroxide, thus releasing sulphate half-esters which will lower the thermal stability. A small-scale composite was prepared by mixing an aqueous suspension of hydroxyazetidinium modified CNCs with a neutralised EAA15 dispersion, and was then hot-pressed after drying. The neutralised composite maintained the increased thermal stability of the modified CNC and showed no sign of degradation when heated to 150 °C, as can be seen in Figure 5.3. When the carboxylates are in their neutral, acid form they are less reactive and thus is less likely affect the sulphate di-esters.

6

CONCLUDING REMARKS

6.1 Conclusions

From the results presented in this thesis, it can be concluded that CNCs can be surface modified by functionalising the CNCs surface sulphate groups with dialkylamines. Azetidinium salts were found to be a suitable reagent for the functionalisation, transforming the sulphate half-esters to di-esters. The functionalisation resulted in increased thermal stability by near 100 °C and significantly increased viscosity and gelation. However, the synthesis of the azetidinium salts proved troublesome as no general reaction conditions were found to yield azetidinium salts, irrespective of amine, and issues with reproducibility also emerged. In the pursuit of a better synthesis route, a dialkyl cyclocarbonate reagent was found, which also reacted with sulphated CNCs. The two-step dialkyl cyclocarbonate synthesis and a new, two-step azetidinium salt synthesis protocol were both found to yield reagent with high purity.

The molecular link could not be verified by any direct characterisation, due to the low concentration of modification (and sulphate groups), but the increase in thermal stability, the shift in wavenumber of the characteristic sulphate peak in FTIR and the correlation between amine and sulphate content after ion exchange supports that conjugation has occurred. Additionally, dialkyl alkylchloride was surprisingly also found to react with the sulphate groups, both in acidic and alkaline conditions, despite what would be expected based on previous reports (Hasani, 2008)

The functionalisation protocols presented in this thesis have distinct advantages and drawbacks, depending on what is most prioritised for the desired application. Azetidinium salts are highly hygroscopic compounds, as well as highly viscous, making them somewhat difficult to handle. Additionally, hydrochloric acid is formed as the side-product when

47

conjugated with CNCs. A great advantage, on the other hand, is that both the reagent synthesis and the functionalisation is water-based, making it an industrially feasible process. The dialkyl cyclocarbonate synthesis appears to be a more robust method compared to the azetidinium salt synthesis, but is performed in organic solvents, although relatively benign, as well as generates more waste during synthesis in the form of sodium chloride. This is somewhat mitigated by the fact that the only waste formed during the conjugation is carbon dioxide when equimolar amounts are used, as long as gas formation is not a major issue in the intended process. Both methodologies work well with the green chemistry principles striving to minimize waste, using safer solvents and the use of renewable feedstock (Anastas and Eghbali, 2010).

Incorporation of CNCs in polymeric composites improved the mechanical properties, irrespective of any modification. The impact of dialkylamine functionalisation was not as great as desired, but resulted in a stronger interphase between matrix and CNCs. The improved thermal stability could also help mitigate the discolouration occurring during processing.

6.2 Future Work

The functionalisation of CNCs utilising the sulphate half-esters is so far a rather unexplored area and there are therefore much to uncover.

The scope of synthesis protocols need to be investigated and optimised, in order to find the limitations of this functionalisation. As part of the optimisation, and in keeping with the green chemistry principles, a revision of the current starting material epichlorohydrin may be needed. Although a commodity chemical of great importance to industry, it is under REACH regulations and more sustainable alternatives ought to be investigated.

The conjugation with dialkylamines and CNCs shows promise as an industrially plausible process, as it is water-based and does not appear to require advanced purification or processing. The only by-product formed during the conjugation between the dialkyl cyclocarbonate and sulphated CNCs should be carbon dioxide, which avoids tedious and time-consuming purification. This of course has to be investigated and confirmed, but should from a theoretical standpoint be a great advantage of the dialkyl cyclocarbonate protocol. Optimisation of the conjugation reactions is needed to find the optimum in time and temperature. The conjugation seems to occur within a large temperature range, and as reaction rates tend to be temperature dependent it could be an indicator that the process could be tuned to either be a fast, high-temperature reaction, or a slower, low-temperature reaction. This allows for flexibility to adjust the process based on what unutilised heated side-streams are available for process integration. Whether or not it

follows typical kinetics requires more research. Based on the fast, ionic interactions, the conjugation may also be suitable for flow reactions, which is advantageous for large-scale, continuous production.

CNCs are biodegradable, but that does not necessarily imply that the functionalised CNCs will be and that should be investigated. The toxicity is another parameter that should be examined before moving to large-scale production.

The functionalisation displayed a great impact on the rheological behaviour of the CNCs. Although we have demonstrated that there is a great difference in viscosity when comparing functionalised CNCs and CNCs mixed with a model reaction, we have not looked into the rheological behaviour of unreacted mixtures of CNCs and dialkylamine reagents. Studying such mixtures could help further our understanding of the conjugations and the properties of the ionic and covalent bonds formed.

The conjugation has previously been demonstrated to work well with carboxylates, so a natural next step would be to try the conjugation with oxidised nanocelluloses, such as CNFs. This would open up for an even broader scope and possibilities to tune nanocellulose for almost any application.

ACKNOWLEDGEMENTS

There are a number of people I would like to thank, as without them this thesis would not have been possible:

First and foremost, my supervisor **Gunnar Westman** for welcoming me as a PhD student and for all your support, encouragement and guidance in the world of research and beyond and for all the ideas and interesting discussions through the years.

My examiner **Nina Kann**, for your positivity, and for always going the extra mile.

My co-supervisor **Merima Hasani** for your support, encouragement and for providing additional perspectives and thoughts.

All my co-authors for fruitful collaborations, with a special thanks to **Lilian Forsgren** and **Abhijit Venkatesh** for a great collaboration and **Mikaela Börjesson** for showing me the ropes.

The **management at Chemistry and Chemical Engineering** for all your help and patience.

Past and present colleagues in the **Westman group** and my friends and colleagues at **Chalmers University of Technology** (especially **Organic chemistry**), in the **Wallenberg Wood Science Center** and at **SIKT** for making me feel right at home, letting me borrow equipment, for all your help and for all the fika over the years.

My **family** and **friends** for all your support and encouragement. A special thanks to **my dad**, for your support and all that you have done for me. Last, but not least, **Alexandra** and **Henrik**, you mean everything to me, thank you for all your love, patience and support! ♥

REFERENCES

ANASTAS, P. & EGHBALI, N. 2010. Green Chemistry: Principles and Practice. *Chemical Society Reviews,* 39, 301-312.

ARAKI, J. & KUGA, S. 2001. Effect of Trace Electrolyte on Liquid Crystal Type of Cellulose Microcrystals. *Langmuir,* 17, 4493-4496.

ARAKI, J., WADA, M., KUGA, S. & OKANO, T. 1999. Influence of surface charge on viscosity behavior of cellulose microcrystal suspension. *J. Wood Sci.,* 45, 258-261.

ARIÑO, R. & BOLDIZAR, A. 2012. Processing and mechanical properties of thermoplastic composites based on cellulose fibers and ethylene—acrylic acid copolymer. *Polymer Engineering & Science,* 52, 1951-1957.

ATALLA, R. H., ATALLA, R. S. & AGARWAL, U. P. 2017. The Nanostructures of Native Celluloses, Their Transformations upon Isolation, and Their Implications for Production of Nanocelluloses. *Nanocelluloses: Their Preparation, Properties, and Applications.* American Chemical Society.

AZIZI SAMIR, M. A. S., ALLOIN, F., SANCHEZ, J.-Y. & DUFRESNE, A. 2004. Cellulose nanocrystals reinforced poly(oxyethylene). *Polymer,* 45, 4149-4157.

BAKALARZ-JEZIORNA, A., HELIŃSKI, J. & KRAWIECKA, B. 2001. Synthesis of multifunctionalized phosphonic acid esters via opening of oxiranes and azetidinium salts with phosphoryl-substituted carbanions. *J. Chem. Soc., Perkin Trans. 1,* 9, 1086-1090.

BECK-CANDANEDO, S., ROMAN, M. & GRAY, D. G. 2005. Effect of Reaction Conditions on the Properties and Behavior of Wood Cellulose Nanocrystal Suspensions. *Biomacromolecules,* 6, 1048-1054.

BECK, S. & BOUCHARD, J. 2014. Auto-catalyzed acidic desulfation of cellulose nanocrystals. *Nordic Pulp & Paper Research Journal,* 29, 006-014.

BONDESON, D., MATHEW, A. & OKSMAN, K. 2006. Optimization of the isolation of nanocrystals from microcrystalline cellulose by acid hydrolysis. *Cellulose,* 13, 171-180.

BRANDRUP, J., IMMERGUT, E. H., GRULKE, E. A., ABE, A. & BLOCH, D. R. 1999. *Polymer handbook*, Wiley New York.

BRAUN, B. & DORGAN, J. R. 2009. Single-Step Method for the Isolation and Surface Functionalization of Cellulosic Nanowhiskers. *Biomacromolecules,* 10, 334-341.

BÖRJESSON, M. & WESTMAN, G. 2016. Branching of hemicelluloses through an azetidinium salt ring-opening reaction. *Carbohydrate Research,* 428, 23-30.

BÖRJESSON, M. H., L.; NYLANDER, F.; KARLSSON, K.; LARSSON, A.; WESTMAN, G. 2018. Arabinoxylan and nanocellulose from a kilogram-scale extraction of barley husk. *BioResources,* 3, 6201-6220.

CAMARERO ESPINOSA, S., KUHNT, T., FOSTER, E. J. & WEDER, C. 2013. Isolation of Thermally Stable Cellulose Nanocrystals by Phosphoric Acid Hydrolysis. *Biomacromolecules,* 14, 1223-1230.

CAO, X., DONG, H. & LI, C. M. 2007. New Nanocomposite Materials Reinforced with Flax Cellulose Nanocrystals in Waterborne Polyurethane. *Biomacromolecules,* 8, 899-904.

CELLUFORCE. 2016. *NanoCrystalline Cellulose applications | CelluForce* [Online]. https://www.celluforce.com/en/markets/. [Accessed 29 December 2020].

CHARLTON, W., HAWORTH, W. N. & PEAT, S. 1926. XVII.—A revision of the structural formula of glucose. *Journal of the Chemical Society (Resumed),* 129, 89-101.

CHATTOPADHYAY, S., KEUL, H. & MOELLER, M. 2012. Functional Polymers Bearing Reactive Azetidinium Groups: Synthesis and Characterization. *Macromolecular Chemistry and Physics,* 213, 500-512.

CHAZEAU, L., CAVAILLÉ, J. Y., CANOVA, G., DENDIEVEL, R. & BOUTHERIN, B. 1999. Viscoelastic properties of plasticized PVC reinforced with cellulose whiskers. *Journal of Applied Polymer Science,* 71, 1797-1808.

CHEN, G., ZHANG, B., ZHAO, J. & CHEN, H. 2013. Improved process for the production of cellulose sulfate using sulfuric acid/ethanol solution. *Carbohydrate Polymers,* 95, 332-337.

COELHO, C. C. S., MICHELIN, M., CERQUEIRA, M. A., GONÇALVES, C., TONON, R. V., PASTRANA, L. M., FREITAS-SILVA, O., VICENTE, A. A., CABRAL, L. M. C. & TEIXEIRA, J. A. 2018. Cellulose nanocrystals from grape pomace: Production, properties and cytotoxicity assessment. *Carbohydrate Polymers,* 192, 327-336.

CONLEY, K., GODBOUT, L., WHITEHEAD, M. A. & VAN DE VEN, T. G. M. 2016. Origin of the twist of cellulosic materials. *Carbohydrate Polymers,* 135, 285-299.

COSGROVE, D. J. 2014. Re-constructing our models of cellulose and primary cell wall assembly. *Current Opinion in Plant Biology,* 22, 122-131.

CSISZÁR, E. & NAGY, S. 2017. A comparative study on cellulose nanocrystals extracted from bleached cotton and flax and used for casting films with glycerol and sorbitol plasticisers. *Carbohydrate Polymers,* 174**,** 740-749.

CUNKLE, G. T. D., DAVID; THOMPSON, THOMAS FRIEND. 2001. *Chlorohydrin and cationic compounds having high affinity for pulp or paper.*

D. KLEMM, B. P., T. HEINZE, U. HEINZE, W. WAGENKNECHT 2004. *Comprehensive Cellulose Chemistry: Fundamentals and Analytical Methods, Volume 1*, Wiley-VCH Verlag GmbH.

DAI, H., OU, S., HUANG, Y. & HUANG, H. 2018. Utilization of pineapple peel for production of nanocellulose and film application. *Cellulose,* 25**,** 1743-1756.

DENHAM, W. S. & WOODHOUSE, H. 1917. XXVII.—Trimethyl glucose from cellulose. *Journal of the Chemical Society, Transactions,* 111**,** 244-249.

DONG, X. M., KIMURA, T., REVOL, J.-F. & GRAY, D. G. 1996. Effects of Ionic Strength on the Isotropic–Chiral Nematic Phase Transition of Suspensions of Cellulose Crystallites. *Langmuir,* 12**,** 2076-2082.

DUFRESNE, A. 2017. Cellulose nanomaterial reinforced polymer nanocomposites. *Current Opinion in Colloid & Interface Science,* 29**,** 1-8.

EL-SAKHAWY, M. & HASSAN, M. L. 2007. Physical and mechanical properties of microcrystalline cellulose prepared from agricultural residues. *Carbohydrate Polymers,* 67**,** 1-10.

ELAZZOUZI-HAFRAOUI, S., NISHIYAMA, Y., PUTAUX, J. L., HEUX, L., DUBREUIL, F. & ROCHAS, C. 2008. The shape and size distribution of crystalline nanoparticles prepared by acid hydrolysis of native cellulose. *Biomacromolecules,* 9**,** 57-65.

EYLEY, S. & THIELEMANS, W. 2014. Surface modification of cellulose nanocrystals. *Nanoscale,* 6**,** 7764-7779.

FAN, L.-T., GHARPURAY, M. M. & LEE, Y.-H. 1987. Acid Hydrolysis of Cellulose. *Cellulose Hydrolysis.* Berlin, Heidelberg: Springer Berlin Heidelberg.

FILSON, P. B. & DAWSON-ANDOH, B. E. 2009. Sono-chemical preparation of cellulose nanocrystals from lignocellulose derived materials. *Bioresource Technology,* 100**,** 2259-2264.

FOSTER, E. J., MOON, R. J., AGARWAL, U. P., BORTNER, M. J., BRAS, J., CAMARERO-ESPINOSA, S., CHAN, K. J., CLIFT, M. J. D., CRANSTON, E. D., EICHHORN, S. J., FOX, D. M., HAMAD, W. Y., HEUX, L., JEAN, B., KOREY, M., NIEH, W., ONG, K. J., REID, M. S., RENNECKAR, S., ROBERTS, R., SHATKIN, J. A., SIMONSEN, J., STINSON-BAGBY, K., WANASEKARA, N. & YOUNGBLOOD, J. 2018. Current characterization methods for cellulose nanomaterials. *Chemical Society Reviews,* 47**,** 2609-2679.

FRENCH, A. D. 2017. Glucose, not cellobiose, is the repeating unit of cellulose and why that is important. *Cellulose,* 24**,** 4605-4609.

GAN, P. G., SAM, S. T., ABDULLAH, M. F. B. & OMAR, M. F. 2020. Thermal properties of nanocellulose-reinforced composites: A review. *Journal of Applied Polymer Science,* 137, 48544.

GARCIA DE RODRIGUEZ, N. L., THIELEMANS, W. & DUFRESNE, A. 2006. Sisal cellulose whiskers reinforced polyvinyl acetate nanocomposites. *Cellulose,* 13, 261-270.

GLASSER, W. G., ATALLA, R. H., BLACKWELL, J., MALCOLM BROWN, R., BURCHARD, W., FRENCH, A. D., KLEMM, D. O. & NISHIYAMA, Y. 2012. About the structure of cellulose: debating the Lindman hypothesis. *Cellulose,* 19, 589-598.

GRUNERT, M. & WINTER, W. T. 2002. Nanocomposites of Cellulose Acetate Butyrate Reinforced with Cellulose Nanocrystals. *Journal of Polymers and the Environment,* 10, 27-30.

GUERRIERO, G., FUGELSTAD, J. & BULONE, V. 2010. What Do We Really Know about Cellulose Biosynthesis in Higher Plants? *Journal of Integrative Plant Biology,* 52, 161-175.

HABIBI, Y. 2014. Key advances in the chemical modification of nanocelluloses. *Chemical Society Reviews,* 43, 1519-1542.

HABIBI, Y. & DUFRESNE, A. 2008. Highly Filled Bionanocomposites from Functionalized Polysaccharide Nanocrystals. *Biomacromolecules,* 9, 1974-1980.

HABIBI, Y., LUCIA, L. A. & ROJAS, O. J. 2010. Cellulose Nanocrystals: Chemistry, Self-Assembly, and Applications. *Chemical Reviews,* 110, 3479-3500.

HAIGLER, C. H. & ROBERTS, A. W. 2019. Structure/function relationships in the rosette cellulose synthesis complex illuminated by an evolutionary perspective. *Cellulose,* 26, 227-247.

HAMAD, W. Y. & HU, T. Q. 2010. Structure–process–yield interrelations in nanocrystalline cellulose extraction. *The Canadian Journal of Chemical Engineering,* 88, 392-402.

HARPER, B. J., CLENDANIEL, A., SINCHE, F., WAY, D., HUGHES, M., SCHARDT, J., SIMONSEN, J., STEFANIAK, A. B. & HARPER, S. L. 2016. Impacts of chemical modification on the toxicity of diverse nanocellulose materials to developing zebrafish. *Cellulose,* 23, 1763-1775.

HASANI, M., CRANSTON, E. D., WESTMAN, G. & GRAY, D. G. 2008. Cationic surface functionalization of cellulose nanocrystals. *Soft Matter,* 4, 2238-2244.

HAWORTH, W. N. 1925. A Revision of the Structural Formula of Glucose. *Nature,* 116, 430.

HAWORTH, W. N. & MACHEMER, H. 1932. 323. Polysaccharides. Part X. Molecular structure of cellulose. *Journal of the Chemical Society (Resumed),* 2270-2277.

HEARLE, J. W. S. 1958. A fringed fibril theory of structure in crystalline polymers. *Journal of Polymer Science,* 28, 432-435.

HERRMANN, K., GERNGROSS, O. & ABITZ, W. 1930. Zur röntgenographischen Strukturerforschung des Gelatinemicells. *Zeitschrift für Physikalische Chemie,* 10B, 371-394.

HEUX, L., CHAUVE, G. & BONINI, C. 2000. Nonflocculating and Chiral-Nematic Self-ordering of Cellulose Microcrystals Suspensions in Nonpolar Solvents. *Langmuir,* 16, 8210-8212.

HIGGINS, R. H., FAIRCLOTH, W. J., BAUGHMAN, R. G. & EATON, Q. L. 1994. Ring Opening of Azetidinols by Phenols: Regiochemistry and Stereochemistry. *J. Org. Chem.,* 59, 2172-2178.

HUBBE, M. A., VENDITTI, R. A. & ROJAS, O. J. 2007. What Happens to Cellulosic Fibers During Papermaking and Recycling? A Review. *BioResources; Vol 2, No 4 (2007).*

HULT, E. L., LARSSON, P. T. & IVERSEN, T. 2001. Cellulose fibril aggregation — an inherent property of kraft pulps. *Polymer,* 42, 3309-3314.

IDSTRÖM, A., BRELID, H., NYDÉN, M. & NORDSTIERNA, L. 2013. CP/MAS 13C NMR study of pulp hornification using nanocrystalline cellulose as a model system. *Carbohydrate Polymers,* 92, 881-884.

IRVINE, J. C. & HIRST, E. L. 1922. CXLV.—2 : 3 : 6-Trimethyl glucose. *Journal of the Chemical Society, Transactions,* 121, 1213-1223.

IRVINE, J. C. & HIRST, E. L. 1923. LXIV.-The constitution of polysaccharides. Part VI. The molecular structure of cotton cellulose. *Journal of the Chemical Society, Transactions,* 123, 518-532.

ISO 1133-1. 2011. Plastics — Determination of the melt mass-flow rate (MFR) and melt volume-flow rate (MVR) of thermoplastics.

ISO 21400. 2018. Pulp — Determination of cellulose nanocrystal sulfur and sulfate half-ester content.

ISO/TS 20477. 2017. Nanotechnologies — Standard terms and their definition for cellulose nanomaterial.

JAKOB, H. F., FRATZL, P. & TSCHEGG, S. E. 1994. Size and Arrangement of Elementary Cellulose Fibrils in Wood Cells: A Small-Angle X-Ray Scattering Study of Picea abies. *Journal of Structural Biology,* 113, 13-22.

JEZIORNA, A., HELIŃSKI, J. & KRAWIECKA, B. 2003. Synthesis of polyfunctional phosphorodithioates and structural analogues mediated by azetidinium ions and epoxides. *Tetrahedron Letters,* 44, 3239-3243.

JIANG, F., ESKER, A. R. & ROMAN, M. 2010. Acid-Catalyzed and Solvolytic Desulfation of H2SO4-Hydrolyzed Cellulose Nanocrystals. *Langmuir,* 26, 17919-17925.

JIANG, F. & HSIEH, Y.-L. 2015. Cellulose nanocrystal isolation from tomato peels and assembled nanofibers. *Carbohydrate Polymers,* 122, 60-68.

KING, A. W. T., MÄKELÄ, V., KEDZIOR, S. A., LAAKSONEN, T., PARTL, G. J., HEIKKINEN, S., KOSKELA, H., HEIKKINEN, H. A., HOLDING, A. J., CRANSTON,

E. D. & KILPELÄINEN, I. 2018. Liquid-State NMR Analysis of Nanocelluloses. *Biomacromolecules,* 19, 2708-2720.

KLEMM, D., HEUBLEIN, B., FINK, H.-P. & BOHN, A. 2005. Cellulose: Fascinating Biopolymer and Sustainable Raw Material. *Angewandte Chemie International Edition,* 44, 3358-3393.

KLEMM, D., KRAMER, F., MORITZ, S., LINDSTRÖM, T., ANKERFORS, M., GRAY, D. & DORRIS, A. 2011. Nanocelluloses: A New Family of Nature-Based Materials. *Angewandte Chemie International Edition,* 50, 5438-5466.

KONTTURI, E. & VUORINEN, T. 2009. Indirect evidence of supramolecular changes within cellulose microfibrils of chemical pulp fibers upon drying. *Cellulose,* 16, 65-74.

KRAUKLIS, A. E. & ECHTERMEYER, A. T. 2018. Mechanism of Yellowing: Carbonyl Formation during Hygrothermal Aging in a Common Amine Epoxy. *Polymers,* 10, 1017.

KRISHNA REDDY, V. V. R. M., UDAYKIRAN, D., CHINTAMANI, U. S., MAHESH REDDY, E., KAMESWARARAO, C. & MADHUSUDHAN, G. 2011. Development of an Optimized Process for the Preparation of 1-Benzylazetidin-3-ol: An Industrially Important Intermediate for Substituted Azetidine. *Organic Process Research & Development,* 15, 462-466.

KUMAR, N. AND KUMBHAT, S. 2016. Unique Properties. In Essentials in Nanoscience and Nanotechnology (eds N. Kumar and S. Kumbhat).

LEE, K.-Y., AITOMÄKI, Y., BERGLUND, L. A., OKSMAN, K. & BISMARCK, A. 2014. On the use of nanocellulose as reinforcement in polymer matrix composites. *Composites Science and Technology,* 105, 15-27.

LI, C.-J. & CHEN, L. 2006. Organic chemistry in water. *Chemical Society Reviews,* 35, 68-82.

LI, D., HENSCHEN, J. & EK, M. 2017. Esterification and hydrolysis of cellulose using oxalic acid dihydrate in a solvent-free reaction suitable for preparation of surface-functionalised cellulose nanocrystals with high yield. *Green Chemistry,* 19, 5564-5567.

LINDSTRÖM, U. M. 2008. *Organic reactions in water: principles, strategies and applications*, John Wiley & Sons.

LU, P. & HSIEH, Y.-L. 2012. Preparation and characterization of cellulose nanocrystals from rice straw. *Carbohydrate Polymers,* 87, 564-573.

LUZI, F., FORTUNATI, E., PUGLIA, D., LAVORGNA, M., SANTULLI, C., KENNY, J. M. & TORRE, L. 2014. Optimized extraction of cellulose nanocrystals from pristine and carded hemp fibres. *Industrial Crops and Products,* 56, 175-186.

MARX-FIGINI, M. 1969. Untersuchungen zur biosynthese der cellulose in der alge valonia. *Biochimica et Biophysica Acta (BBA) - General Subjects,* 177, 27-34.

MEDRONHO, B., ROMANO, A., MIGUEL, M. G., STIGSSON, L. & LINDMAN, B. 2012. Rationalizing cellulose (in)solubility: reviewing basic physicochemical aspects and role of hydrophobic interactions. *Cellulose,* 19**,** 581-587.

MELIKOĞLU, A. Y., BILEK, S. E. & CESUR, S. 2019. Optimum alkaline treatment parameters for the extraction of cellulose and production of cellulose nanocrystals from apple pomace. *Carbohydrate Polymers,* 215**,** 330-337.

MOON, R. J., MARTINI, A., NAIRN, J., SIMONSEN, J. & YOUNGBLOOD, J. 2011. Cellulose nanomaterials review: structure, properties and nanocomposites. *Chemical Society Reviews,* 40**,** 3941-3994.

NEWMAN, R. H. 2004. Carbon-13 NMR evidence for cocrystallization of cellulose as a mechanism for hornification of bleached kraft pulp. *Cellulose,* 11**,** 45-52.

NICKERSON, R. F. & HABRLE, J. A. 1947. Cellulose Intercrystalline Structure. *Industrial & Engineering Chemistry,* 39**,** 1507-1512.

NIELSEN, L. E. 1974. *Mechanical properties of polymers and composites*, Dekker.

NOBEL MEDIA AB. 14 October 1987. [Press release] https://www.nobelprize.org/prizes/chemistry/1987/press-release/. [Accessed 2 January 2021]

O'SULLIVAN, A. C. 1997. Cellulose: the structure slowly unravels. *Cellulose,* 4**,** 173-207.

OBOKATA, T. & ISOGAI, A. 2007. The mechanism of wet-strength development of cellulose sheets prepared with polyamideamine-epichlorohydrin (PAE) resin. *Colloid Surface A,* 302**,** 525-531.

ORTS, W. J., SHEY, J., IMAM, S. H., GLENN, G. M., GUTTMAN, M. E. & REVOL, J.-F. 2005. Application of Cellulose Microfibrils in Polymer Nanocomposites. *Journal of Polymers and the Environment,* 13**,** 301-306.

PARZUCHOWSKI, P. G., ŚWIDERSKA, A., ROGUSZEWSKA, M., FRĄCZKOWSKI, T. & TRYZNOWSKI, M. 2018. Amine functionalized polyglycerols obtained by copolymerization of cyclic carbonate monomers. *Polymer,* 151**,** 250-260.

PAYEN, A. 1838. Mémoire sur la composition du tissu propre des plantes et du ligneux. *Comptes Rendus,* 7**,** 1052–1056.

PÉREZ, S. & MAZEAU, K. 2004. Conformations, Structures, and Morphologies of Celluloses. *In:* DUMITRIU, S. (ed.) *Polysaccharides: Structural Diversity and Functional Versatility, Second Edition.* Boca Raton: CRC Press.

PROCESSUM, R. 2015. *Europe's first pilot facility for nanocrystalline cellulose - RISE Processum* [Online]. https://www.processum.se/en/sp-processum/information/news-archive/1376-europe-s-first-pilot-facility-for-nanocrystalline-cellulose. [Accessed 29 December 2020].

REDDY, N. & YANG, Y. 2015. The N-Methylmorpholine-N-Oxide (NMMO) Process of Producing Regenerated Fibers. *Innovative Biofibers from Renewable Resources.* Berlin, Heidelberg: Springer Berlin Heidelberg.

REVOL, J.-F., GODBOUT, L., DONG, X.-M., GRAY, D. G., CHANZY, H. & MARET, G. 1994. Chiral nematic suspensions of cellulose crystallites; phase separation and magnetic field orientation. *Liquid Crystals,* 16, 127-134.

REVOL, J. F. 1982. On the cross-sectional shape of cellulose crystallites in Valonia ventricosa. *Carbohydrate Polymers,* 2, 123-134.

REVOL, J. F., BRADFORD, H., GIASSON, J., MARCHESSAULT, R. H. & GRAY, D. G. 1992. Helicoidal self-ordering of cellulose microfibrils in aqueous suspension. *International Journal of Biological Macromolecules,* 14, 170-172.

REVOL, J. F. & MARCHESSAULT, R. H. 1993. In vitro chiral nematic ordering of chitin crystallites. *International Journal of Biological Macromolecules,* 15, 329-335.

ROMAN, M. 2015. Toxicity of Cellulose Nanocrystals: A Review. *Industrial Biotechnology,* 11, 25-33.

ROMAN, M. & WINTER, W. T. 2004. Effect of Sulfate Groups from Sulfuric Acid Hydrolysis on the Thermal Degradation Behavior of Bacterial Cellulose. *Biomacromolecules,* 5, 1671-1677.

ROSS, J. H., BAKER, D. & COSCIA, A. T. 1964. Some Reactions of Epichlorohydrin with Amines. *J. Org. Chem.,* 29, 824-826.

ROWLAND, S. P. & ROBERTS, E. J. 1972. The nature of accessible surfaces in the microstructure of cotton cellulose. *Journal of Polymer Science Part A-1: Polymer Chemistry,* 10, 2447-2461.

RÅNBY, B. G. 1949. Aqueous Colloidal Solutions of Cellulose Micelles. *Acta Chemica Scandinavica,* 3, 649-650.

SADEGHIFAR, H., FILPPONEN, I., CLARKE, S. P., BROUGHAM, D. F. & ARGYROPOULOS, D. S. 2011. Production of cellulose nanocrystals using hydrobromic acid and click reactions on their surface. *Journal of Materials Science,* 46, 7344-7355.

SALAS, C., NYPELÖ, T., RODRIGUEZ-ABREU, C., CARRILLO, C. & ROJAS, O. J. 2014. Nanocellulose properties and applications in colloids and interfaces. *Current Opinion in Colloid & Interface Science,* 19, 383-396.

SHAFIZADEH, F. & BRADBURY, A. G. W. 1979. Thermal degradation of cellulose in air and nitrogen at low temperatures. *Journal of Applied Polymer Science,* 23, 1431-1442.

SIQUEIRA, E. J., SALON, M.-C. B., BELGACEM, M. N. & MAURET, E. 2015. Carboxymethylcellulose (CMC) as a model compound of cellulose fibers and polyamideamine epichlorohydrin (PAE)–CMC interactions as a model of PAE–fibers interactions of PAE-based wet strength papers. *J. Appl. Polym. Sci.,* 132, 42144.

SIQUEIRA, G., BRAS, J. & DUFRESNE, A. 2009. Cellulose Whiskers versus Microfibrils: Influence of the Nature of the Nanoparticle and its Surface Functionalization on the Thermal and Mechanical Properties of Nanocomposites. *Biomacromolecules,* 10, 425-432.

SIXTA, H., MICHUD, A., HAURU, L., ASAADI, S., MA, Y., KING, A. W. T., KILPELÄINEN, I. & HUMMEL, M. 2015. Ioncell-F: A High-strength regenerated cellulose fibre. *Nordic Pulp & Paper Research Journal,* 30, 43-57.

SJÖSTRÖM, E. 1993. *Wood Chemistry (Second Edition),* San Diego, Academic Press.

SMYTH, M., GARCÍA, A., RADER, C., FOSTER, E. J. & BRAS, J. 2017. Extraction and process analysis of high aspect ratio cellulose nanocrystals from corn (Zea mays) agricultural residue. *Industrial Crops and Products,* 108, 257-266.

STAUDINGER, H., JOHNER, H., SIGNER, R., MIE, G. & HENGSTENBERG, J. 1927. Der polymere Formaldehyd, ein Modell der Zellulose. *Zeitschrift für Physikalische Chemie.*

STRØMME, M., MIHRANYAN, A. & EK, R. 2002. What to do with all these algae? *Materials Letters,* 57, 569-572.

SUGIYAMA, J., CHANZY, H. & MARET, G. 1992. Orientation of cellulose microcrystals by strong magnetic fields. *Macromolecules,* 25, 4232-4234.

UNITED STATES NATIONAL NANOTECHNOLOGY INITIATIVE. *Nanotechnology Timeline* [Online]. https://www.nano.gov/timeline. [Accessed 2020-12-29 2020].

VENKATESH, A., THUNBERG, J., MOBERG, T., KLINGBERG, M., HAMMAR, L., PETERSON, A., MÜLLER, C. & BOLDIZAR, A. 2018. Cellulose nanofibril-reinforced composites using aqueous dispersed ethylene-acrylic acid copolymer. *Cellulose,* 25, 4577-4589.

WANG, N., DING, E. & CHENG, R. 2007. Thermal degradation behaviors of spherical cellulose nanocrystals with sulfate groups. *Polymer,* 48, 3486-3493.

YU, H., QIN, Z., LIANG, B., LIU, N., ZHOU, Z. & CHEN, L. 2013. Facile extraction of thermally stable cellulose nanocrystals with a high yield of 93% through hydrochloric acid hydrolysis under hydrothermal conditions. *Journal of Materials Chemistry A,* 1, 3938-3944.

ZHANG, H., CHEN, Y., WANG, S., MA, L., YU, Y., DAI, H. & ZHANG, Y. 2020. Extraction and comparison of cellulose nanocrystals from lemon (Citrus limon) seeds using sulfuric acid hydrolysis and oxidation methods. *Carbohydrate Polymers,* 238, 116180.

A.1 Conductometric Titration Data Processing

The surface charge was calculated graphically from the intersect points determined by plotting the conductivity against the volume of added NaOH solution. For the acidic surface charges there will be an intersect point (inflection) between the initial decreasing slope and the increasing slope (Foster et al., 2018) and for the weak surface charges the charge is determined from the second intersect point, between the plateau and the increasing slope, subtracting any NaOH required for any acidic groups present. The surface charges (mmol charge per kg CNC) are calculated using:

$$Amount\ of\ strong\ acid\ groups = \frac{V_{NaOH\ 1st\ intersect} * c_{NaOH}}{m_{CNC}} \qquad Eq.\ A1$$

$$Amount\ of\ weak\ acid/base\ groups = \frac{(V_{NaOH\ 2nd\ intersect} - V_{NaOH\ 1st\ intersect}) * c_{NaOH}}{m_{CNC}} \qquad Eq.\ A2$$

where c_{NaOH} is the concentration of the sodium hydroxide solution, m_{CNC} is the dry weight of the CNCs and $V_{NaOH\ 1st\ intersect}$ and $V_{NaOH\ 2nd\ intersect}$ are the volumes of sodium hydroxide required to neutralise the strong acid groups and weak acid/base groups respectively, which are calculated from the slope and intersects according to

$$V_{NaOH\ 1st\ intersect} = \frac{intersept_{base\ or\ plateau} - intersept_{acid}}{slope_{acid} - slope_{base\ or\ plateau}} \qquad Eq.\ A3$$

$$V_{NaOH\ 2n\ \ intersect} = \frac{intersept_{base} - intersept_{plateau}}{slope_{plateau} - slope_{base}} \qquad Eq.\ A4$$

In a typical titration curve for a sample containing strong acid groups, the conductivity initially decreases as the protons associated to the strong acidic surface groups are consumed by the added OH⁻, see Figure 3.1 a) and b). Once the strong acid groups have been neutralised, the equivalence point is reached and any additional base added will, if no weak acid or base groups are present, merely increase the ion concentration leading to an increase in conductivity. When weak acid and base groups are present, a plateau will appear as they are neutralised, see Figure 3.1 b) and c).

The conductivity was corrected for the increasing total volume during the measurement accordingly:

$$\kappa_c = \kappa_m * \left(\frac{V_i + V_0}{V_i}\right) \qquad\qquad Eq.\,A5$$

where κ_c is the corrected conductivity (μS/cm), κ_m is the measured conductivity (μS/cm), V_i (mL) is the initial volume of the suspension prior, and V_0 (mL) is the total added volume of NaOH solution at each data point (mL).

A.2 Cellulose Nanocrystal Properties Data

Table A1. Compilation of sulphate and amine contents, determined by elemental analysis or conductometric titration and the onset of thermal degradation determined from TGA of the dialkylamine functionalised and non-functionalised CNCs presented in this thesis.

Sample		Sulphate half-ester content (µmol/g)	Amine content (µmol/g)	Onset of thermal degradation (°C)	Paper
CNC	Dialkylamine				
CNC-OH	-	0 [a]	-	277	
CNC-OSO$_3$H-part	-	146 [a]	-	158	I
CNC-OSO$_3$H	-	171 [a]	-	156	
CNC-OSO$_3$H-over	-	265 [a]	-	155	
CNC-OSO$_3$H	-	350 [b]	-	157	II & III
CNC-OSO$_3$H-self	-	129 [b]	-	156	
CNC-OH	-	20 [b]	-	201	
CNC-OSO$_3$H-part	-	136 [b]	-	152	IV
CNC-OSO$_3$H	-	187 [b]	-	152	
CNC-OSO$_3$H		216 [b]	-	-	
CNC-OH		0 [a]	0 [a]	-	
CNC-OSO$_3$H-part		0 [a]	43 [a]	-	
CNC-OSO$_3$H	DEA-AzOH	0 [a]	57 [a]	246	
CNC-OSO$_3$H-over		47 [a]	121 [a]	-	
CNC-OSO$_3$H	DEA-AzOMe	209 [a]	29 [a]	278	I
CNC-OH		6 [a]	50 [a]	-	
CNC-OSO$_3$H-part		14 6 [a]	228 [a]	-	
CNC-OSO$_3$H	DHA-AzOH	162 [a]	257 [a]	250	
CNC-OSO$_3$H-over		159 [a]	228 [a]	-	
CNC-OSO$_3$H	DHA-AzOMe	-	-	246	

CNC	Dialkylamine	Sulphate half-ester content (µmol/g)	Amine content (µmol/g)	Onset of thermal degradation (°C)	Paper
CNC-OSO$_3$H	M-AzOMe	215 [a], 102 [b]	357 [a]	250	
CNC-OSO$_3$H	DHA-AzOMe	352 [a], 180 [b]	378 [a]	246	II
CNC-OSO$_3$H	DAA-AzOMe	305 [a], 119 [b]	357 [a]	242	
CNC-OSO$_3$H	M-AzOH	-	-	224	
CNC-OSO$_3$H	DHA-AzOH	-	-	248	III
CNC-OSO$_3$H	DAA-AzOH	-	-	247	
CNC-OH	DAA-CC	63 [b]	0 [b]	244	
CNC-OSO$_3$H-part		78 [b]	83 [b]	213	
CNC-OSO$_3$H		97 [b]	101 [b]	213	
CNC-OH	DAA-AzOH	29 [b]	0 [b]	280	
CNC-OSO$_3$H-part		41 [b]	61 [b]	222	
CNC-OSO$_3$H		79 [b]	106 [b]	220	
CNC-OH	DAA-AC	37 [b]	0 [b]	248	
CNC-OSO$_3$H-part		81 [b]	68 [b]	218	IV
CNC-OSO$_3$H		105 [b]	98 [b]	219	
CNC-OH	DAA-AC-alk	33 [b]	0 [b]	250	
CNC-OSO$_3$H-part		82 [b]	64 [b]	219	
CNC-OSO$_3$H		109 [b]	73 [b]	215	
CNC-OSO$_3$H	No reagent, 90 °C, 5, 15, 30 min, 2 h and 24 h	137 [b]	-	156	
		136 [b]	-	157	
		136 [b]	-	157	
		118 [b]	-	153	
		34 [b]	-	164	

Sample		Sulphate half-ester content (µmol/g)	Amine content (µmol/g)	Onset of thermal degradation (°C)	Paper
CNC	Dialkylamine				
CNC-OSO$_3$H	No reagent, 70 °C, 15, 30 min, 2 h, 5 h and 24 h	121 [b]	-	156	
		125 [b]	-	157	
		121 [b]	-	158	
		122 [b]	-	156	
		101 [b]	-	160	
CNC-OSO$_3$H	No reagent, 50 °C, 15, 30 min, 2 h, 5 h and 24 h	124 [b]	-	156	
		128 [b]	-	158	
		128 [b]	-	157	
		134 [b]	-	158	
		120 [b]	-	159	IV
CNC-OSO$_3$H	DAA-CC 5 min mixing	0	99	-	
CNC-OSO$_3$H	DAA-CC 5 min mixing ion exchange	212	0	-	
CNC-OSO$_3$H	DAA-CC mixing dialysis	117	0	-	
CNC-OSO$_3$H	DAA-CC 24 h mixing ion exchange	84	121	-	
CNC-OSO$_3$H	DAA-CC 90 °C, 20 min ion exchange	97	90	-	
CNC CelluForce	-	293 [b]	-	236	V
CNC CelluForce	DAA-CC			238	
CNC CelluForce	DAA-AzOH			263	-

[a] determined by elemental analysis

[b] determined by conductometric titration

A.3 CNC Composite Properties

Table A2. Compilation of the mechanical properties of the composite materials presented in this thesis.

Matrix	Reinforcing agent	Amount CNC (wt.-%)	Young's modulus (MPa)	Yield stress (MPa)	Ultimate tensile strength (MPa)	Elongation at break (%)	Paper
LLDPE	-	-	108 (13)		25 (4)	11 (2)	
LLDPE	CNC-OSO$_3$H	3.2[a]	216 (19)		18 (1)	8 (0)	
LLDPE	CNC-DEA-AzOMe	3.5[a]	211 (19)		14 (1)	7 (0)	I
LLDPE	CNC-DHA-AzOMe	2.9[a]	223 (11)		15 (1)	7 (1)	
LDPE	-	-	150 (7)	7 (0.1)	13 (0.3)	62 (3.6)	
LDPE	CNC-OSO$_3$Na	10	210 (2)	8.5 (0.3)	12.1 (0.3)	39.4 (1)	
LDPE	CelluForce-DAA-CC	10	209 (6)	9 (0.2)	12.6 (0.1)	38 (2.1)	
EAA7	-	-	109 (2)	5.7 (0.1)	16.8 (0.6)	90.6 (2.6)	V
EAA7	CNC-OSO$_3$Na	10	197 (14)	12.9 (0.3)	17.5 (0.3)	36.7 (3.6)	
EAA7	CelluForce-DAA-CC	10	166 (4)	8 (0.2)	16 (0.5)	59 (3.2)	
EAA7	CelluForce-DAA-AzOH	10	783 (27)	-	16 (0.3)	58 (8)	
EAA15	CNC-OSO$_3$Na	10	948 (35)	-	23 (0.2)	8 (0.7)	
EAA15	CelluForce-DAA-CC	10	544 (14)	14 (0.2)	17 (2)	115 (43)	-
EAA15	CelluForce-DAA-AzOH	10	697 (17)	16 (0.2)	22 (1)	206 (18)	
EAA15	-	-	322 (5)	15.1 (0.6)	25.8 (1.2)	255 (6)	III
EAA15	CNC-OSO$_3$H	10	921 (64)	-	21.9 (0.9)	6 (1)	
EAA15	CNC-M-AzOH	10	678 (46)	15.1 (0.4)	14.2 (2.3)	11 (10)	III
EAA15	CNC-DHA-AzOH	10	678 (21)	17.9 (0.4)	16.5 (1.0)	28 (15)	
EAA15	CNC-DAA-AzOH	10	864 (32)	21.1 (0.7)	19.7 (0.8)	31 (22)	
EAA15	CNC-OSO$_3$H	1	353 (18)	15.3 (0.5)	25.3 (1.7)	246 (7)	
EAA15	CNC-M-AzOH	1	367 (22)	15.2 (0.6)	23.4 (1.3)	252 (10)	III
EAA15	CNC-DHA-AzOH	1	295 (16)	14.1 (0.4)	23.7 (1.2)	267 (10)	
EAA15	CNC-DAA-AzOH	1	314 (21)	14.1 (0.6)	22.9 (1.0)	261 (10)	
EAA15	CNC-OSO$_3$H	0.1	270 (13)	13.5 (0.3)	24.5 (0.7)	278 (6)	
EAA15	CNC-M-AzOH	0.1	294 (28)	14.1 (0.5)	24.3 (0.8)	284 (11)	III
EAA15	CNC-DHA-AzOH	0.1	249 (24)	12.8 (0.6)	23.5 (1.4)	288 (15)	
EAA15	CNC-DAA-AzOH	0.1	237 (25)	12.1 (1.0)	21.2 (1.3)	276 (11)	

Table A3. Compilation of the crystallinity and colorimetry data for some of the composite materials presented in this thesis.

Matrix	Reinforcing agent	Crystallinity (%)	"Colour"				Paper
			CIEL*	CIEa*	CIEb*	Gloss (%)	
LLDPE	-	-	83.7	-1.3	6.8	82.8 (0.2)	
LLDPE	CNC-OSO$_3$H	-	-59.0 (0.1)	1.3 (0)	-7.2 (0)	79.1 (5.3)	I
LLDPE	CNC-DEA-AzOMe	-	-3.6 (0.2)	0.1 (0)	3 (0.1)	80.9 (6.8)	
LLDPE	CNC-DHA-AzOMe	-	-2 (0.2)	-0.2 (0)	1.5 (0.1)	86 (1.6)	
LDPE	-	22 (0.6)	77.3 (0.5)	2.6 (0.1)	-4.6 (0.3)	26.7 (1.0)	
LDPE	CNC-OSO$_3$Na [a]	21 (0.6)	68.2 (0.7)	2.2 (0.2)	13.2 (0.7)	22.8 (2.2)	
LDPE	CelluForce-DAA-CC [a]	20 (0.9)	69.1 (0.3)	0.9 (0.1)	13.2 (0.6)	26.1 (2.4)	V
EAA7	-	16 (1.0)	84.0 (0.1)	2.5 (0)	-3.5 (0.1)	26.9 (3.7)	
EAA7	CNC-OSO$_3$Na [a]	16 (1.1)	58.9 (0.1)	4.7 (0)	21.3 (0.1)	19.9 (0.8)	
EAA7	CelluForce-DAA-CC [a]	14 (0.1)	52.2 (0.9)	6.0 (0.2)	19.2 (0.3)	21.7 (1.8)	
EAA15	-	17	-	-	-	-	III
EAA15	CNC-OSO$_3$H [a]	18	-	-	-	-	
EAA15	CNC-M-AzOH [a]	18	-	-	-	-	
EAA15	CNC-DHA-AzOH [a]	15	-	-	-	-	III
EAA15	CNC-DAA-AzOH [a]	19	-	-	-	-	

[a] 10 wt.-% CNCs added.

A.4 Nuclear Magnetic Resonance Spectroscopy Data

NMR analysis of the diallyl substituted dialkylamine reagents. The following pages contain NMR spectra of the compounds presented in this thesis.

NMR analysis of 1-chloro-3-(diallylamino)propan-2-ol:

^{1}H NMR (400 MHz, CDCl$_3$). δ = 5.82 m (=CH), 5.18 broad t (=CH$_2$) *(J=16 Hz)*, 3.89 broad dddd (CHOH) (J=7 Hz), 3.52 m (CH$_2$Cl), 3.25 m (CH$_2$), 3.08 dd (CH$_2$) *(J=8, 16 Hz)*, 2.55 m (CH$_2$).

^{13}C NMR (101 MHz, CDCl$_3$). δ = 134.32 (=CH), 119.46 (=CH$_2$), 67.19 (CHOH), 57.06 (CH$_2$), 56.12 (CH$_2$), 47.10 (CH$_2$Cl) ppm.

NMR analysis of 4-((diallylamino)methyl)-1,3-dioxan-2-one)

^{1}H NMR (400 MHz, CDCl$_3$). δ = 5.77 dddd (=CH) *(J=6, 6, 10 and 17 Hz)*, 5.17 dddd (=CH$_2$) *(J=1, 1, 7 and 12 Hz)*, 4.75 dddd (CHOR) *(J=6, 7, 8 and 14 Hz)*, 4.46 dd (CH$_2$OR) *(J=7 and 8 Hz)*, 4.22 dd (CH$_2$OR) *(J=7 and 8 Hz)*, 3.13 dddd (CH$_2$) *(J=,1, 1, 6 and 14 Hz)* 2.74 d (CH$_2$) *(J=4 Hz)*.

^{13}C NMR (101 MHz, CDCl$_3$). δ = 155.11 (CO$_3$), 135.11 (=CH), 118.47 (=CH$_2$), 75.56 (CHOR), 68.07 (CH$_2$OR), 58.24 (CH$_2$), 54.76 (CH$_2$) ppm.

NMR analysis of *N,N*-diallyl-3-hydroxyazetidium chloride

^{1}H NMR (400 MHz, DMSO-*d₆*). δ = 6.67 m (OH), 5.99 m (=CH), 5.63 m (=CH$_2$), 4.62 ddd (CHOH) *(J=7, 14 and 14 Hz)*, 4.44 ddd (CH$_2$, ring) *(J=6, 6 and 12 Hz)*, 4.23 ddd (CH$_2$, ring) *(J=6, 6 and 12 Hz)*, 4.10 dd (CH$_2$) *(J=7 and 7 Hz)*, 3.95 dd (CH$_2$) *(J=7 and 7 Hz)*.

^{13}C NMR (101 MHz, DMSO-*d₆*). δ = 127.65 (=CH), 126.36 (=CH$_2$), 67.75 (CH$_2$, ring), 63.82 (CH$_2$), 61.83 (CH$_2$), 57.69 (CHOH, ring).

NMR analysis of *3-(diallylamino)propan-1,2-diol)*

^{1}H NMR (400 MHz, CDCl$_3$). δ = 5.74 m (=CH), 5.10 m (=CH$_2$), 3.72 dtd *(J=6, 12 and 18 Hz)* (CR$_2$HOH), 3.59 dd (CH$_2$) *(J=6 and 18 Hz)*, 3.42 dd (CH$_2$) *(J=6 and 17 Hz)*, 3.09 dddt (CH$_2$) *(J=1, 6, 18, 84 and 114 Hz)*, 2.53 dd (CRH$_2$OH) *(J=12 and 18 Hz)*, 2.40 dd (CRH$_2$OH) *(J=8 and 18 Hz)*.

^{13}C NMR (101 MHz, CDCl$_3$). δ = 134.50 (=CH), 118.39 (=CH$_2$), 67.80 (CR$_2$HOH), 65.08 (CH$_2$), 57.00 (CH$_2$), 55.66 (CRH$_2$OH) ppm

Diallyl alkylchloride (1-chloro-3-(diallylamino)propan-2-ol)

^{1}H NMR (400 MHz, CDCl$_3$)

^{13}C NMR (101 MHz, CDCl$_3$)
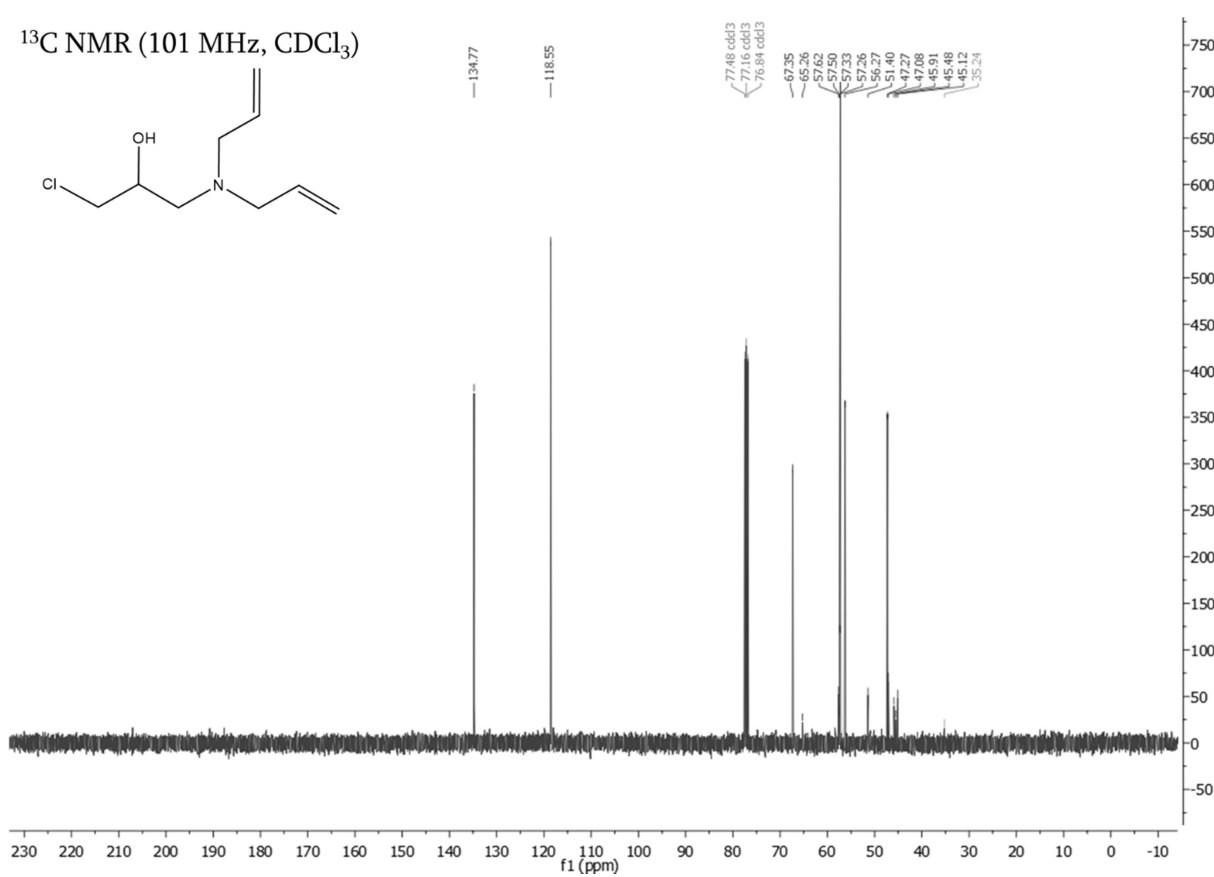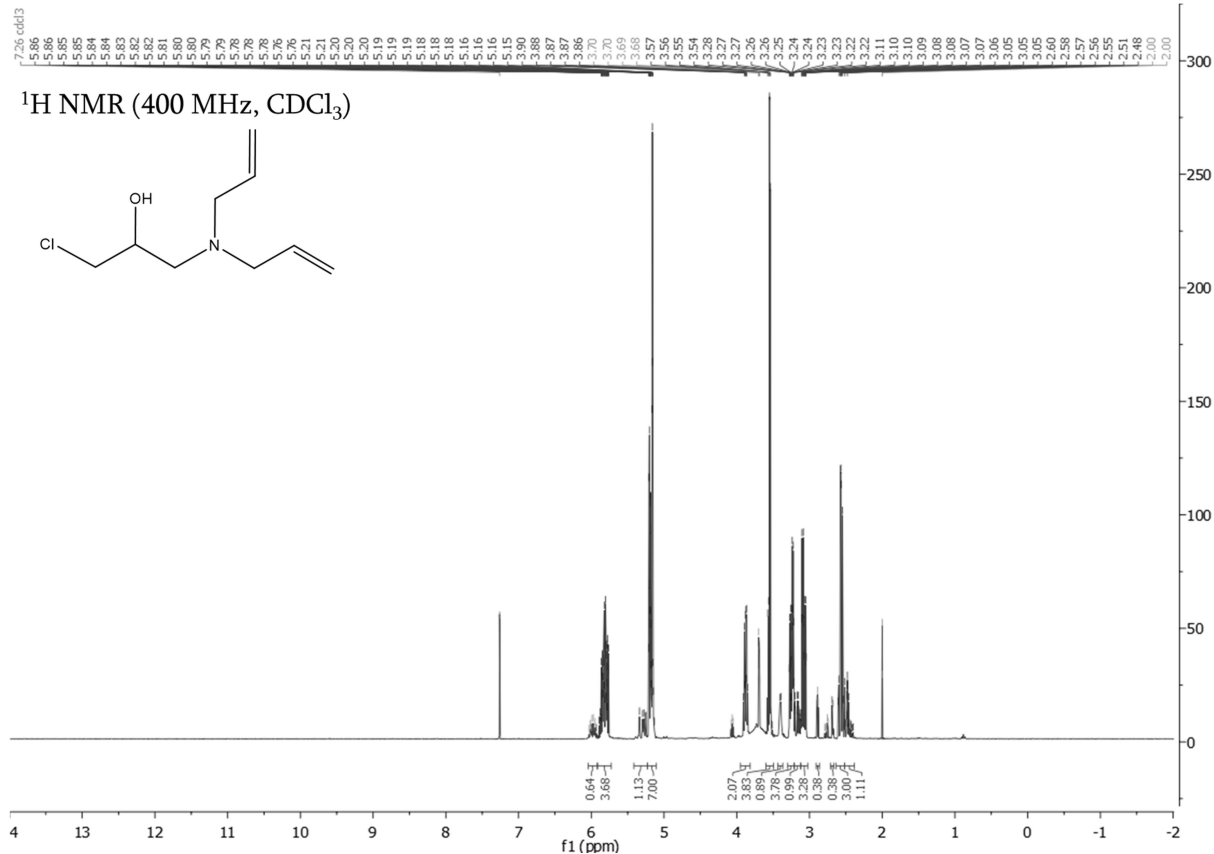
COSY

HSQC

Diallyl cyclocarbonate (4-((diallylamino)methyl)-1,3-dioxan-2-one)

^{1}H NMR (400 MHz, CDCl$_3$)

^{13}C NMR (101 MHz, CDCl$_3$)
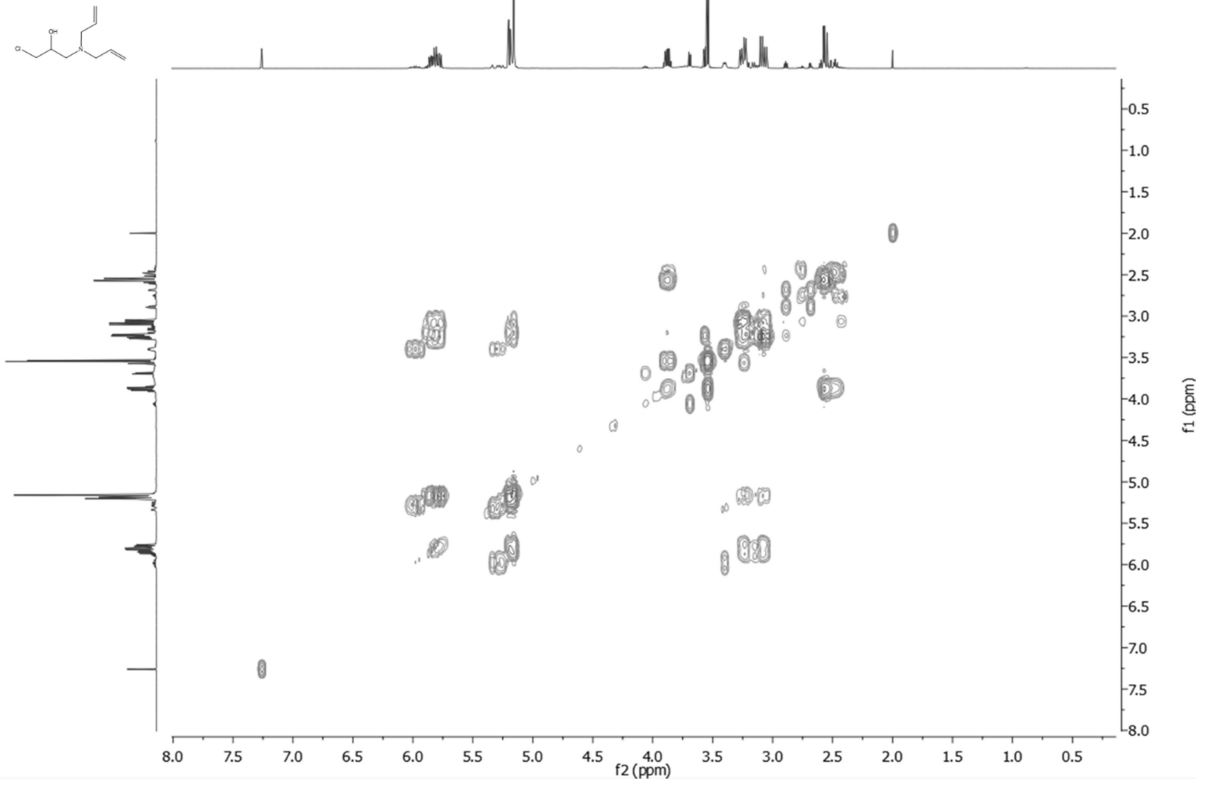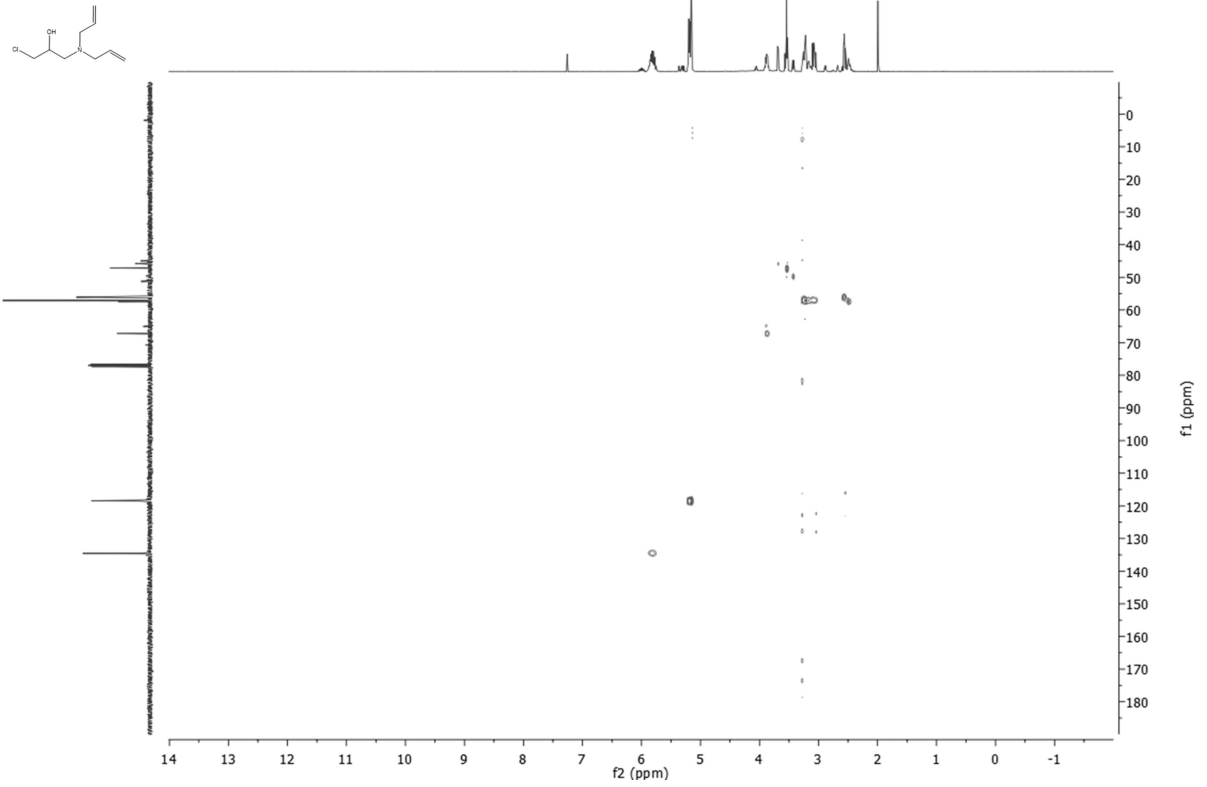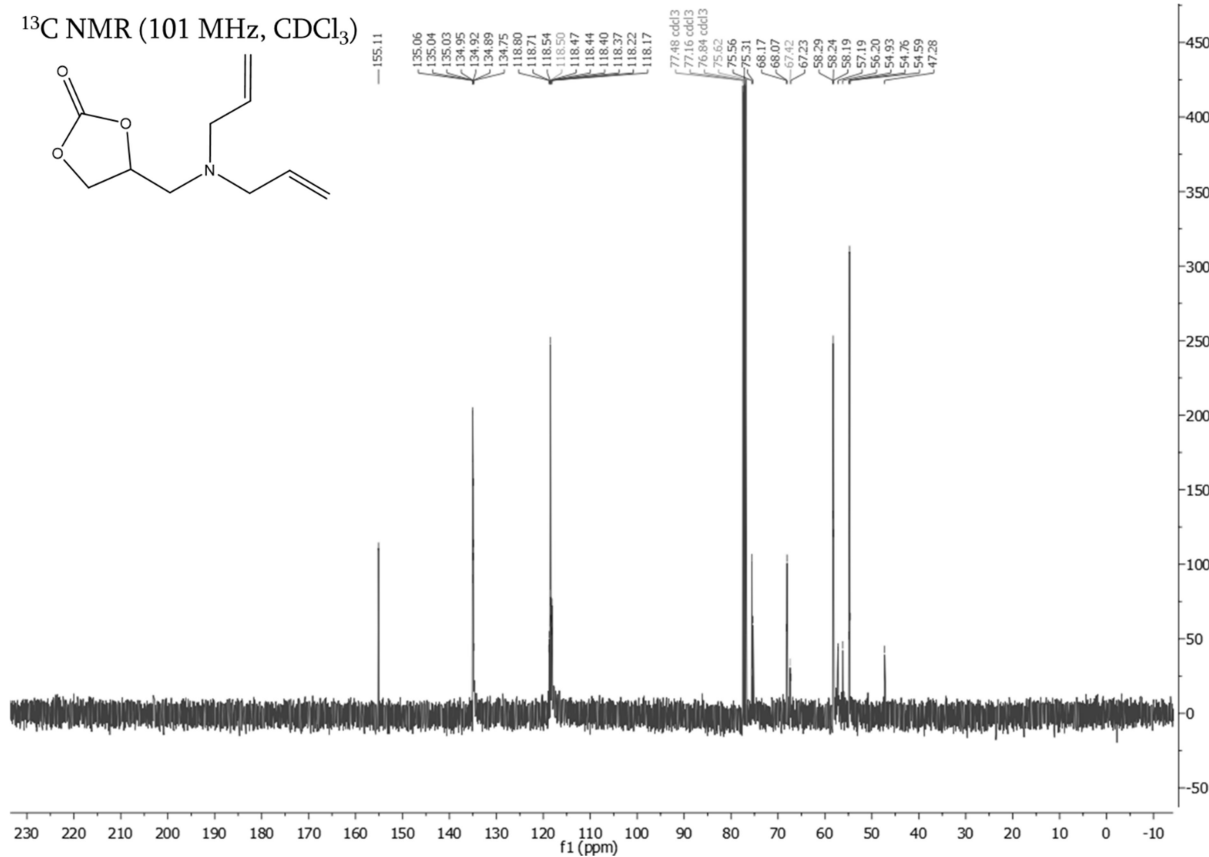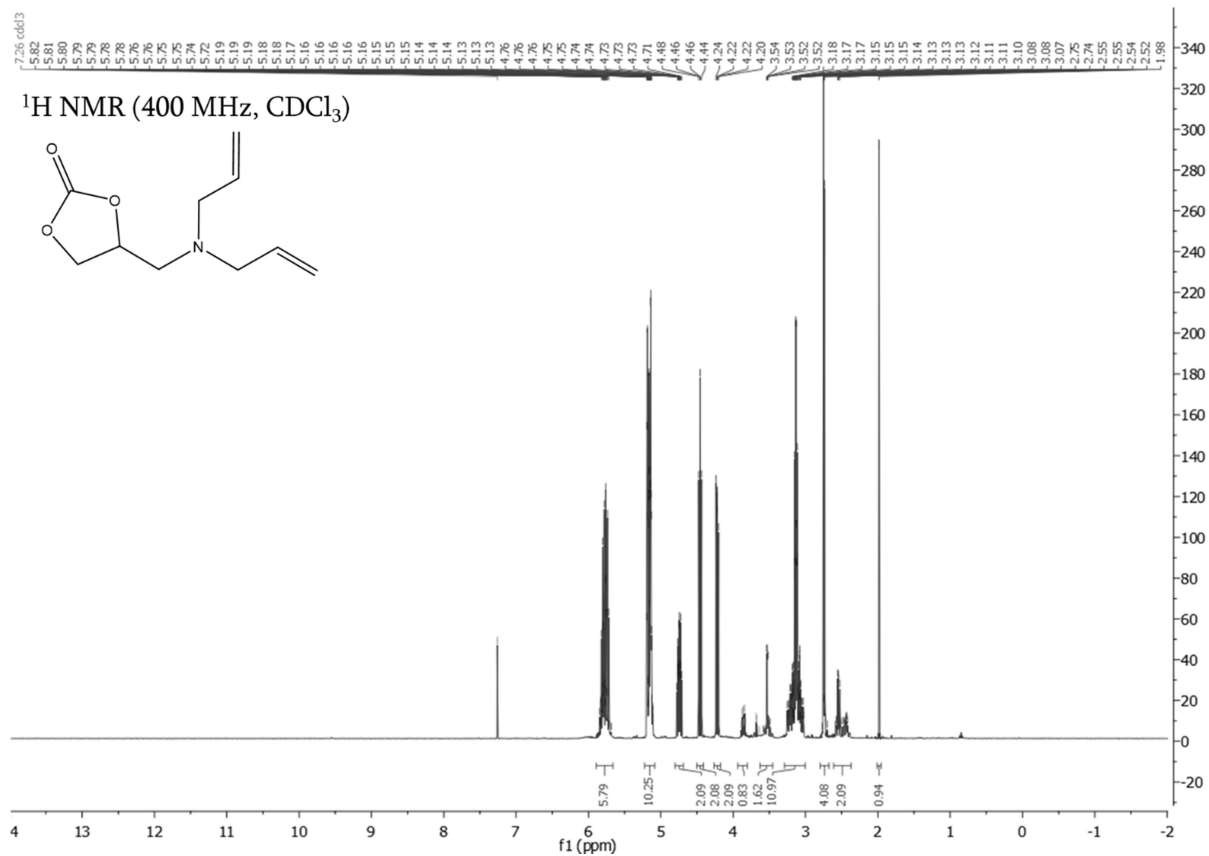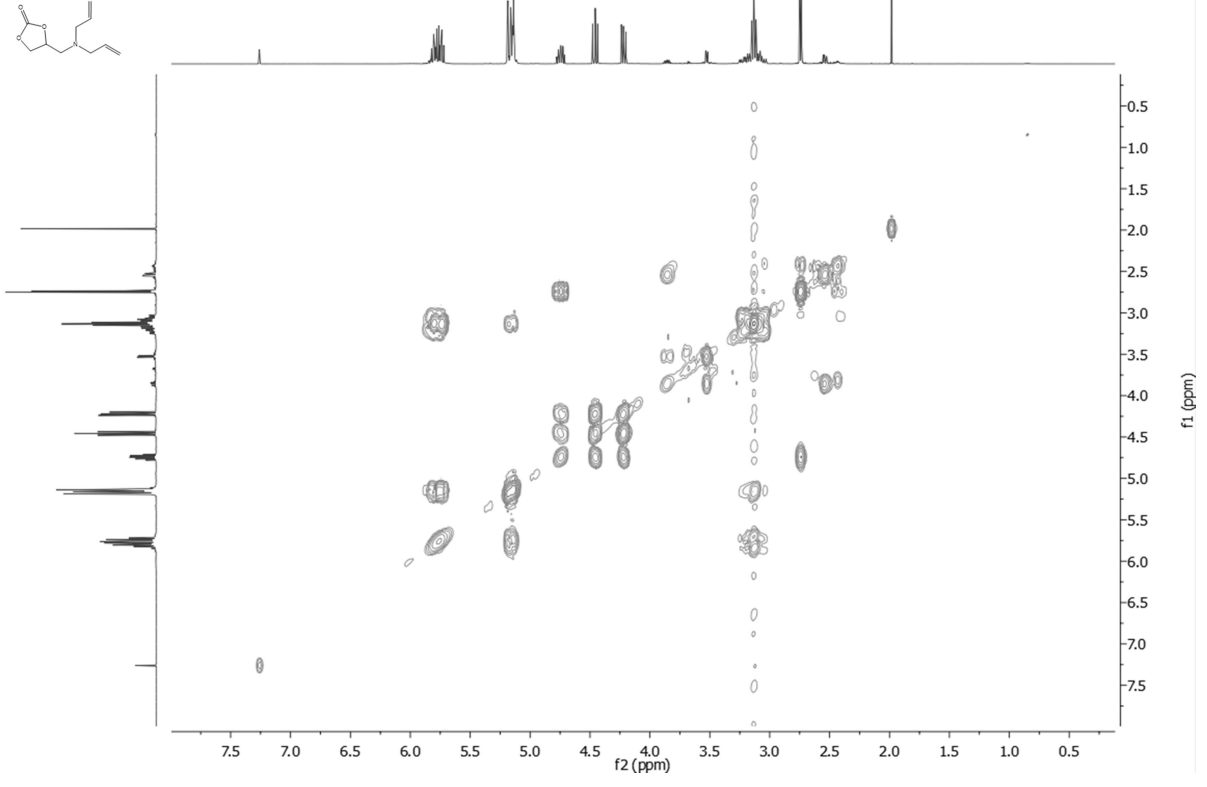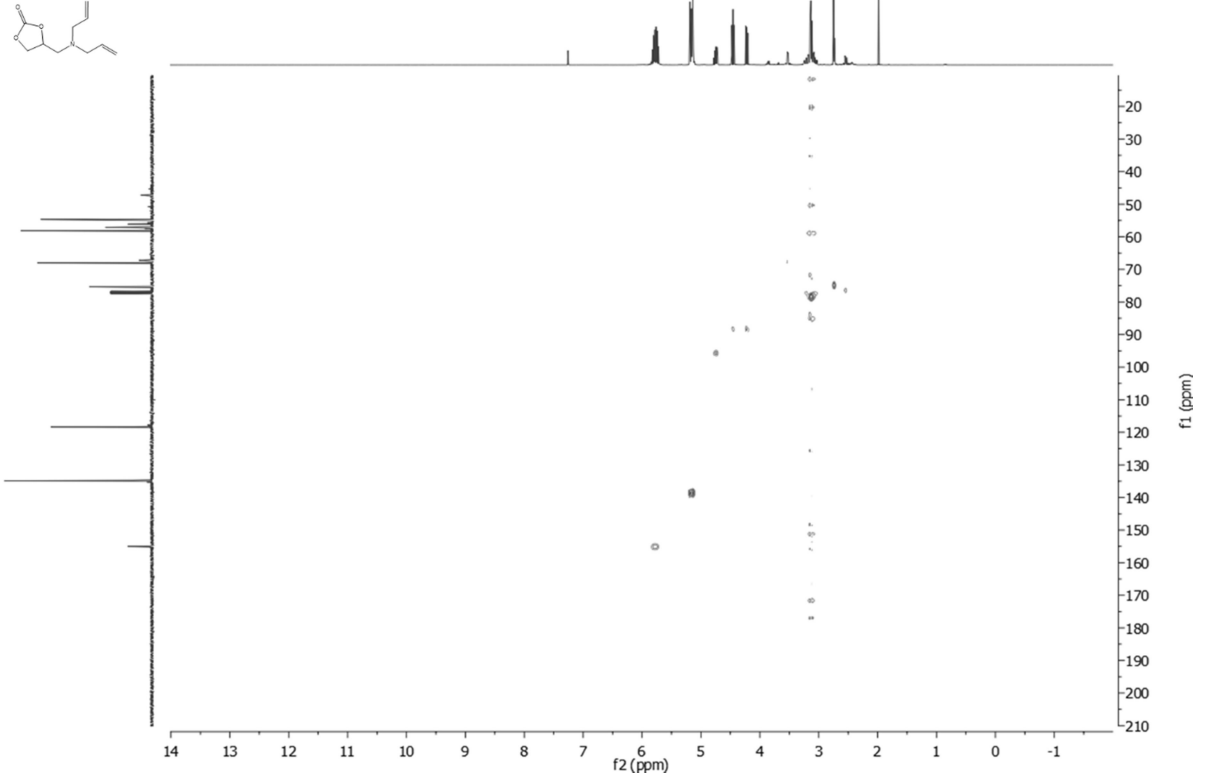
COSY

HSQC

Diallyl hydroxyazetidinium salt (N,N-diallyl-3-hydroxyazetidium chloride)

^{1}H NMR (400 MHz, DMSO-d_6)

^{13}C NMR (101 MHz, DMSO-d_6)
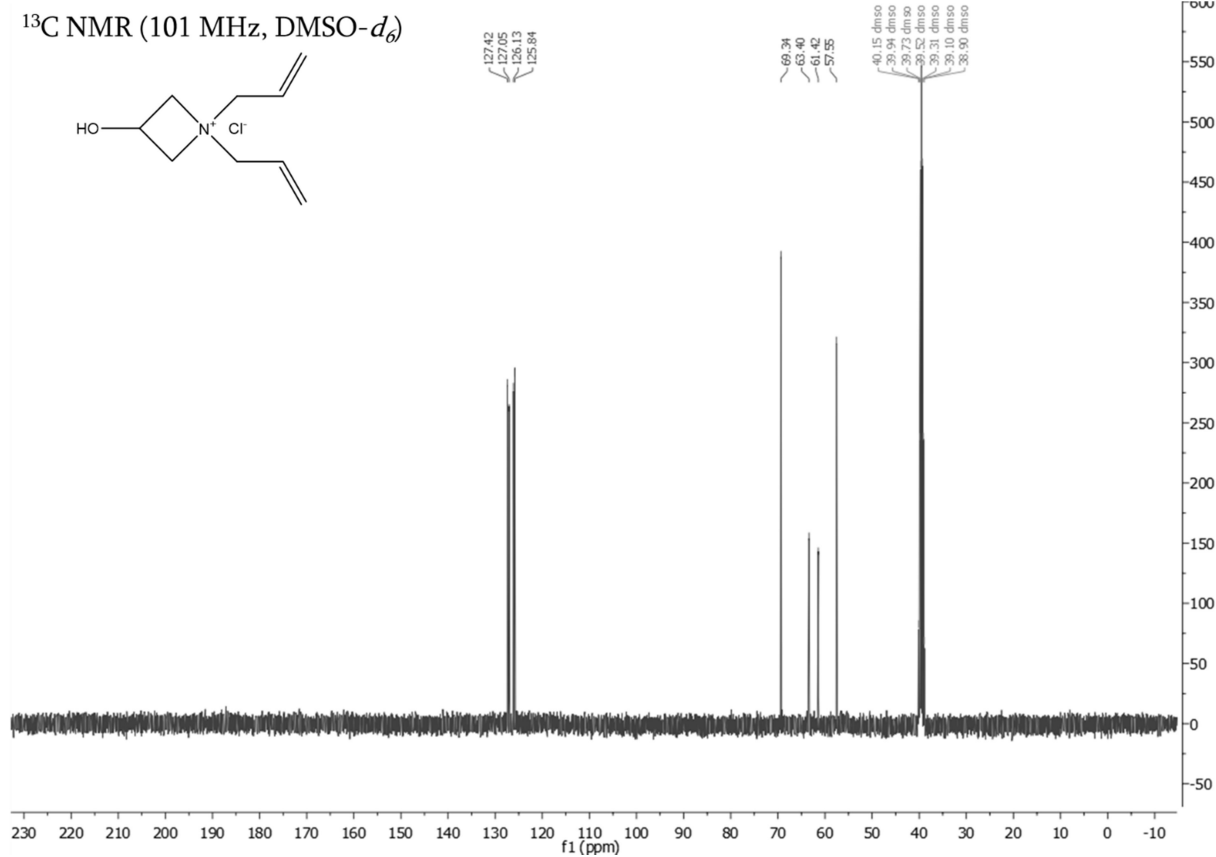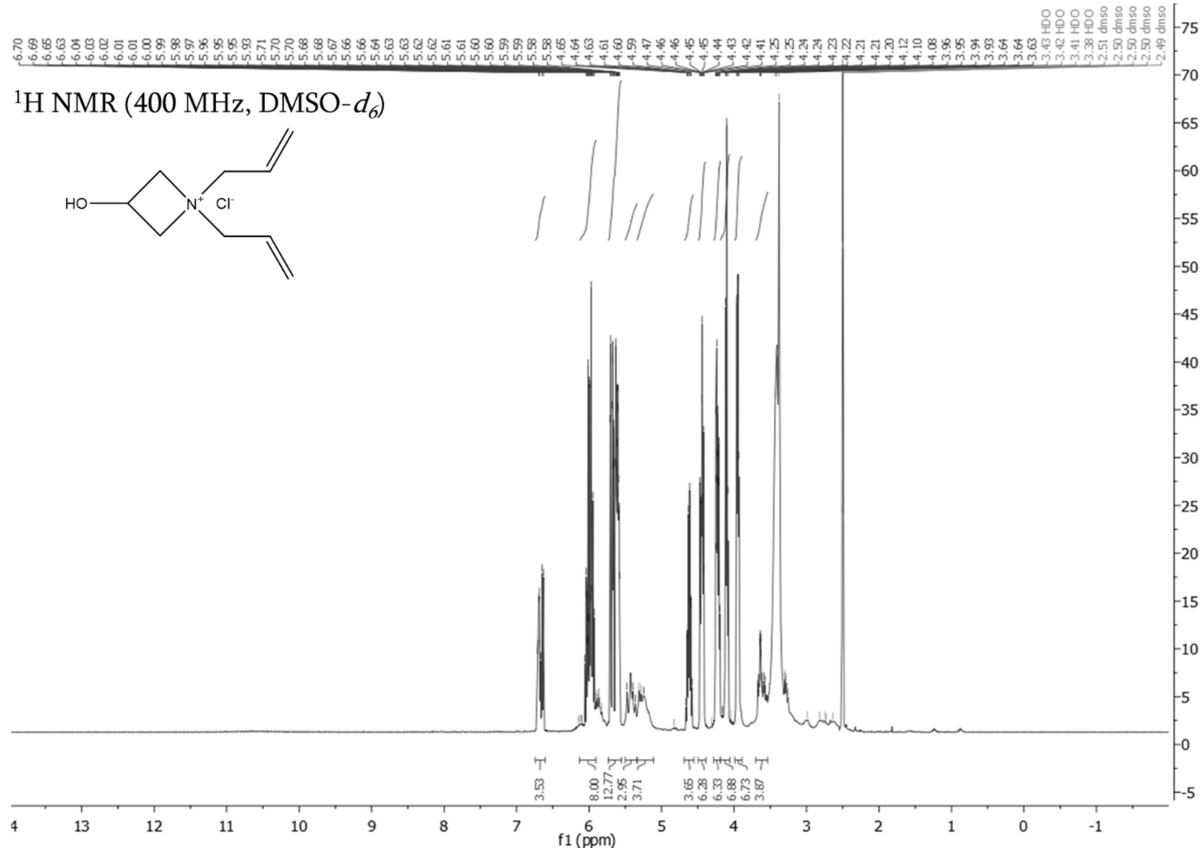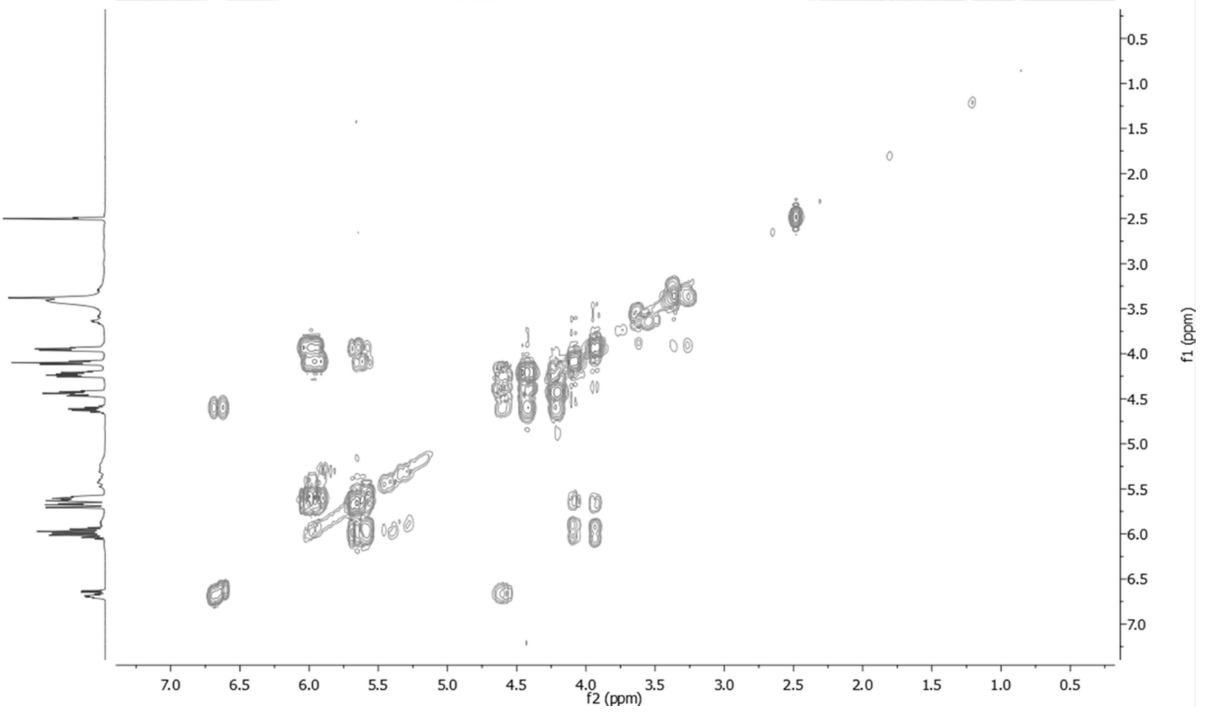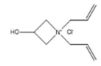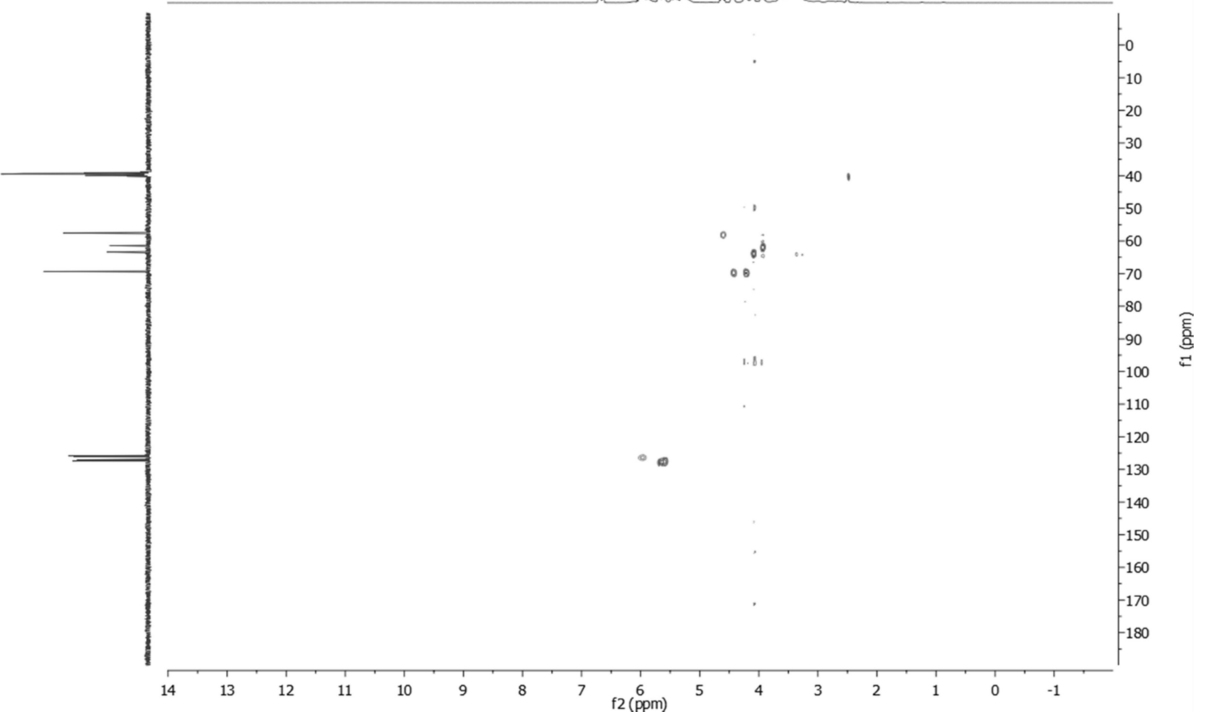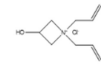
COSY

HSQC

Diallyl diol (3-(diallylamino)propan-1,2-diol)

¹H NMR (400 MHz, CDCl₃)

¹³C NMR (101 MHz, CDCl₃)
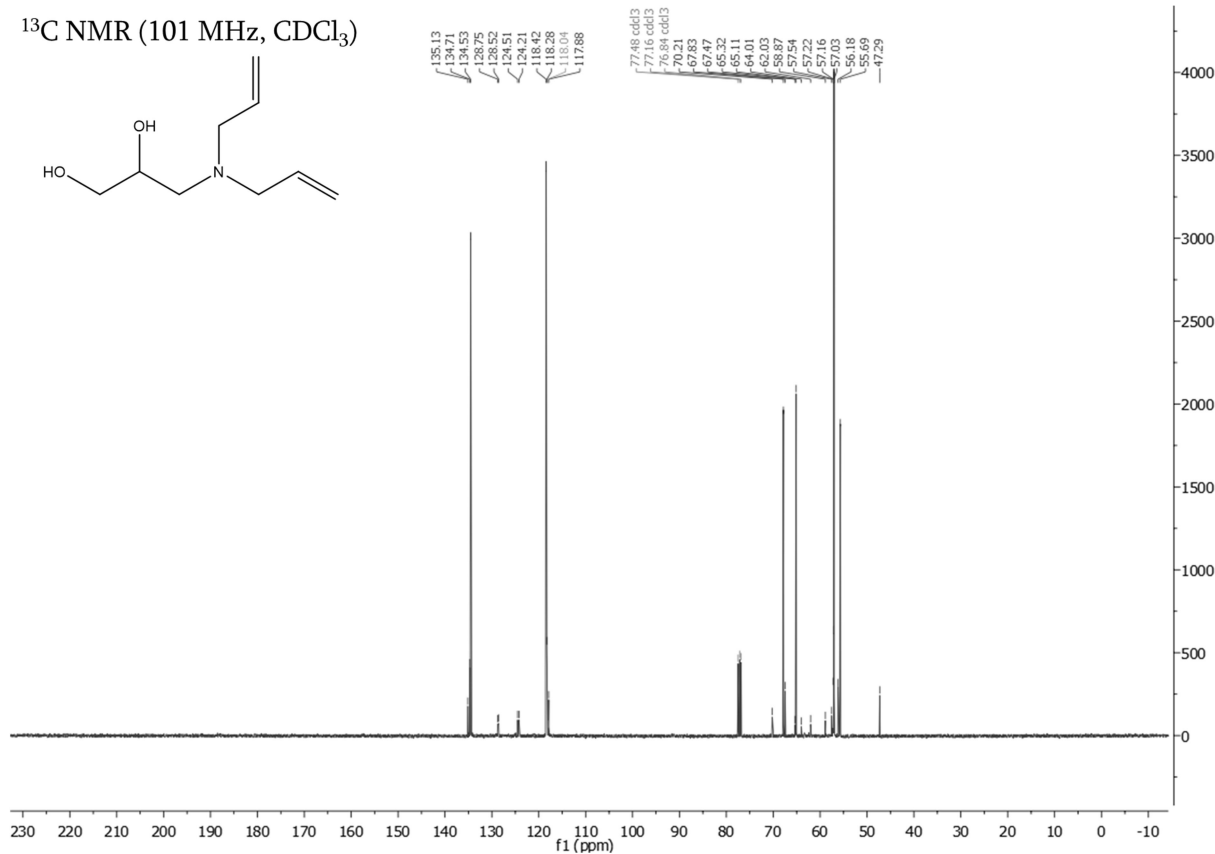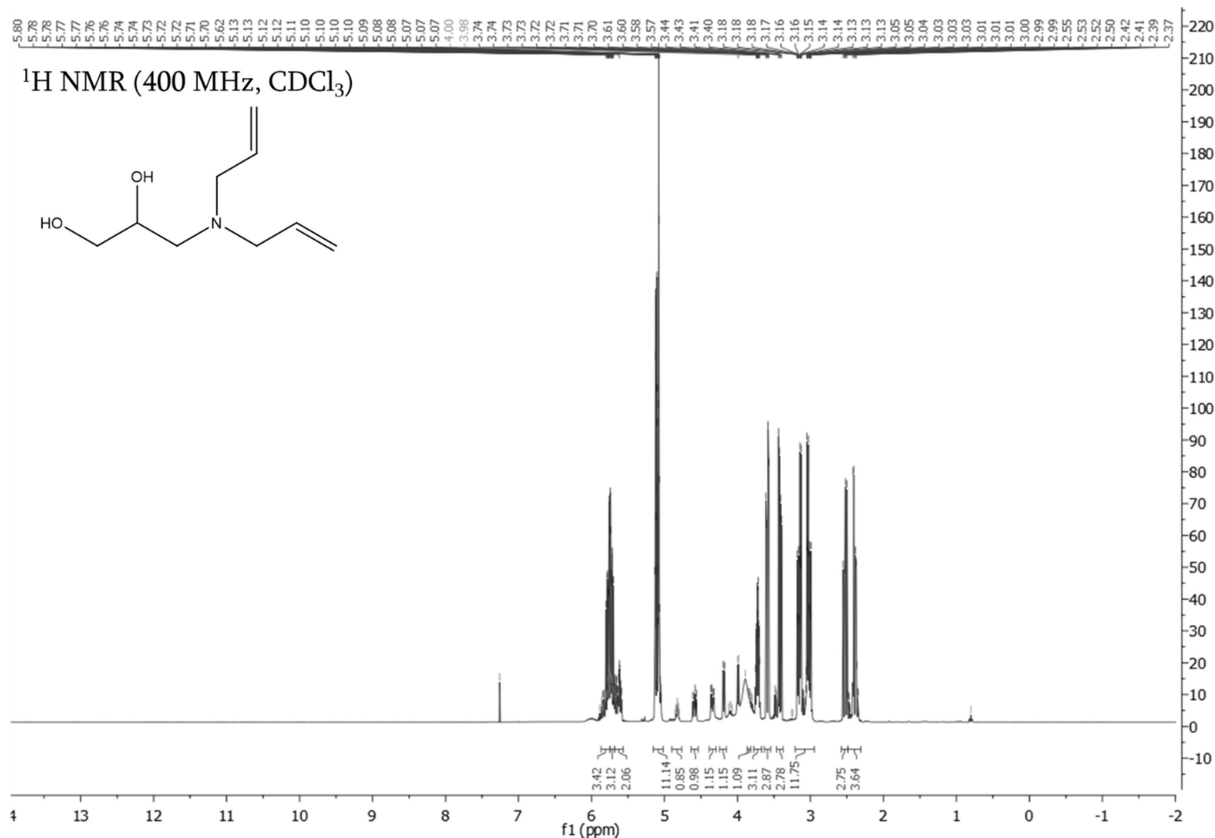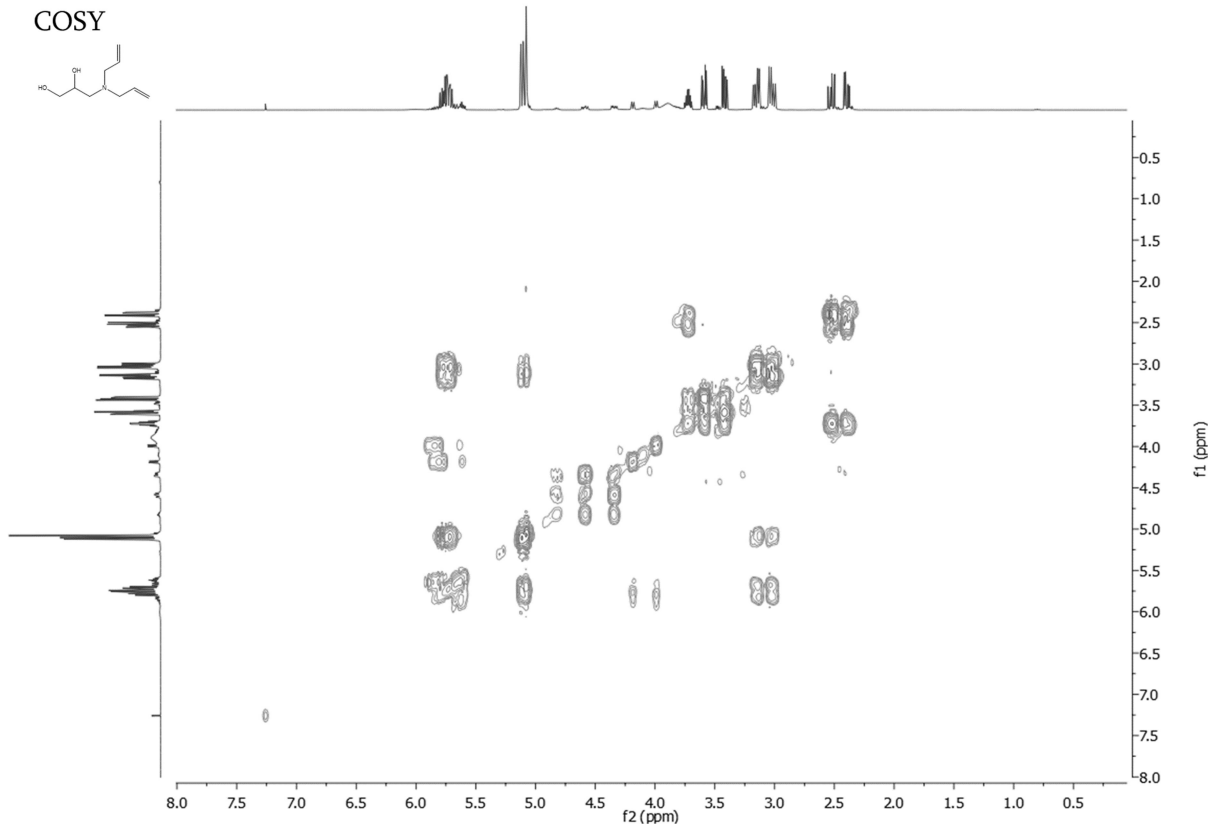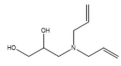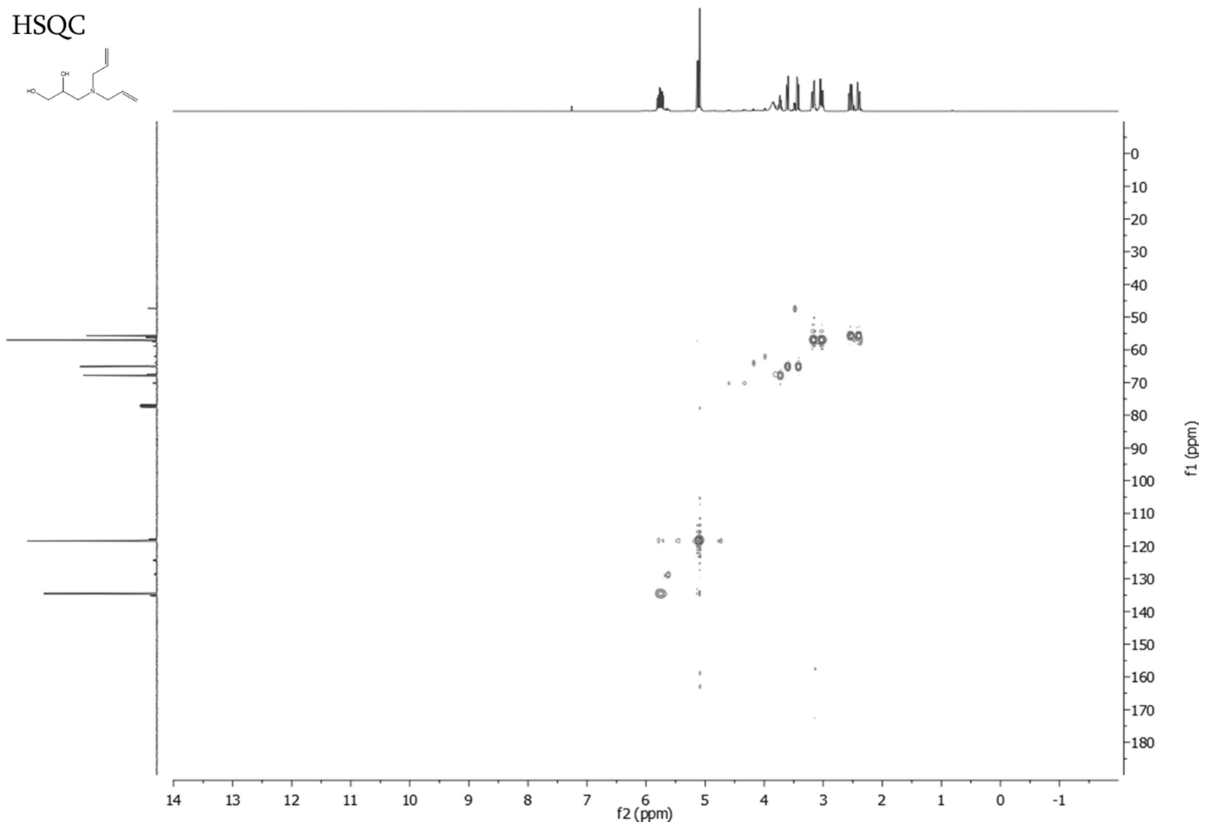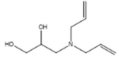
COSY

HSQC

Morpholine hydroxyazetidinium salt
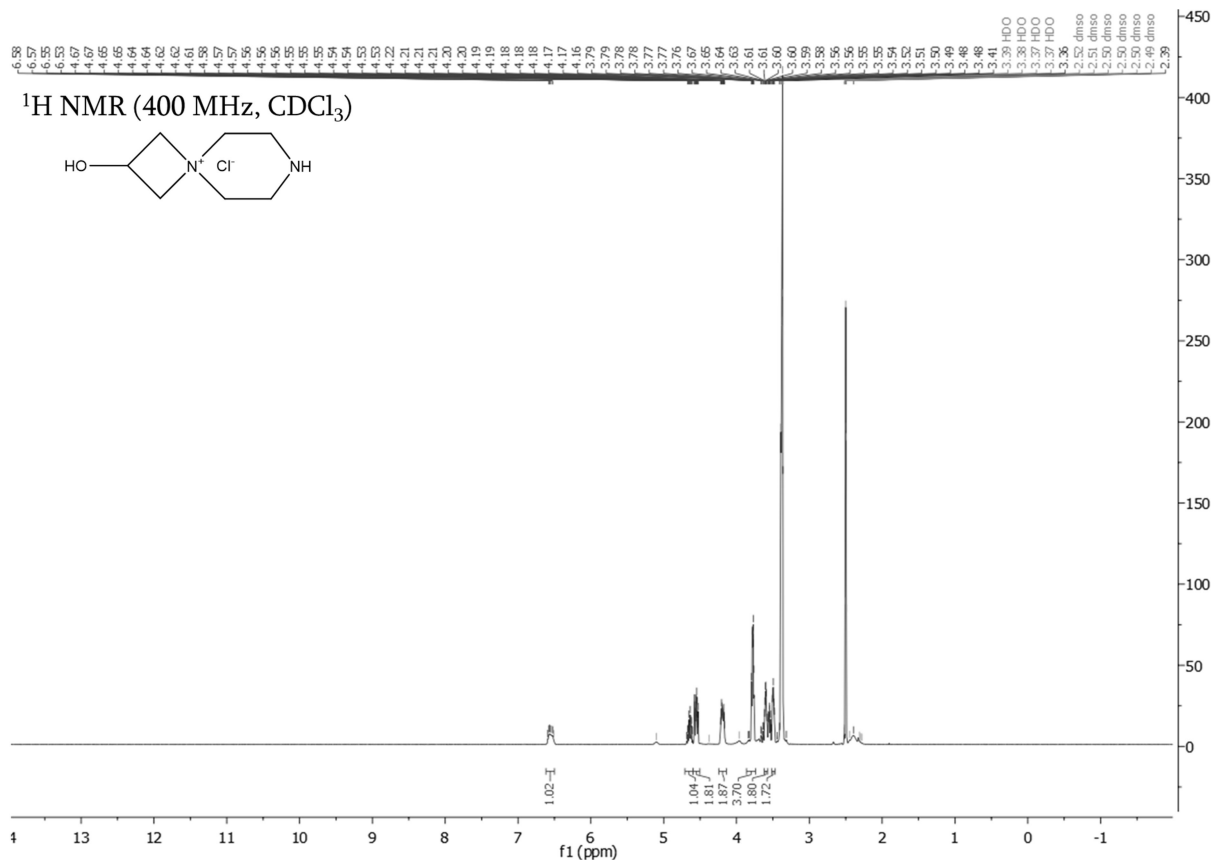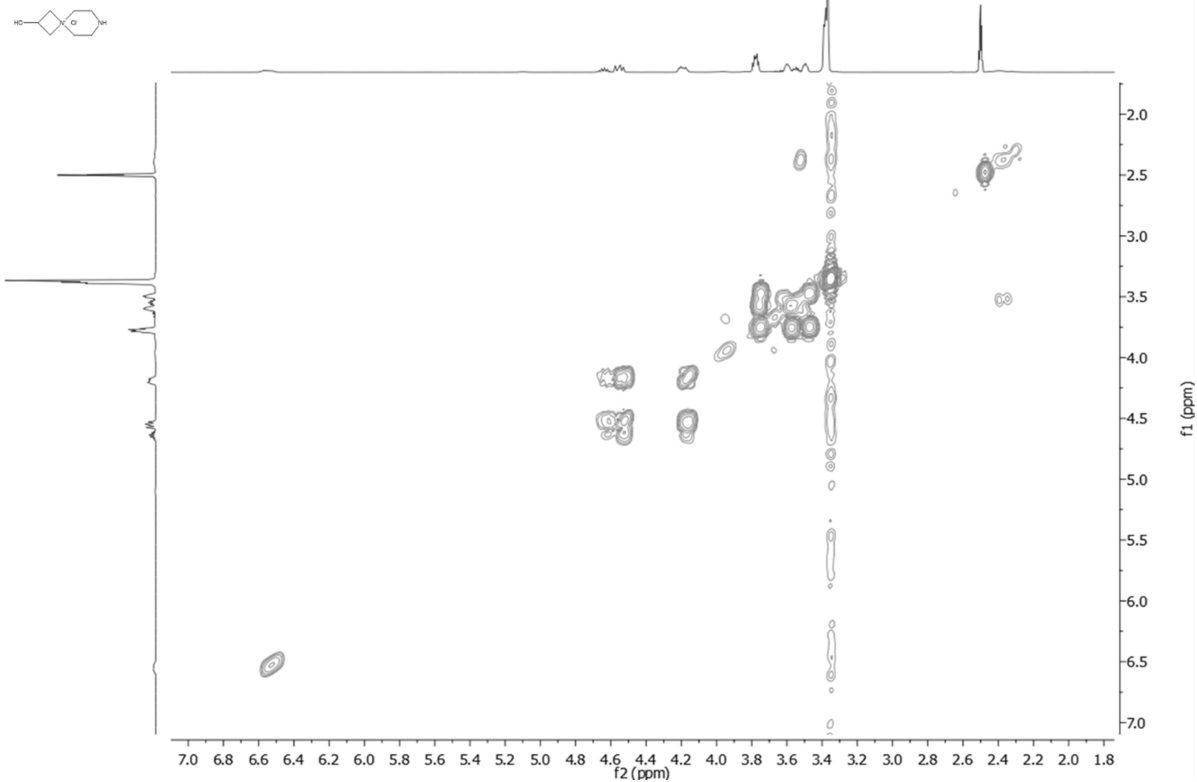
^{1}H NMR (400 MHz, CDCl$_3$)

COSY

79

Diethylamine hydroxyazetidinium salt

¹H NMR (400 MHz, DMSO-d_6)

¹³C NMR (101 MHz, DMSO-d_6)

Dihexylamine hydroxyazetidinium salt

^{1}H NMR (400 MHz, DMSO-d_6)

^{13}C NMR (101 MHz, DMSO-d_6)

COSY

HSQC

Dihexylamine alkylchloride and hydroxyazetidinium salt (mixed products)

¹H NMR (400 MHz, DMSO-*d₆*)
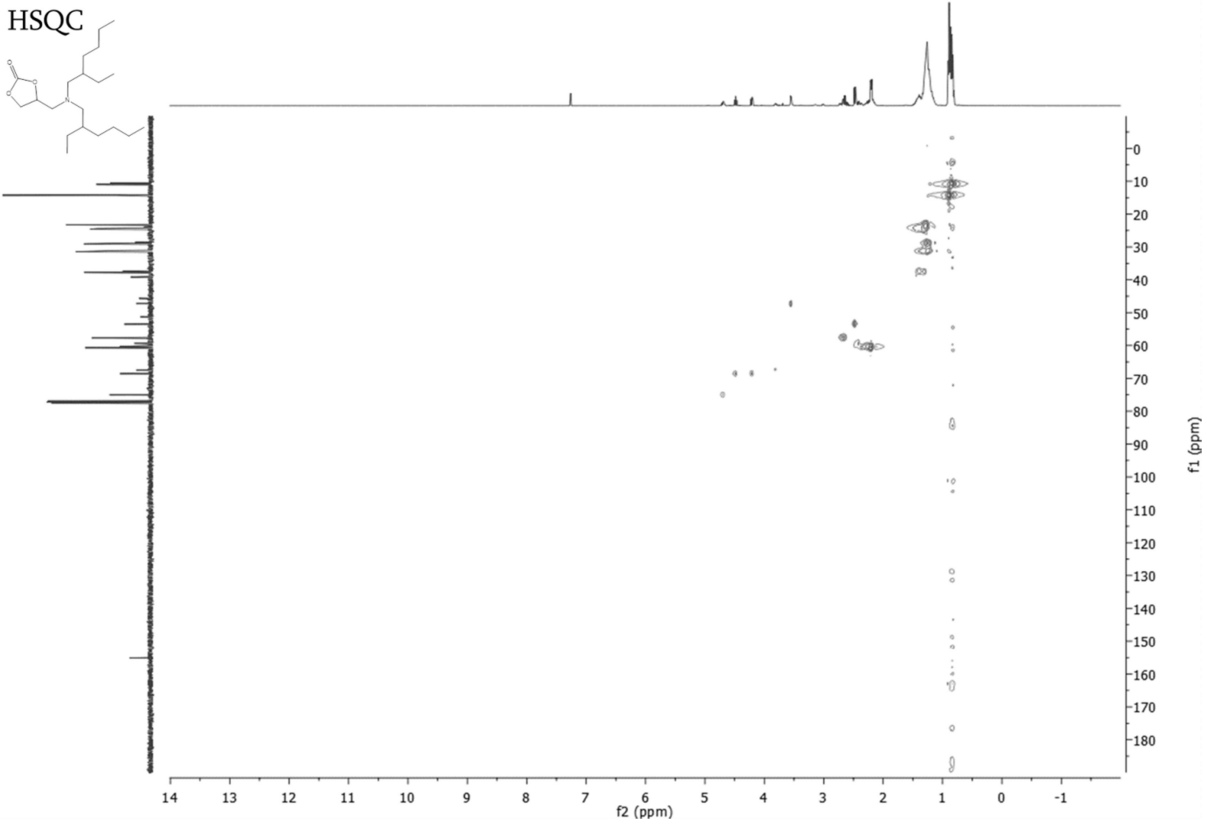

¹³C NMR (101 MHz, DMSO-*d₆*)
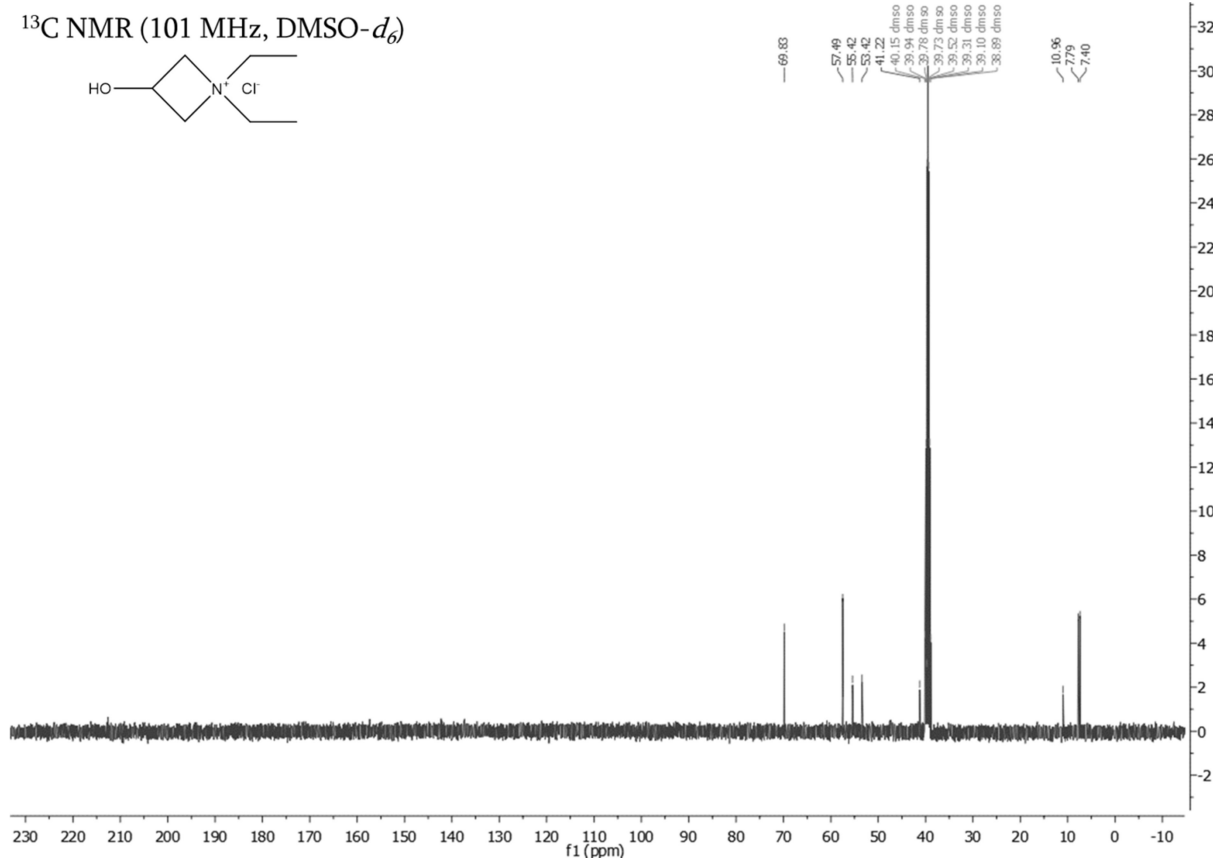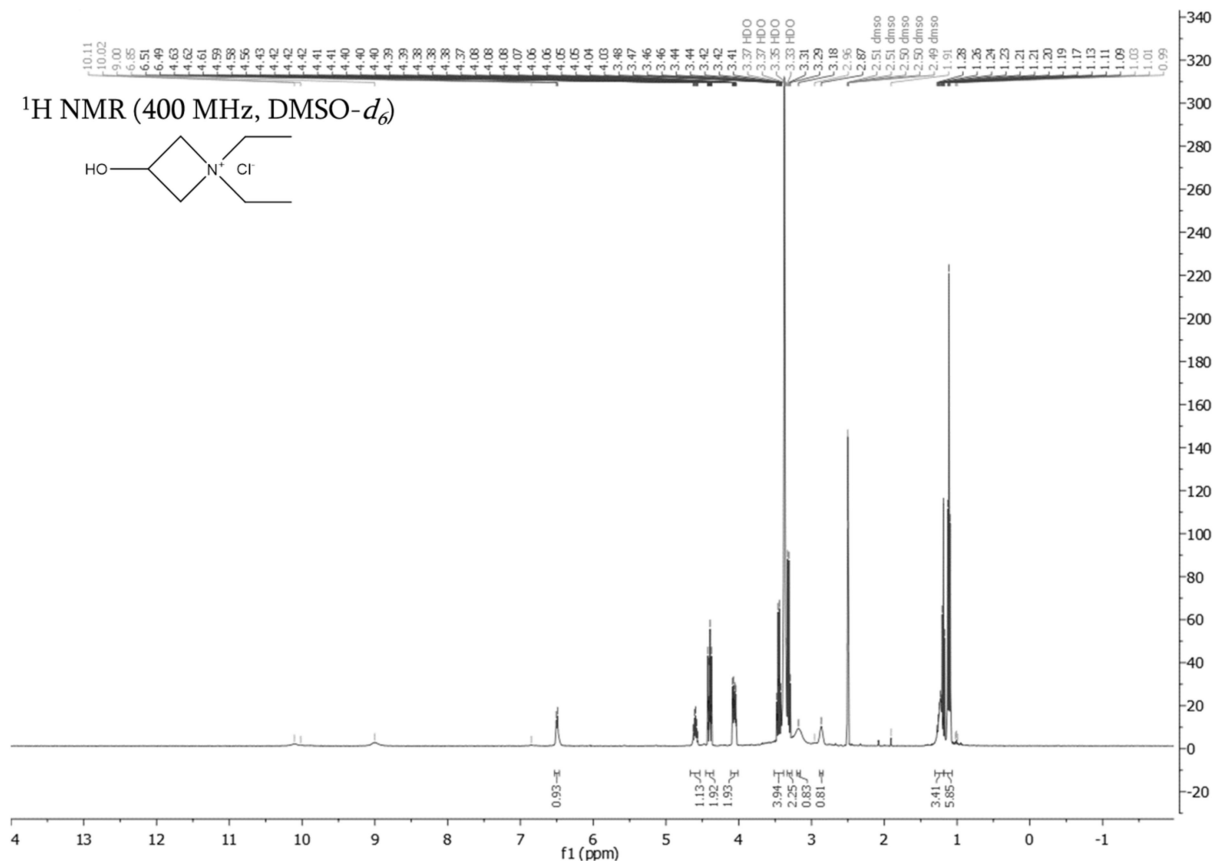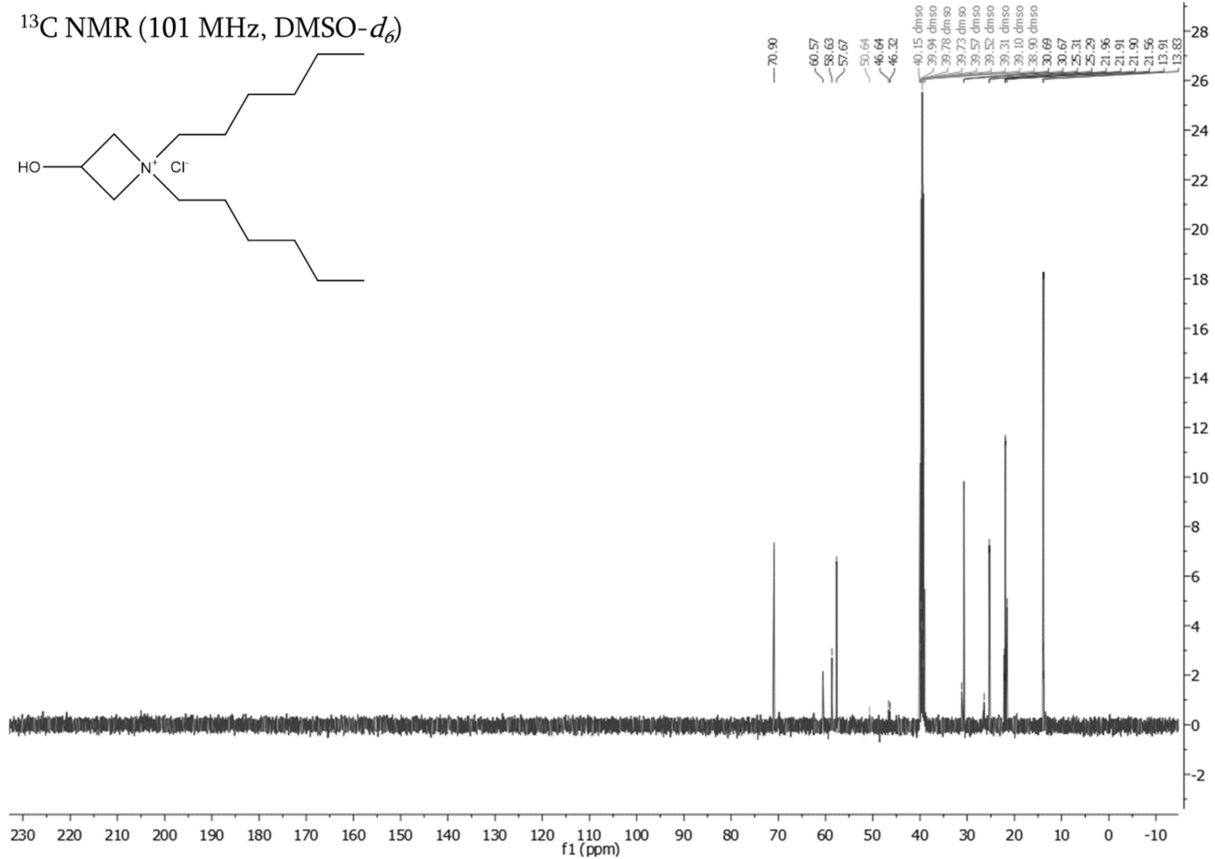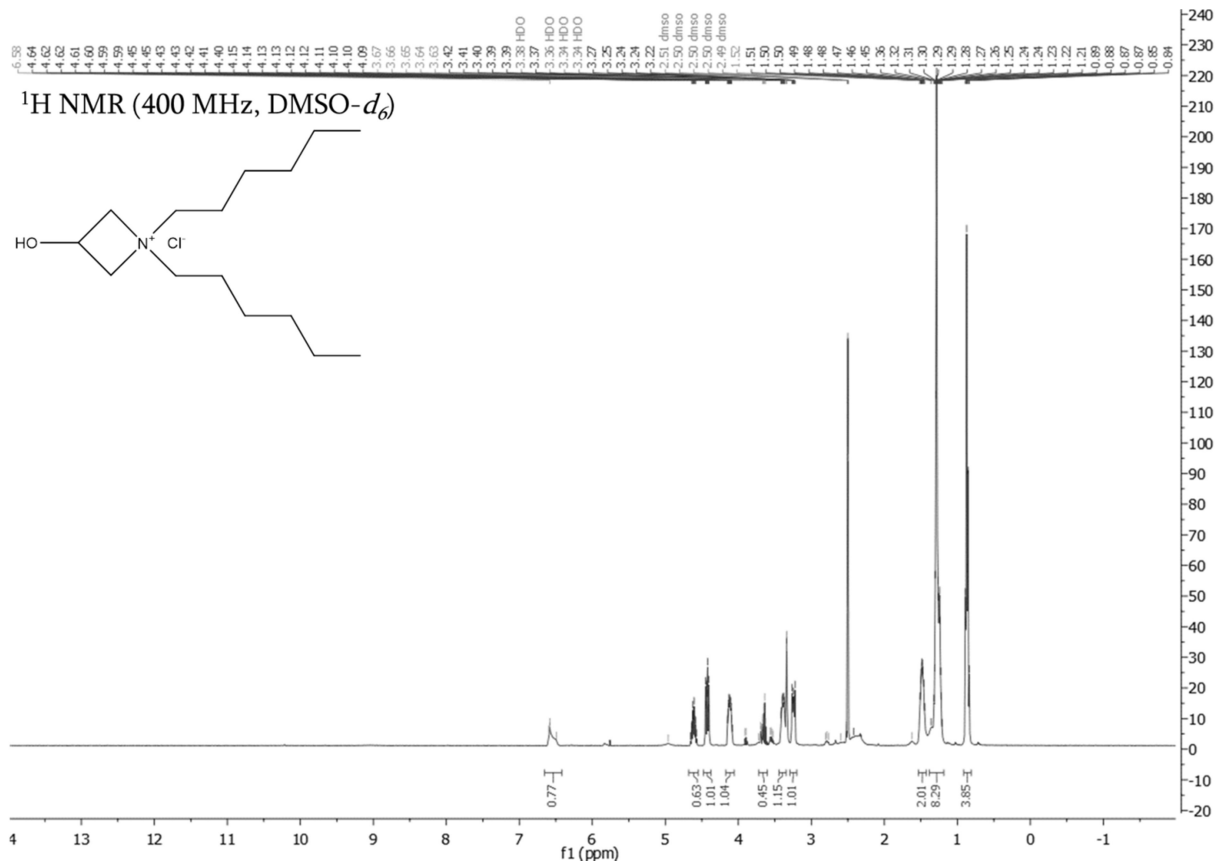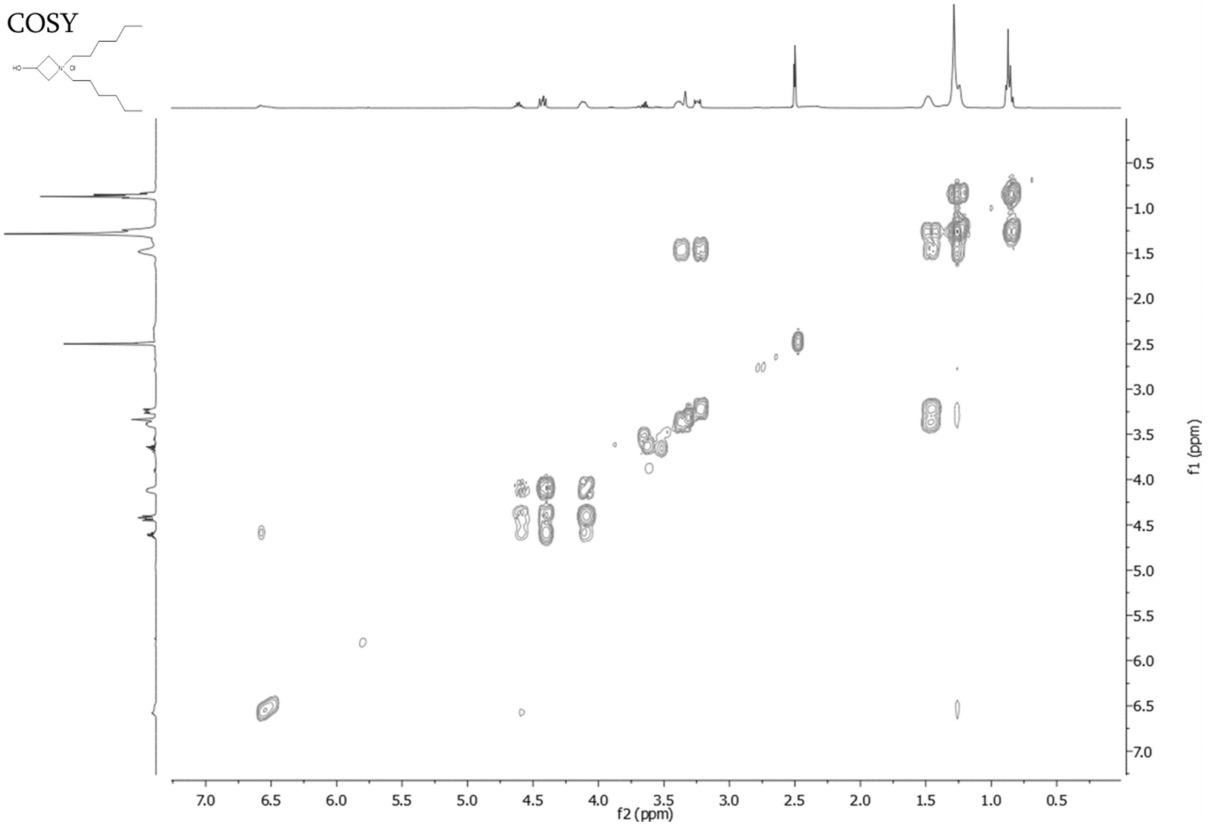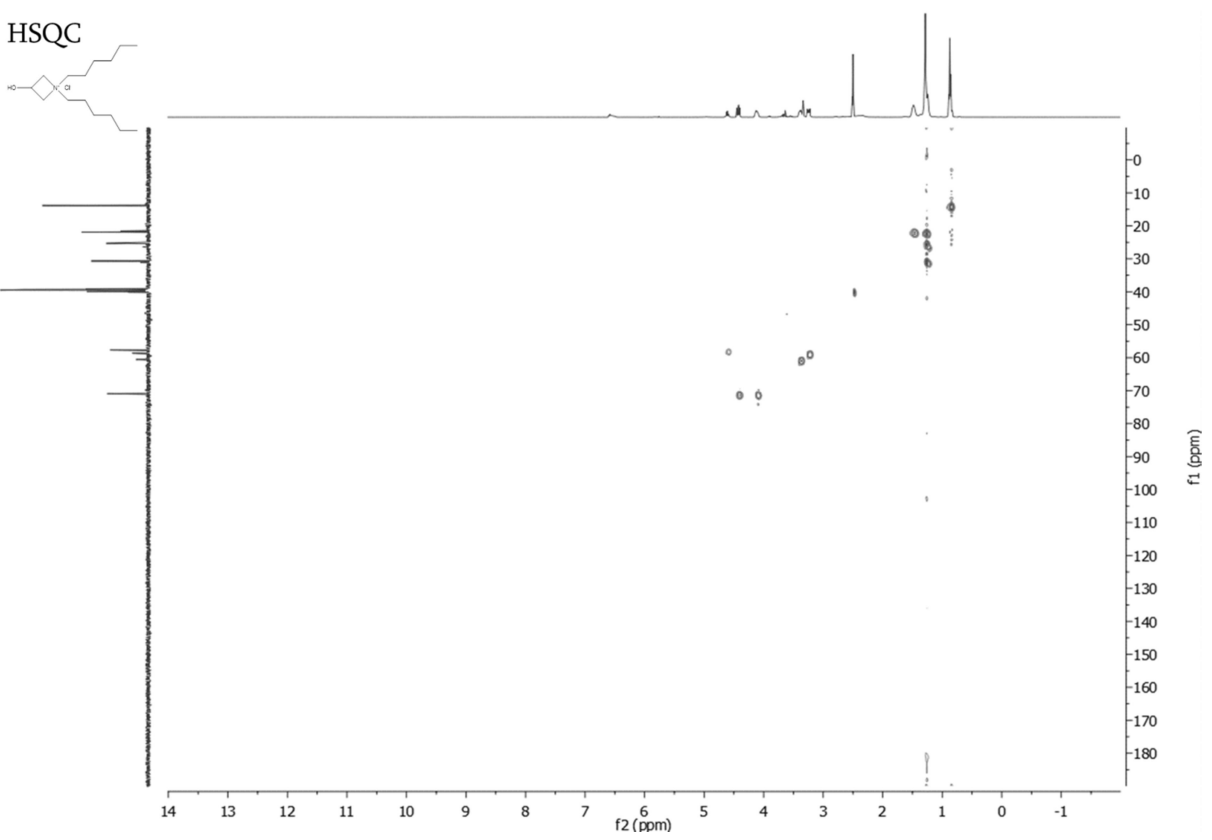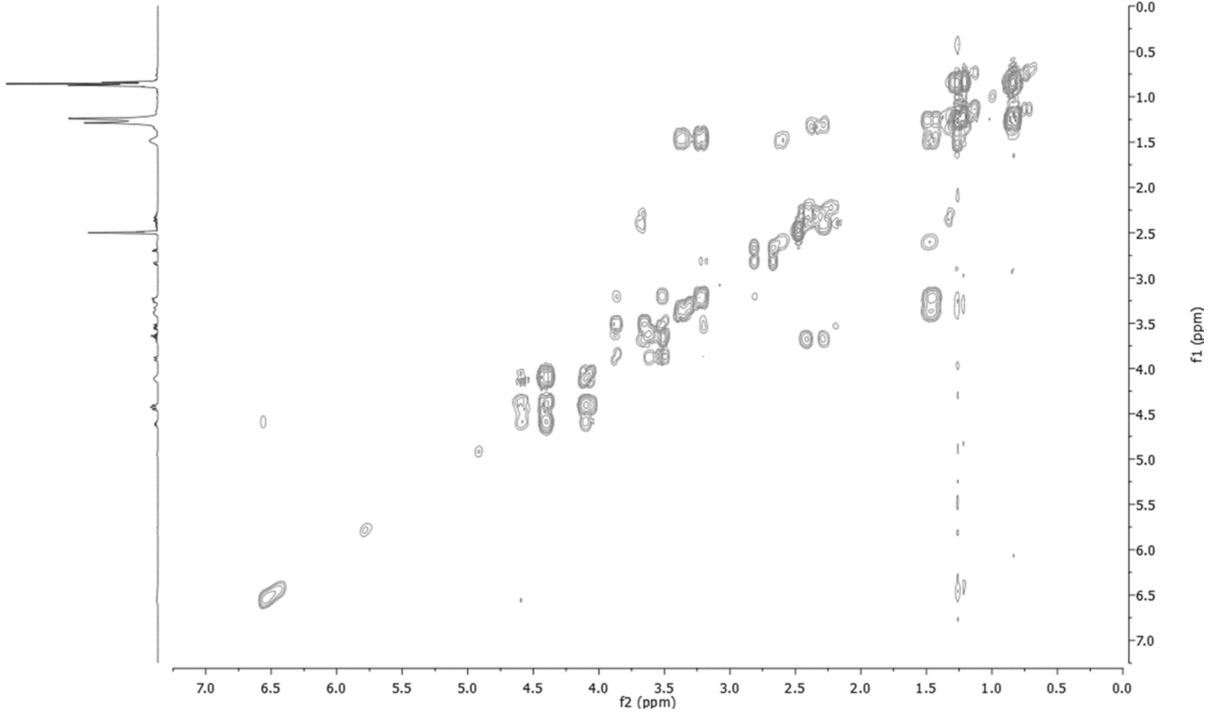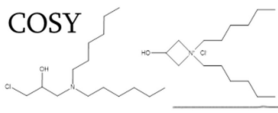
COSY

HSQC

Di(ethylhexyl)amine alkylchloride

^{1}H NMR (400 MHz, DMSO-d_6)
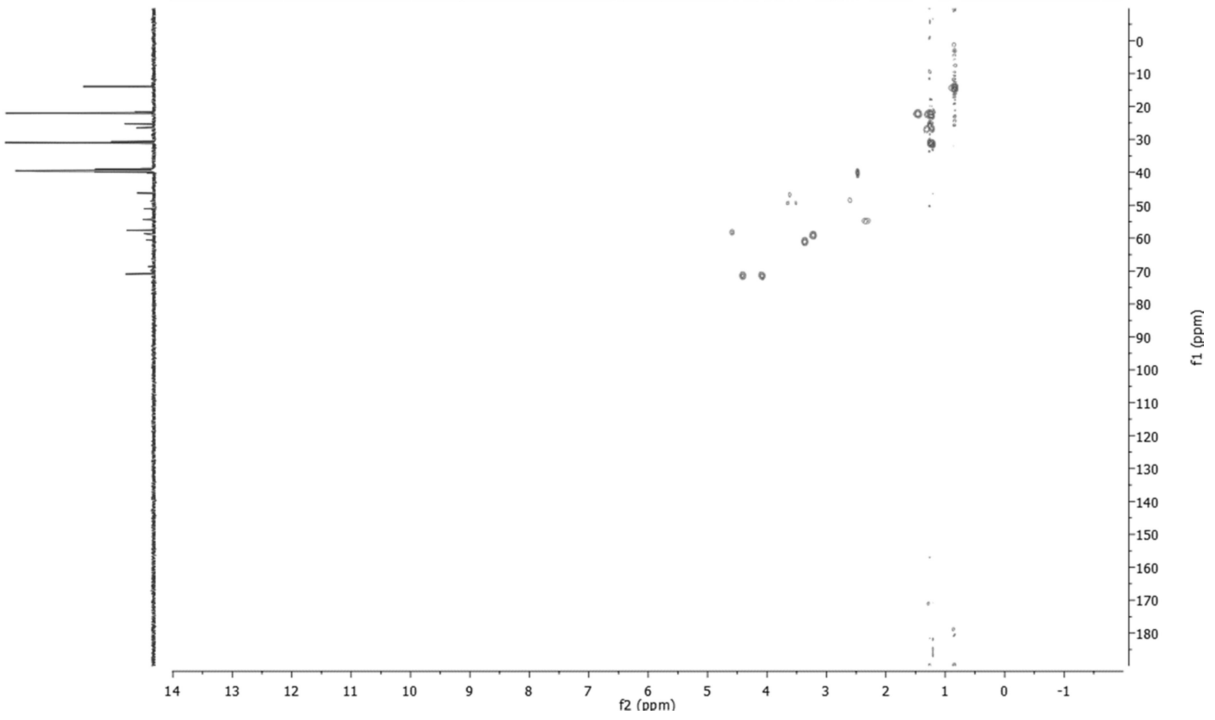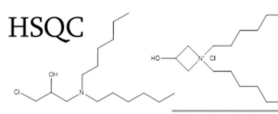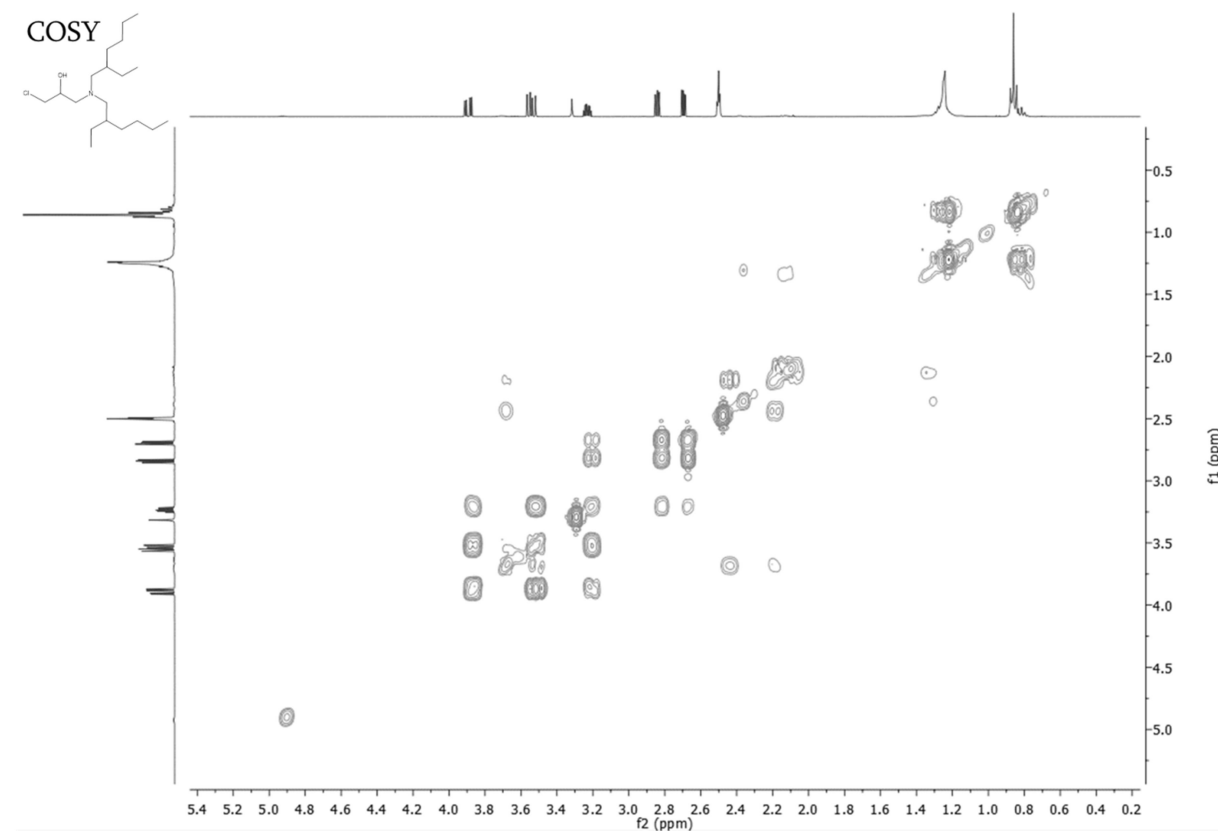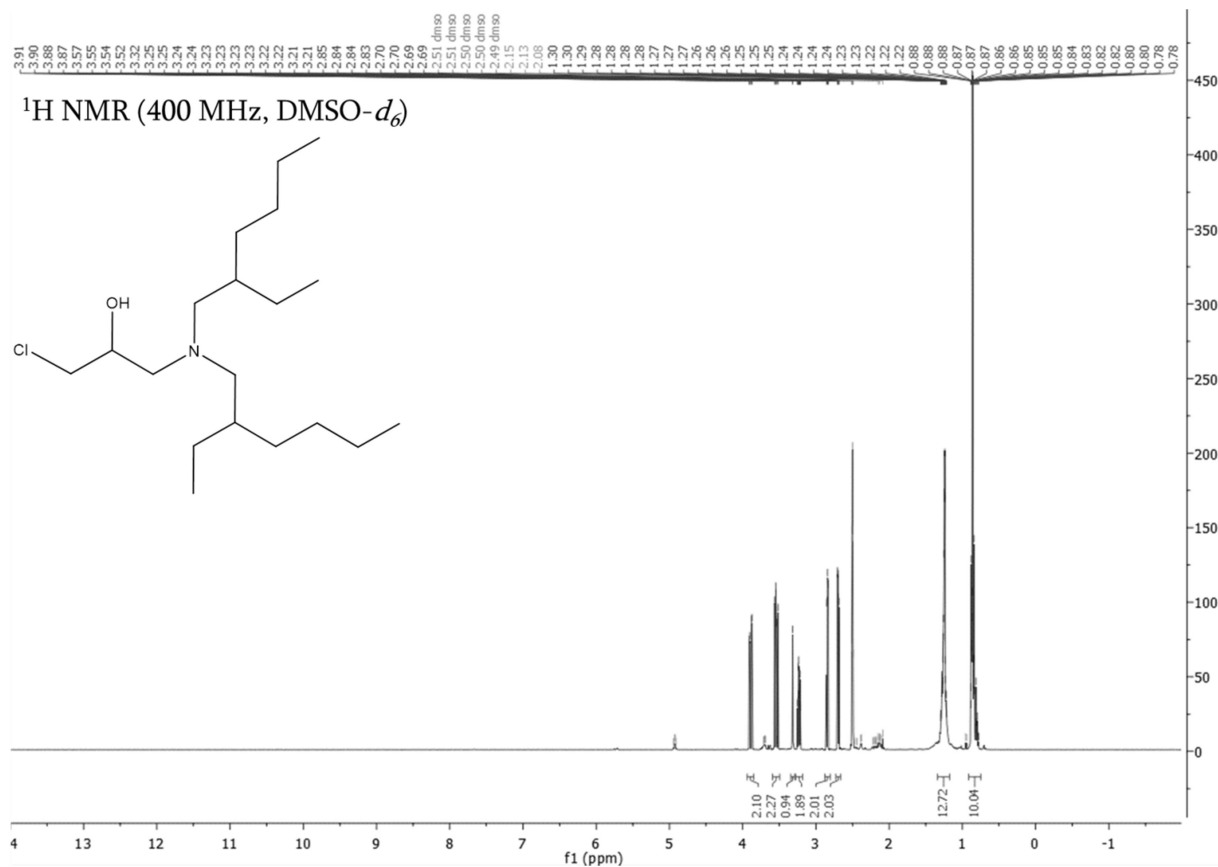
COSY

Di(ethylhexyl)amine cyclocarbonate

^{1}H NMR (400 MHz, CDCl$_3$)
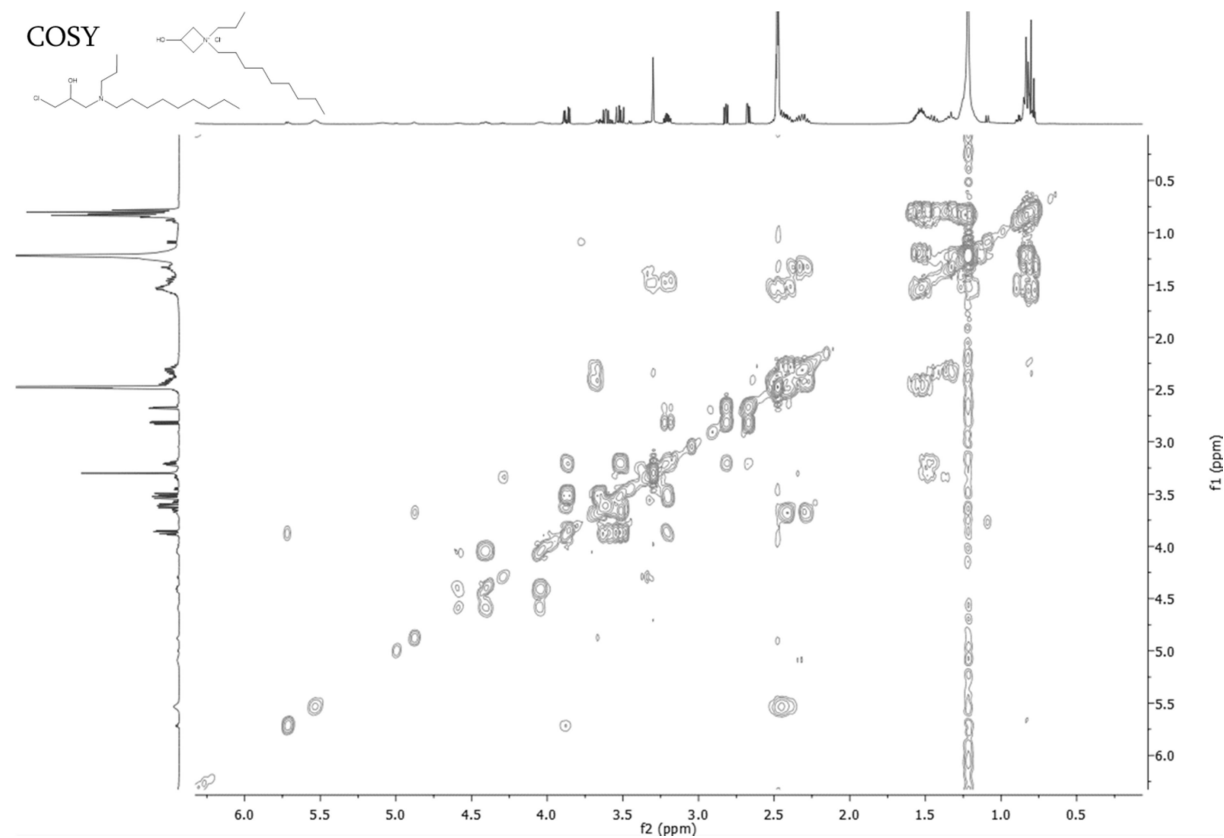

^{13}C NMR (101 MHz, CDCl$_3$)

COSY

HSQC

Propylnonylamine alkylchloride and hydroxyazetidinium salt (mixed products)

^{1}H NMR (400 MHz, DMSO-d_6)

COSY

Methylundecylamine alkylchloride and hydroxyazetidinium salt (mixed products)

¹H NMR (400 MHz, DMSO-*d₆*)

COSY

Dibenzylamine alkylchloride

¹H NMR (400 MHz, DMSO-*d₆*)

COSY
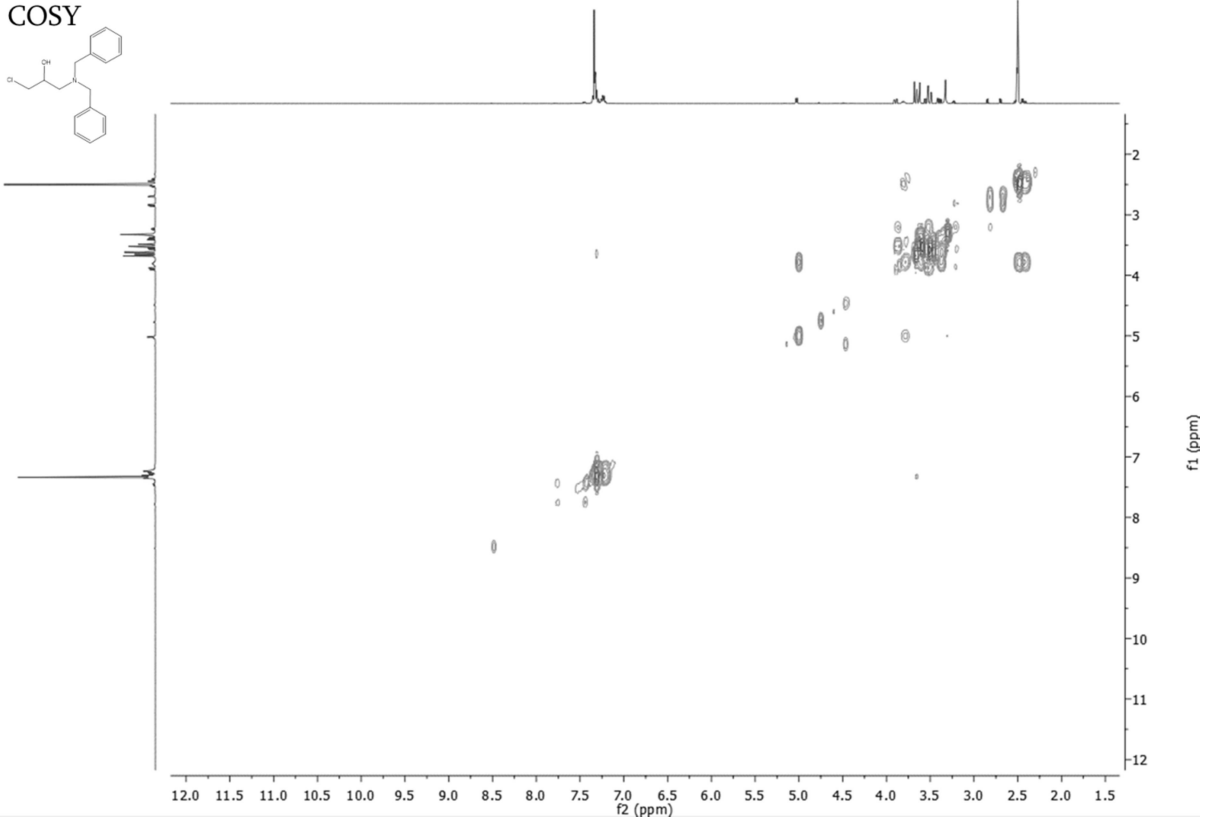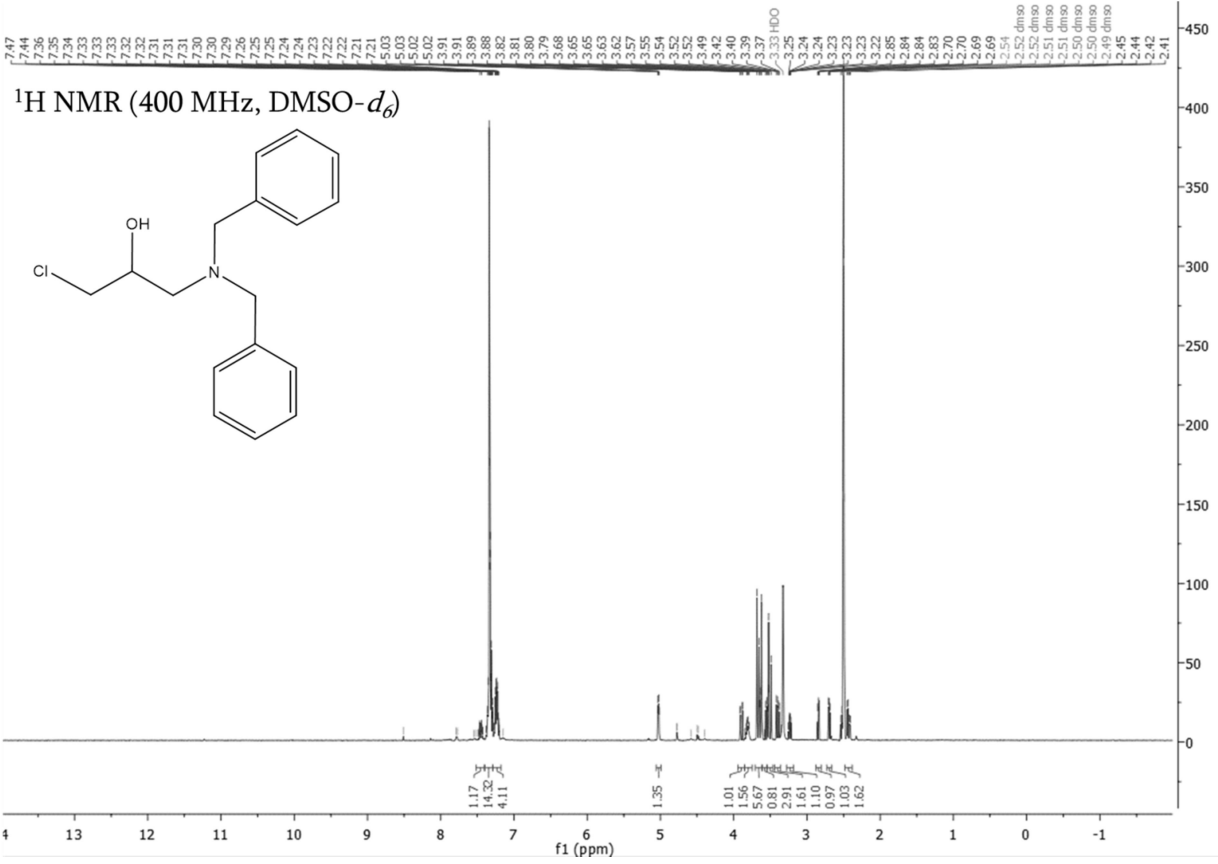
Iminodipropionitril alkylchloride

^{1}H NMR (400 MHz, DMSO-d_6)

COSY